

Tohoku (30-Inch) Bubble Chamber
Magnet Stress Analysis

Wes Craddock
September 5, 1984

Table of Contents

- 1) History of Design and Fabrication
- 2) Magnet Parameters
- 3) Simple Analytical Analysis
- 4) Axisymmetric Coil/Cryostat ANSYS Analysis
- 5) 3D Finite Element Analysis by Computerized Engineering
- 6) Finite Element Analysis of Radial Arm Bracket
- 7) Strength of Materials Cryostat Analysis
- 8) Coil Stress Analysis with W. Young's Program
- 9) Discussion and Summary of Coil Stresses
- 10) Preload Screw Torque Values
- 11) Special Area Stress Analysis
- 12) Summary of Cryostat Stress Analysis and Comparison to ASME Pressure Vessel Code

- Appendix A Computerized Engineering's Finite Element Report
Appendix B Welding Certification Documents
Appendix C Cryostat Stress Due to Internal Helium Pressure
Appendix D Safety of Cryostat Closure Welds
Appendix E Material Properties

TOHOKU (30-INCH) BUBBLE CHAMBER MAGNET STRESS ANALYSIS

HISTORY OF DESIGN AND FABRICATION

The Tohoku Bubble Chamber superconducting magnet was originally planned and conceived by Fermilab's old Technical Services department as part of an energy conservation program. Technical Services purchased the superconductor along with the Chicago Cyclotron wire. After very preliminary designs were proposed, this project was taken over by Research Services. This superconducting magnet was intended to replace the 8 MW water cooled copper coils of the hydrogen filled 30-Inch Bubble Chamber. The following decisions were made at the very outset of design.

1. The central field should reach the old maximum value of 32 kg.
2. The magnet should fit in the existing iron without remachining.
3. Damaged wire from the Chicago Cyclotron Magnet project would be used for this magnet.
4. Liquid helium boiloff should be kept to a minimum because no liquifier decision could be made that far in advance.
5. The magnet would be cryostable.

Magnet design was made with "hand" calculations and a special purpose relatively simple solenoid magnet stress program acquired from W. Young at the University of Wisconsin. Material tests of the wire in tension and conductor/G-10 stacks in compression provided accurate hoop and radial moduli data. Axial and radial electromagnetic loads were calculated assuming cylindrical symmetry with the program TRIM. Upper bounds on the radial decentering forces were made with various combinations of hand calculations and a few Hall probe measurements made with the old copper coils.

Coil bobbin, outer cryostat wall, and the vacuum shell were all fabricated by Youngstown Welding. Many inspection trips were made during this manufacturing. Just as these pieces were being completed, it was decided that a finite element analysis should be performed. Up to this point Fermilab had very little exposure to the finite element method. An \$11,000 analysis was completed by Computerized Engineering based on a 1/4 model using ANSYS 3D solid elements. Only the cryostat was analyzed as opposed to the coil/cryostat combination. Assumed worse case radial forces were given to Computerized Engineering by Fermilab on the assumption that their results would always be scaled up or down based on future more accurate material property data and solenoid stress runs. In any event, their work only included radial and axial electromagnetic forces. It was in my opinion a rather course model. In an effort to check their results and my calculations, B. Wands ran a simplified ANSYS axisymmetric model. He also made a detail ANSYS analysis of the vertical support bracket and its connection to the cryostat.

Both coils were wound by Research Services personnel and welded in Lab 3. During cryostat fabrication it was decided that a large portion of the original I.G.C. superconducting cable was totally unusable. Approximately 1/3 new wire was ordered from New England Electric Co. Left over substandard Energy Doubler strands were supplied to manufacture the new cable. After both cryostats were welded shut, the new Tohoku Bubble Chamber was proposed to Research Services. This involved reworking the vacuum and LN2 shells and machining a chamfer on the top inside corner of the cryostat. Production Tool Corporation manufactured the new vacuum shell inner and transition ring.

In an effort to get accurate stresses I have made a detailed axisymmetric model which incorporates the cryostat, coil, push bars, preload screws, and axial support brackets. These answers are considered to be the most reliable, accurate, and easy to interpret. Previous hand calculations, W. Young's solenoid stress program results, and ANSYS runs are used for verification and to provide stress information from the radial decentering forces which are not available with this 2D model. It will be shown that W. Young's program, measurements during winding, and a little intuition are all that are available to predict the winding stress distribution. Refer to reference 1 for construction and assembly details.

MAGNET PARAMETERS AND DIMENSIONS

Figures 1 to 8 show the magnet cross section and some of its more important dimensions. Listed below are the important magnet dimensions and the values, if different, used in all the analyses. Analysis has been based on thickness less than or equal to the minimum thickness obtained after machining.

All forces are based on my TRIM run #47 which is the final field run for the magnet with the muon notches filled with iron. Little difference is found when the muon notches have the iron removed.

Many of the following calculated values are used only in the more complete axisymmetric ANSYS analysis. Values that are used exclusively in this particular analysis are marked with an *. They are thought to be the most accurate values available.

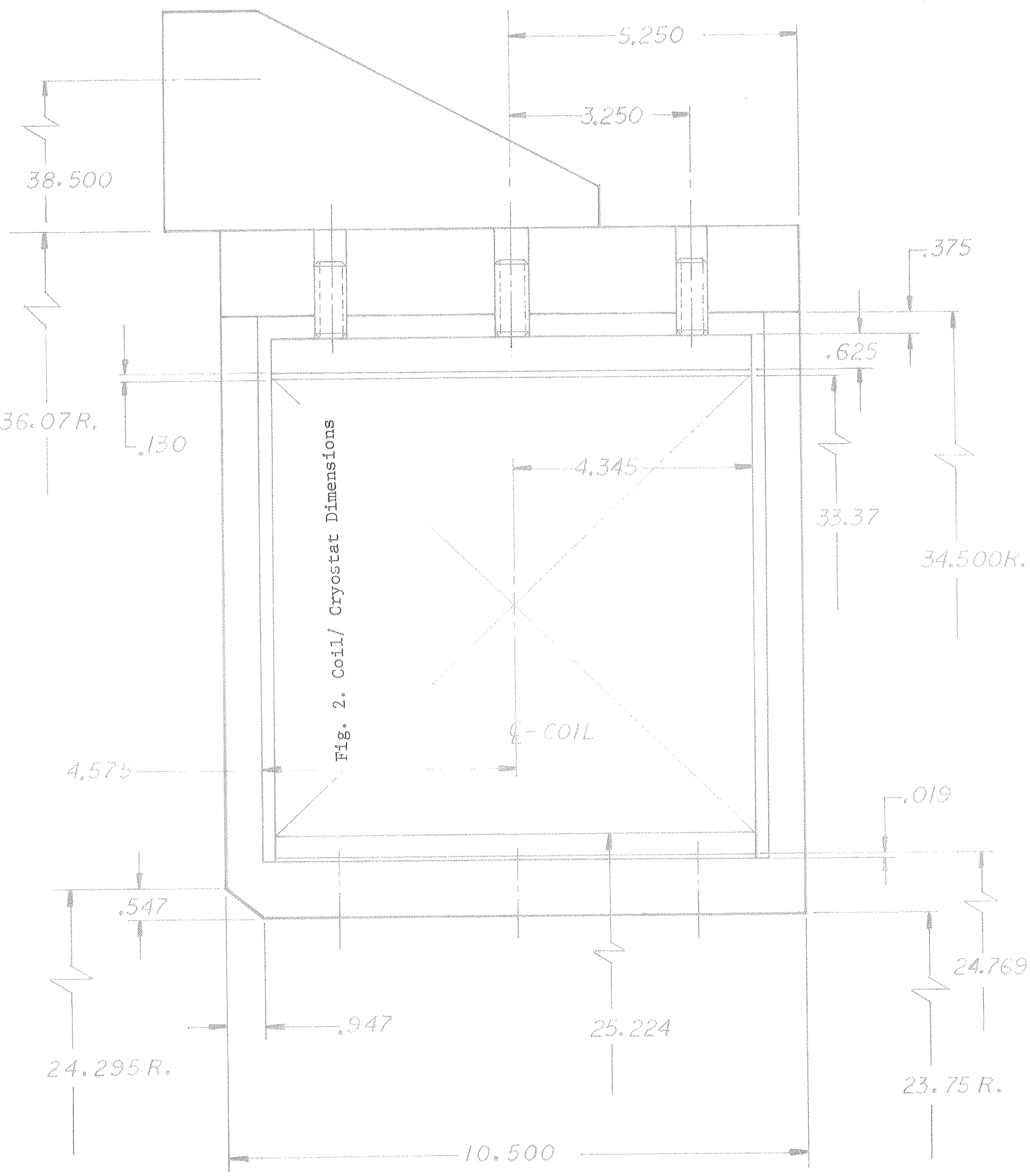


Fig. 2. Coil/ Cryostat Dimensions

C-COIL

(3)

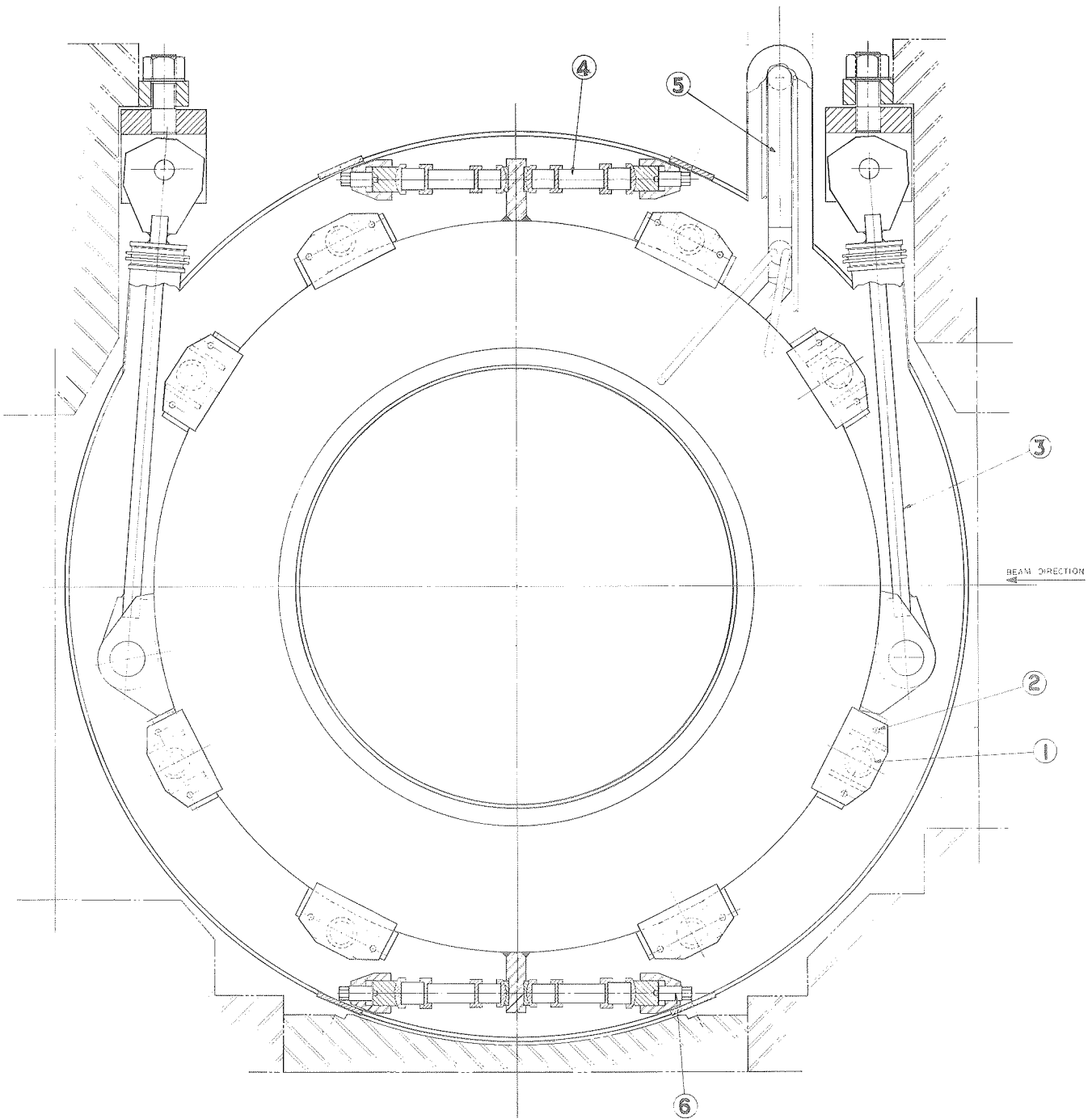
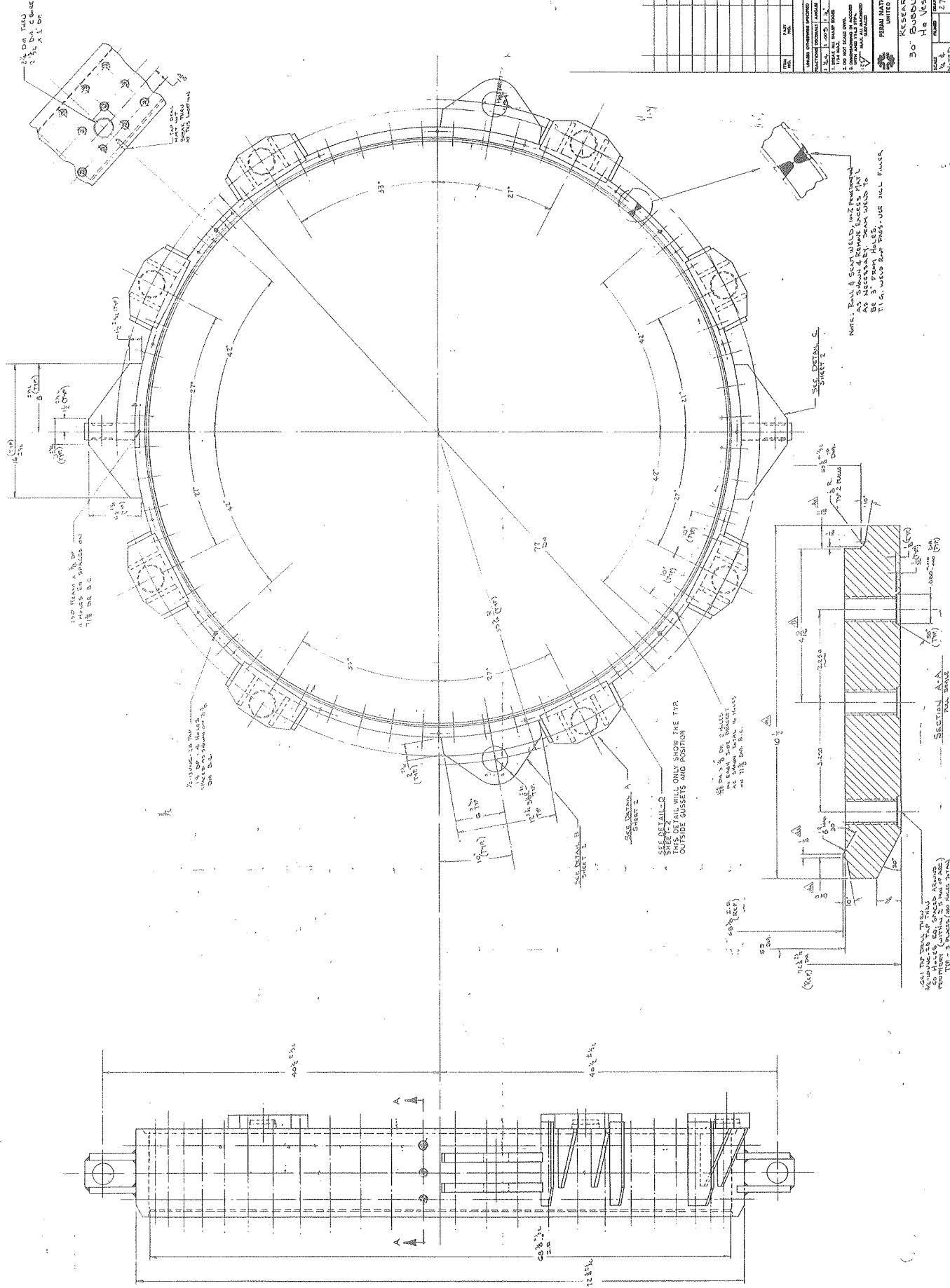


Fig. 3. Axial View of Magnet

Fig. 4. Cryostat Outer Ring



| REV. | DESCRIPTION | DATE | BY |
|------|---|----------|-------------|
| A | ISSUED FOR FABRICATION | 12/22/50 | J.C. GIBSON |
| B | REVISIONS MADE TO DRAWING | 1/10/51 | J.C. GIBSON |
| C | ADDED 16-BUSSETS TOTAL. ONE RADIAL COMP. POST PAD REMOVED FOR SINK ADDED. 1-1/2\"/> | | |
| E | 4-9/16 WAS 4-7/8 | 9/30 | J.C. GIBSON |
| F | 3-81 | 11-11-51 | J.C. GIBSON |

| REV. | DATE | DESCRIPTION OF REV. | BY |
|------|----------|---|-------------|
| 1 | 12/22/50 | ISSUED FOR FABRICATION | J.C. GIBSON |
| 2 | 1/10/51 | REVISIONS MADE TO DRAWING | J.C. GIBSON |
| 3 | 9/30/51 | ADDED 16-BUSSETS TOTAL. ONE RADIAL COMP. POST PAD REMOVED FOR SINK ADDED. 1-1/2\"/> | |
| 4 | 11-11-51 | 3-81 | J.C. GIBSON |

RESEARCH SERVICES
 30" BUDDLE CHAMBER CAL GANESSON
 He VESSEL-OUTER RING
 2771 MC-5455
 SHEET 1 OF 2

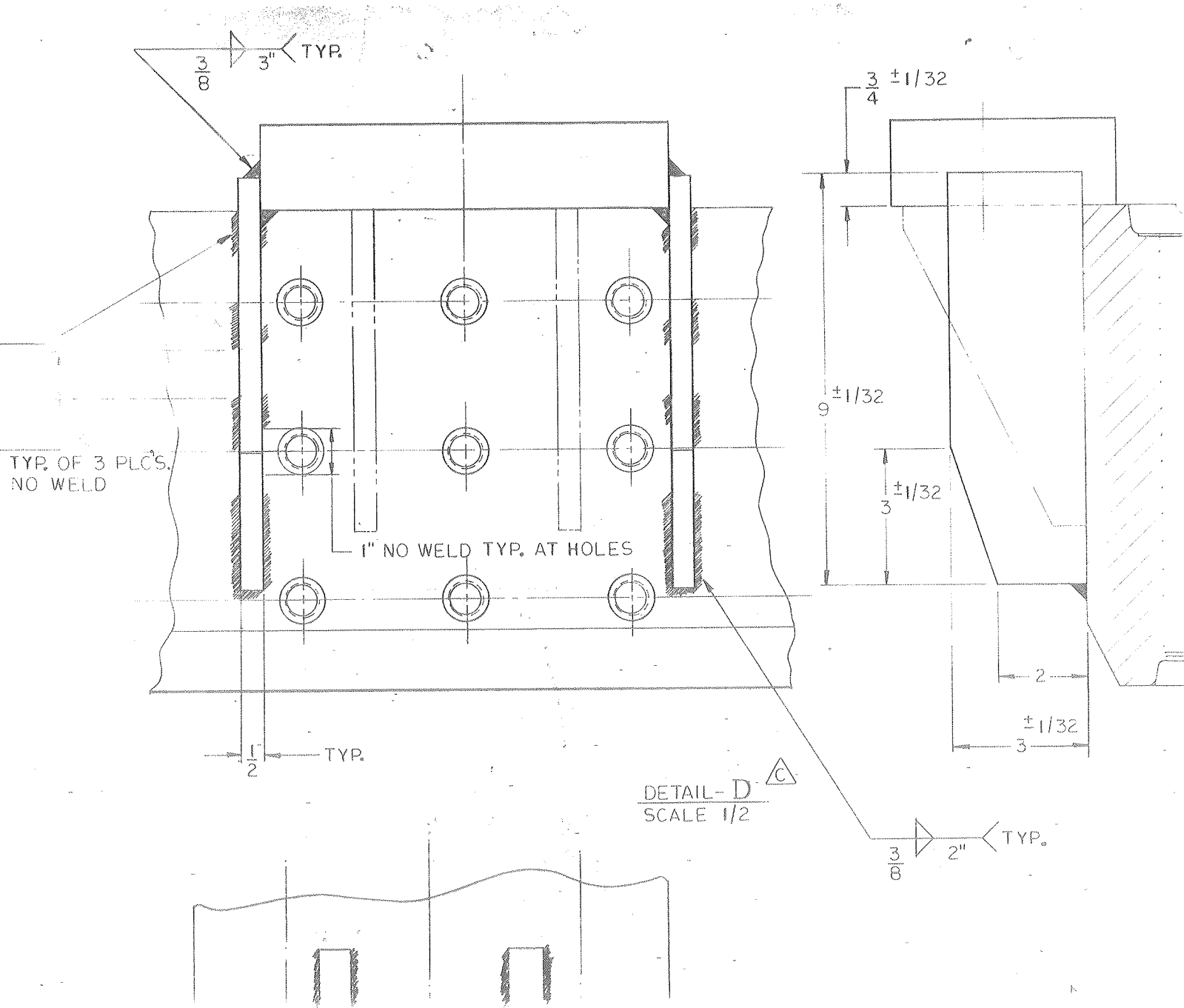


Fig. 5. Axial Support Bracket

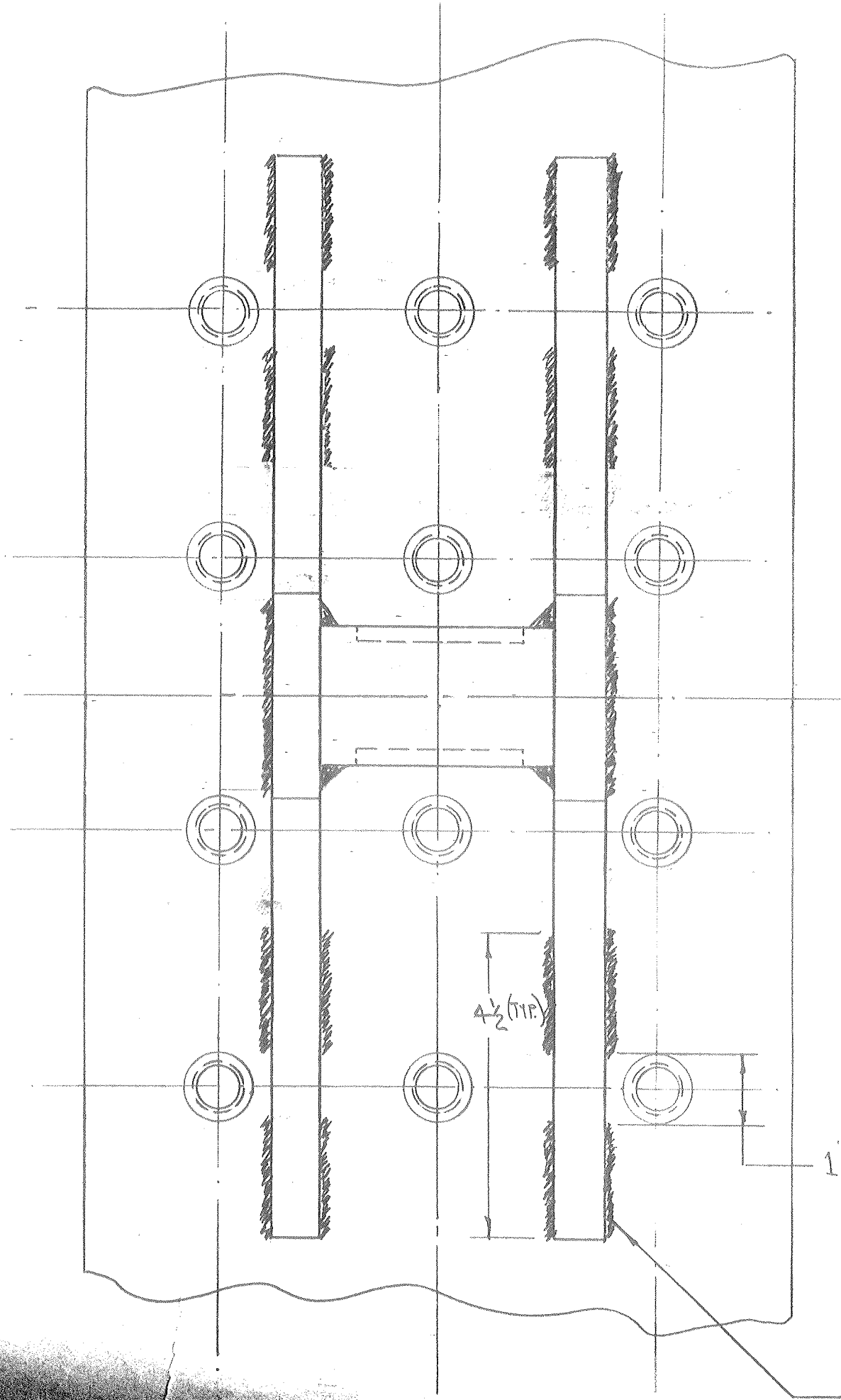


Fig. 8. Horizontal Support Gussets

1" No WELD (TYP.)

$\frac{1}{2}$ $\frac{3}{4}$ TYP.

Tohoku Magnet Dimensions
(inches)

| | Nominal as Built | Used in Analysis |
|----------------------------------|---|-----------------------------------|
| Inner cryostat wall | 23.75 to 24.75 | --- |
| Outer cryostat wall | 34.5 to 36.188 | 34.50 to 36.07 |
| Outer wall thickness | 1.688 | 1.57 |
| Top & bottom plate thickness | .6875 | .675 |
| Inner push bar (60 per coil) | .375 t x 1.24 w | --- |
| Inner push bar G-10 insulator | .03 solid G-10 + .050 G-10 spacer | --- |
| Outer push bar (60 per coil) | .625 t x 1.24 w | --- |
| Outer push bar G-10 insulator | .03 solid G-10 + two .050 G-10 spacer = .130 | --- |
| Inner radius of first coil layer | 25.224 warm 25.14 (4.2 k) | 25.224 (ANSYS) 25.14 (TRIM 47) |
| Outer radius of last coil layer | 33.37 warm 33.27 (4.2 k) | 33.37 (ANSYS) 33.27 (TRIM 47) |
| Axial height of coil winding | 8.69 | 8.69 (ANSYS) 8.66 (TRIM 47) |
| Extent of inner screw | ~.019 | .019 |
| Extent of outer screw | ~.375 + .050 preload | .375 |
| Inner screw | 5/8 UNC | --- |
| Outer screw | 3/4 UNC | --- |
| Numbr of conductor layers | 63 | --- |
| Total number of turns per coil | 2840 | --- |
| Turns per layer | 45.08 | --- |

| | |
|----------------------------|---|
| Wire size | ~.088" x .178" (I.G.C. spec) --- ~.091" x .183" (typical measured size) |
| Turn to turn insulation | .006 --- |

Assume the conductor is ~ .089" x .178"

Radial thickness of conductor package = $33.37 - 25.224 = 8.146"$

Thickness of each wire G-10 layer = $\frac{8.146}{63} = .129"$

Then G-10 average thickness ~ .0403

--- means same as nominal dimension

Material Properties

Thermal Contraction $\Delta L/L$ (300 K to 4.2 K)

| | |
|--------------------------------------|---|
| Stainless steel | .003 |
| Conductor, hoop direction | .0032 |
| G-10 CR (normal direction) | .0075 |
| Conductor, normal or radial | .0033 |
| Conductor/G-10 composite (radial) | $\frac{.040}{.129} \times .0075 + \frac{.089}{.129} \times .0032 = .0045$ |
| Coil (axial) | .0032 (assumed) |
| Inner push bar (radial) | $\frac{.08 \times .0075 + .375 \times .003}{.455} = .00379^*$ |
| Outer push bar (radial) | $\frac{.130 \times .0075 + .625 \times .003}{.755} = .00378^*$ |

For push bars axial and hoop thermal contractions are assumed to be the same as the radial thermal contractions.

Young's Modulus (psi)

| | |
|---------------------|---|
| 304 stainless steel | 30×10^6 |
| G-10 (normal) | 4×10^6 at 300 K 5.2×10^6 at 4.2 K |
| Conductor (hoop) | 8.2×10^6 at 300 K 12.5×10^6 at 4.2 K |

(based on an area of $.091 \times .183 = .0167 \text{ in}^2$)

Coil package modulus (hoop):

$$E_{\text{parallel}} A_{\text{total}} = \sum E_i A_i$$

for the coil package hoop direction, $E_{\text{G-10}} = 0$

.asis

$$E_{\text{hoop coil}} = \frac{E_{\text{conductor}} A_{\text{conductor}}}{A_{\text{total}}} = \frac{E_c \times .0167 \times 2840}{(33.37-25.224) \times 8.69}$$

$$E_{\text{hoop coil}} = 5.5 \times 10^6 \text{ at } 300 \text{ K} \quad 8.38 \times 10^6 \text{ at } 4.2 \text{ K}$$

Coil package modulus (radial):

| | | |
|--------------------------------|-------------------|----------------|
| Alternating stack of conductor | 3.7×10^5 | unheated 300 K |
| and .050" thick G-10 without | 1.2×10^6 | baked 300 K |
| B-staged epoxy | | |

Since the coil was baked 4 times during winding and the spacers were coated with B-staged epoxy, the upper value of radial modulus is assumed for all load cases. Furthermore, it is anticipated that a test at 4.2 K would yield higher modulus values. Thus the following value is reasonable.

Each of the 60 G-10 spacers has a 3/4" width in contact with the wire.

$$\text{Avg. radial modulus} = E_{\text{G-10/wire}} \times \frac{\text{Contact Area}}{\text{Total Area}} = E \times \frac{60 \times .75}{2 \pi r}$$

| | | |
|--------------------------------|---|------|
| First layer contact area ratio | = | .284 |
| Last layer contact area ratio | = | .215 |
| Average contact area ratio | = | .249 |

$$E_{r \text{ coil}} = E_{r \text{ wire/G-10}} \times .249$$

$$E_{r \text{ coil}} = 3.0 \times 10^5 \text{ *}$$

$$E_{\text{axial coil}} = 1 \times 10^6 \text{ * assumed value; little effect on calculation}$$

Inner and outer push bar modulus (radial):

There are 60 inner and outer preload push bars which are composed of G-10 bonded to stainless steel.

For materials in series,

$$\frac{1}{A E_{\text{composite}}} = \frac{1}{L_{\text{total}}} \sum_i \frac{L_i}{A_i E_i}$$

$$\text{Area of stainless steel per bar} = 1.25 \times 9.15 = 11.44$$

$$\text{Area of G-10 per bar} = .75 \times 9.15 = 6.863$$

Let $A = A_{s.s.} = 1$, then $A_{G-10} = \frac{6.863}{11.44} = .60$

$$\frac{1}{E_{\text{composite}}} = \left[\frac{1}{.455} \frac{.375}{3 \times 10^7} + \frac{.08}{.6 \times 4 \times 10^6} \right]$$

$$E_{\text{composite}} = 9.9 \times 10^6$$

But in the axisymmetric ANSYS calculation, the modulus must be reduced by the fraction of perimeter the push bar occupies. For the inner push bar the effective radial modulus is given by

$$E_{r_e} = \frac{9.9 \times 10^6 \times 1.25 \times 60}{2 \pi \times 25.228} = 4.7 \times 10^6*$$

Similarly for the outer push bar;

$$E_{r_e} = \frac{1}{.755} \frac{.625}{3 \times 10^7} + \frac{.13}{.6 \times 4 \times 10^6} \times \frac{1.25 \times 60}{2 \pi \times 33.37} = 3.6 \times 10^6*$$

Inner and outer push modulus (axial):

The preload push bars are composed of G-10 epoxied to stainless steel. In calculating the axial or bending stiffness, the G-10 is assumed to have a modulus of zero. The bars are modeled as a single material with a reduced modulus which will give the same deflection as the stainless steel alone.

$$y \propto \frac{1}{EI} \propto \frac{1}{wt^3}$$

$$\text{For the inner bar, } \frac{I}{I_0} = [.375 / (.375 + .08)]^3$$

$$\text{For the outer bar, } \frac{I}{I_0} = [.625 / (.625 + .130)]^3$$

where I/I_0 is the ratio of the bending moment of inertia of stainless steel bar to the bending moment of inertia of the composite stainless steel/G-10 bar. Naturally the value of E must be further reduced to reflect the azimuthal discontinuity of the bars.

$$\text{For the inner bar, } E_y = \frac{3 \times 10^7 \times 60 \times 1.25/}{2 \pi \times 25.228} \times .560 = 7.95 \times 10^6*$$

$$\text{For the outer bar, } E_y = \frac{3 \times 10^7 \times 60 \times 1.25/}{2 \pi \times 33.37} \times .567 = 6.09 \times 10^6*$$

The hoop modulus, E_y , is given the small value of 1000* for both bars.

Inner and outer preload screws:

$$E_x = E_y = E_z = \frac{3 \times 10^7*}{50*} \quad \begin{array}{l} \text{when in contact} \\ \text{when not in contact or} \\ \text{when applying preload} \end{array}$$

Preload is applied in the ANSYS model by two forces acting in opposite directions at each end of the spar elements (screws). A very small modulus is required to ensure that all preload forces end up in the conductor and cryostat as opposed to a tensile force in the spar elements. Also a small modulus is required when the outer screw is not in physical contact during winding and inner preloading. Actually E_z (hoop) should always have a small modulus since the screws are discontinuous, but the area of the screws are small so the effect can be neglected.

Area for the 2D spars (preload screws) must be input on a per radian basis. The screws are assumed to have an effective area equal to their major diameter area.

For the inner screw

$$\text{Area} = \frac{60 \times .307}{2 \pi} = 2.93 \frac{\text{in}^2*}{\text{rad}}$$

For the other screw

$$\text{Area} = \frac{60 \times .442}{2 \pi} = 4.22 \frac{\text{in}^2*}{\text{rad}}$$

By mistake values of 5.12 in^2/rad and 6.23 in^2/rad were used. This changes answers by less than 1/3%.

Modulus of 2D spars axially connecting to push bars and cryostat:

Each preload bar has two spar elements connecting it to the cryostat. These spars have an area of 1 in^2/rod and essentially zero stiffness for all loads except for the axial electromagnetic load case. A value of $E = 1 \times 10^6$ was

chosen arbitrarily to simulate the partial transference of axial loads in shear through the coil to the push bars which then bear against the cryostat.

Cryostat outer wall and axial support bracket moduli:

Eight axial support brackets are welded to the outer wall of the cryostat. During winding both bracket and outer wall were given essential zero stiffness or modulus. This enables one to include these two items as part of the complete model without having to assign them any significant stress when they were not physically attached during the winding process. This feature is important when load cases are added together.

Each outer bracket is composed of four 1/2" thick gussets and a top plate welded to the outer wall. Thus we obtain,

$$E_x \text{ (radial)} = E_y \text{ (axial)} = \frac{(4 \times 1/2) \times 8}{2 \pi \times 36.07} \times 3 \times 10^7 = 2.1 \times 10^6*$$

$$E_z = 1000$$

Both inner and outer walls were given a modulus of 3×10^7 with the exception of the outer wall during winding. No reduction in modulus was used to simulate the reduced stiffness of these walls due to the threaded preload screw holes. Simple estimates give a modulus ~7% lower. This will have no noticeable effect on the solution because the modulus of the coil is so much lower in comparison.

Loads:

There are 6 different load cases to consider as follows:

1. Winding loads
2. Preloading of inner radius of cryostat/coil
3. Preloading of outer radius of cryostat/coil
4. Thermal stresses from cooldown
5. Radial electromagnetic loads
6. Axial electromagnetic loads

Winding loads are by far the most difficult to analyze. Warren Young's computer program and physical measurements of the coil are the basis for the estimated stress distribution in the coil and the radial pressure on the bobbin accumulated during winding. Even though the final radial pressure from winding

is a rough estimate, the sum of inner preload and winding is known very accurately by actual torque loadings of the screws.

| Load case | Pressure (psi) | Radius of applied load | Load on a single screw (lbs) | Load on one row of 60 screws (lbs/radian) |
|---------------|----------------|------------------------|------------------------------|---|
| Winding | 230 | 24.75" | 1730 | 1.65×10^4 |
| Inner preload | 740 | 24.75" | 5560 | 5.31×10^4 |
| Outer preload | 400 | 34.5" | 4190 | 4.00×10^4 |

Cooldown stresses are obtained by using the appropriate values of thermal contraction for each material. Radial and axial electromagnetic loads are taken from my TRIM/FORGY run #47.

The axisymmetric ANSYS analysis was modeled to represent the specific columns in FORGY. Note for example that the inner and outer columns of the coil in the ANSYS model are only 1/2 as thick as the rest of the columns. Listed below are the specified radial pressures used as input to the axisymmetric ANSYS analysis. See the section on simplified analytic analysis for conversion from tension given by FORGY to radial pressure. Positive pressure is radially outward.

Radial Pressure Distribution

| Column # | Radius (inches) | Tension (Newtons) | Pressure input to ANSYS (psi) |
|----------|-----------------|---------------------|-------------------------------|
| 21 | 25.14 | 1.643×10^5 | 169 |
| 22 | 25.62 | 3.491 | 353 |
| 23 | 26.10 | 3.420 | 345 |
| 24 | 26.57 | 3.224 | 320 |
| 25 | 27.05 | 3.007 | 288 |
| 26 | 27.53 | 2.781 | 261 |
| 27 | 28.01 | 2.546 | 235 |
| 28 | 28.49 | 2.302 | 209 |
| 29 | 28.97 | 2.048 | 183 |
| 30 | 29.44 | 1.780 | 156 |
| 31 | 29.92 | 1.497 | 129 |

| | | | |
|----|-------|---------------------------|-------|
| 32 | 30.40 | 1.196 | 102 |
| 33 | 30.88 | 8.734×10^4 | 73.2 |
| 34 | 31.36 | 5.26 | 43.4 |
| 35 | 31.84 | 1.47×10^4 | 11.9 |
| 36 | 32.31 | -2.69×10^4 | -21.5 |
| 37 | 32.79 | -6.97 | -55.0 |
| 38 | 33.27 | -4.59×10^4 | -35.7 |
| | | Total 29.06×10^5 | |

The distribution of axial loads through the coil pack to the cryostat is difficult to predict because of highly variable material properties in the axial direction. Three mechanisms exist for the transfer of this axial force. Each layer of conductor was tightly packed with wedges. It is expected that most of the axial force is transmitted directly through the turns to the cryostat. Layer to layer G-10 spacers are not expected to transmit much of the load since their fit to the cryostat was loose. The inner and outer preload bars have a close fit ($\sim .025''$) with the cryostat and are expected to transmit at least some of the axial load carried in shear through the coil. In any event the axial loads are distributed as pressures to the top and bottom cryostat plates. "Weak" spar elements are attached between top and bottom of preload bars and cryostat to simulate the partial shear load transfer to these bars.

Since the 2D program TRIM was used on our 3D problem, the actual magnitude of the axial force is not assumed to be accurately known. An arbitrary uncertainty of 1" axial misplacement was chosen as a conservative upper bound on the axial load. This is equivalent to an extra 200,000 lbs. Total loads are listed below.

| | F_z (TRIM) | F_z (worse case) |
|----------------------------------|------------------------|------------------------|
| TRIM 47 muon notches filled | 2.05×10^5 lbs | 4.22×10^5 lbs |
| TRIM 41 muon notches unfilled | 2.38×10^5 lbs | 4.38×10^5 lbs |

The actual total load used in the axisymmetric ANSYS analysis was 462,000 lbs.

Axial Pressure Distribution

| Column # | Radius (inches) | F_z (Newtons) | Psi | Psi for 462,000 lbs |
|----------|--------------------|---------------------|-------|------------------------|
| 21 | 25.14 | -2.05×10^4 | -122 | -275 |
| 22 | 25.618 | -3.43 | -100 | -226 |
| 23 | 26.10 | -2.40 | -68.8 | -155 |
| 24 | 26.57 | -1.20×10^4 | -33.8 | -76.1 |
| 25 | 27.05 | $+3.6 \times 10^2$ | +1.0 | 2.3 |
| 26 | 27.53 | 1.28×10^4 | +34.8 | 78.4 |
| 27 | 28.01 | 2.52 | 67.3 | 152 |
| 28 | 28.49 | 3.76 | 98.8 | 223 |
| 29 | 28.97 | 4.98 | 129 | 290 |
| 30 | 29.44 | 6.19 | 157 | 355 |
| 31 | 29.92 | 7.38 | 185 | 416 |
| 32 | 30.40 | 8.54 | 210 | 474 |
| 33 | 30.88 | 9.67 | 234 | 528 |
| 34 | 31.36 | 10.77 | 257 | 579 |
| 35 | 31.84 | 11.86 | 279 | 628 |
| 36 | 32.31 | 12.92 | 299 | 674 |
| 37 | 32.79 | 13.71 | 313 | 705 |
| 38 | 33.27 | 6.70 | 302 | 679 |

$$\text{Pressure} = \frac{F_z (\text{FORGY}) \times .2248 \text{ lbs/N}}{2 \pi r \Delta r}$$

where Δr is the column radial thickness = .478". Positive pressures are applied on the lower cryostat plate and negative pressures are applied on the upper cryostat plate. Figure 9 is a plot of this pressure distribution assuming each column of conductors is independent.

W. Crockett

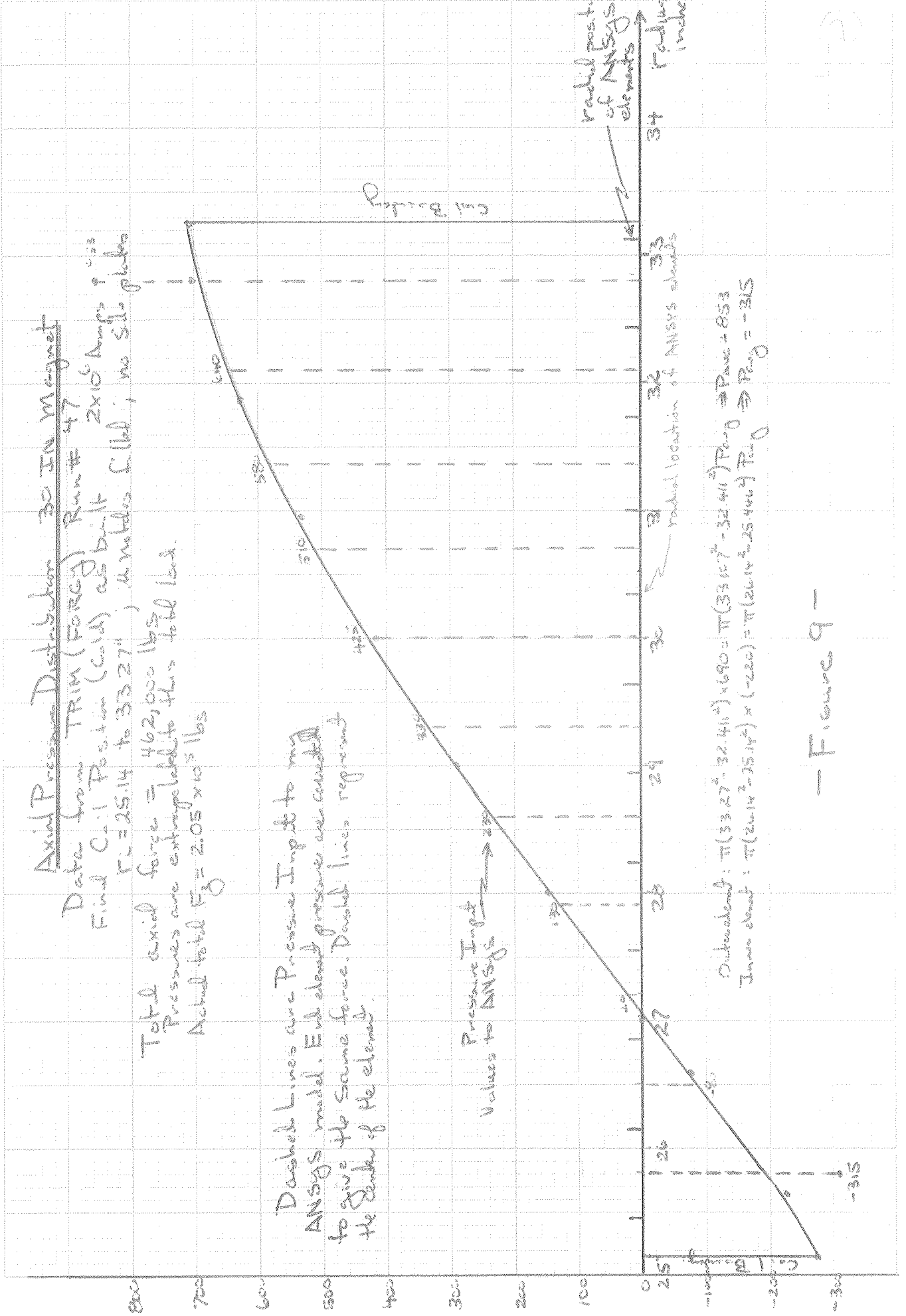
Axial Pressure Distribution 30 IN Magnet

Data from TRIM (FORC) Run # 47
 Final Coil Position (Cold) as built 2×10^6 Amps @ 115
 $r_c = 25.14$ to 33.27 , 4 needles (1.6d); no side plates

Total axial force = $462,000$ lbs
 Pressures are extrapolated to this total load.
 Actual total $F_0 = 2.05 \times 10^5$ lbs

Dashed lines are Pressure Input to my ANSYS model. End element pressure are corrected to give the same force. Dashed lines represent the center of the element

Pressure Input Values to ANSYS \rightarrow



Outer element: $\pi(33.27^2 - 32.41^2) \times 690 = \pi(33.10^2 - 32.41^2) P_{avg} \Rightarrow P_{avg} = 853$
 Inner element: $\pi(26.14^2 - 25.14^2) \times (-220) = \pi(26.14^2 - 25.44^2) P_{avg} \Rightarrow P_{avg} = -315$

- Figure 9 -

SIMPLE ANALYTIC ANALYSIS

This coil is much too complex to analyze accurately with an analytic approach. It is worth while, however, to make some initial hand calculations for a worse case analysis.

Self Supported Turns:

The hoop stress is calculated for the inner layer which has no radial constraint from the cryostat or the outer layers of the coil.

$$F_{\text{hoop}} = B I R$$

where F is in Newtons, B_z is the axial field component in Tesla, and R is in meters. From Trim 47, $B_{z\text{max}}$ for the inner layer is 5.42 T at 2×10^6 amp-turns per coil (704 amps/turn).

$$F = 5.42 \times 704 \times \frac{25.14}{39.37} \times .2248 \frac{\text{lb}}{\text{N}} = 547 \text{ lbs}$$

$$= 32,800 \text{ psi based on a } .0167 \text{ in}^2 \text{ cross section}$$

From wire tests at 300K and 4.2K the coil should be self supporting. This, of course, neglects any tension from winding. The cable breaks at 640 lbs. at room temperature and 780 lbs. at 4.2K.

Magnetic Pressure Approximation

FORGY output from TRIM only gives hoop tension. Radial forces from run #47 are calculated treating each column as a thin wall cylinder. The summation of these forces are applied to the ID of the coil which is treated as an isotropic thick walled cylinder with internal pressure and no reinforcement.

$$P_r = \frac{\sigma_{\theta} t}{r} \quad \text{thin wall formula}$$

Then the total radial force on the cylinder or a specific column used in TRIM is given by

$$F_r = 2\pi r h P_r = 2\pi (\sigma_{\theta} t h) = 2\pi T$$

where

$$P_r = \text{radial pressure}$$

$$h = \text{cylinder length or column height in TRIM}$$

$$r = \text{radius}$$

σ_{θ} = hoop stress

t = cylinder thickness or mesh thickness

T = total hoop tension

Thus the total radial force on all columns is given by

$$F_{r\text{total}} = 2\pi \Sigma T$$

where T is the tension given for each column of the FORGY output.

If this total radial force were applied at one specific radius r, the equivalent pressure at that radius is then

$$P_r(r) = \frac{F_{r\text{ total}}}{2\pi r h} = \frac{\Sigma T}{rh}$$

From FORGY output of run #47 the total tension is 2.91×10^6 N. The equivalent radial pressure on the inner layer would then be

$$P_r(r=25.22) = \frac{2.91 \times 10^6 \times .2248 \text{ lbs/N}}{25.22 \times 8.66}$$

$$P_r = \sigma_{r\text{max}} = 2995 \text{ psi}$$

By comparison the actual magnetic pressure on the inner layer is

$$5.42^2 \times 57 \frac{\text{psi}}{\text{Telsa}^2} = 1675 \text{ psi}$$

The peak hoop stress for a thick walled cylinder under internal pressure is on the inside

$$\sigma_{\theta\text{max}} = \frac{P_i r_i^2 + r_o^2}{r_o^2 - r_i^2} = 10970 \text{ psi}$$

The hoop stress is an average stress based on the full cross sectional area of the coil. The G-10 spacers can carry no hoop load, however. Thus

$$\sigma_{\theta\text{conductor max}} = 10970 \frac{.089 + .040}{.089} = 15,900 \text{ psi}$$

This value is reasonable when compared to the computer calculated values in the following sections.

Linear Distribution of Body Forces:

An extension of the results from Westendorp and Kilb² are used to analyze an isotropic cylinder with reinforcement and distributed body forces. From this paper

$$\Delta r = \frac{1-\nu^2}{E} \left[\frac{C_1 r}{1+\nu} + \frac{C_2}{(1-\nu)r} - \frac{\alpha r^2}{3} + \frac{\beta r^3}{8} \right]$$

$$\sigma_\theta = C_1 + \frac{C_2}{r^2} - \alpha \frac{(1+2\nu)r}{3} + \frac{\nu(1+3\nu)r^2}{8}$$

$$\sigma_r = C_1 - \frac{C_2}{r^2} - \frac{\alpha(2+\nu)r}{3} + \frac{\beta(3+\nu)r^2}{8}$$

$$\alpha = J_\theta \frac{(B_i r_o - B_o r_i)}{r_o - r_i} = 1.5 \times 10^9 \text{ A-T/m}^2$$

$$\beta = J_\theta \frac{(B_i - B_o)}{r_o - r_i} = 1.42 \times 10^9 \text{ A-T/m}^2$$

From TRIM #47

| | | | | |
|-------|-------|----------|----------|--|
| R_i | R_o | B_{zi} | B_{zo} | J_θ |
| .639m | .845m | 5.42T | -1.24T | $2.84 \times 10^4 \text{ A/in}^2 = 4.40 \times 10^7 \text{ A/m}^2$ |

and the body force is of the form $\alpha - \beta r$. A 1.56" thick outer stainless steel ring was chosen. The coefficients C_1 and C_2 for both the coil and the outer band must be solved from the following boundary conditions:

$$\sigma_r = 0 \text{ at } r = r_i \text{ and } r = r_x \text{ the outside of the band}$$

$$\Delta r_{\text{coil}} = \Delta r_{\text{band}} \text{ at } r = r_o$$

$$\sigma_{r\text{coil}} = \sigma_{r\text{band}} \text{ at } r = r_o$$

Alternatively Westendorp and Kilb's results for a free coil can be combined with stresses obtained from a shrink fit of the outer band.

An effective coil modulus of 8.38×10^6 psi was selected. This represents the reduction in E_0 due to the spacers. Again hoop stress needs to be multiplied by the factor $(.089 + .04)/.089 = 1.45$ to obtain the actual conductor stress.

Stress & Displacement Values

| | σ_{θ} (coil) | σ_{θ} (wire) | σ_{θ} (band) | σ_r (coil) | Δr |
|-----------|--------------------------|--------------------------|--------------------------|-------------------|------------|
| $r = r_i$ | 7840 | 11400 | --- | 0 | .024 |
| $r = r_o$ | 5000 | -7250 | 18,400 | -860 | .020 |

Axial forces are considered next. The effect of axial force on the coil package can only be estimated with simplified hand calculations. Axial forces can be carried to the cryostat shell by direct turn to turn loading of the conductor, by a transmission of axial force to the layer to layer spacers, and by a shear force carried through the coil to the inner and outer preload bars. The peak pressure of 710 psi at the cryostat boundary is found in the last layer. This is an average pressure with the area of the spacers included. Assuming direct turn to turn loading, the maximum conductor pressure must be multiplied by $(.089 + .04)/.089$ to give 1030 psi. Actually the peak conductor bearing pressure is found almost exactly in the center of the coil. Using TRIM 47 extrapolating to 500,000 lbs., and taking into account the spacer effect, the maximum axial conductor bearing pressure is found to be

$$\sigma_{\max} = 1050 \times \frac{5 \times 10^5}{2.05 \times 10^5} \times 1.45 = 3700 \text{ psi}$$

This greater turn to turn bearing pressure is a result of the pinch force in the coil. If the 500,000 lb. axial force is considered to be transmitted in shear to the outer push bars, the shear stress on the outer G-10 strips is calculated to be 1300 psi. Both the maximum shear stress and the maximum bearing pressure are considered acceptable.

AXISYMMETRIC COIL/CRYOSTAT ANSYS ANALYSIS

Three different axisymmetric ANSYS models have been created. The first two are simple half model runs analyzing only the radial pressure distribution. They were created to check the validity of using only one element through the cryostat wall in the 3D ANSYS run. The course model cryostat elements were chosen to be very similar to Computerized Engineering 3D element size. All three models use the axisymmetric option of the STIF 42 (2D isoparametric stress solid) and STIF 1 (2D spar) elements. Spar elements model the preload screws and the partial contact between preload bars and cryostat annular plates. Spar elements were chosen to eliminate any bending moments. Figures 10 to 12 are the course half model and Figures 13 to 15 are the refined half model. Figures 38 to 40 in the next section are the results of radial electromagnetic loads on the full axisymmetric model.

Table 1 is a comparison summary of these three radial load cases. The course model underestimates cryostat peak bending stresses by roughly 30%, peak hoop stresses by 9%, and peak Von Mises stresses and stress intensities by only 4%. Loads in the outer screws are 14% greater for the full model than either of the other two half models, while loads on the inner screws are within 3% for all three cases. Peak cryostat stresses are up to 6% lower, and peak coil stresses are up to 9% lower in the full model than the refined half model. As expected, the outer support bracket stiffens the outer wall forcing it to carry a greater fraction of the total load. This reduces stress levels in the coil and stress levels in the inner wall where the peak stresses are located. Maximum displacements at the center of the inner wall are very close for all three cases.

Comparison of Radial Electromagnetic
Loads for Three Different Axisymmetric
Models

Table 1

| Nodal Cryostat Stresses | Course 1/2 Model | Refined 1/2 Model | Full Model |
|--------------------------------------|---------------------|----------------------|------------|
| S_z min | 5039 | 4919 | ----- |
| max | 23664 | 25852 | 25398 |
| S_x min | -10,041 | -13230 | -12745 |
| max | 6806 | 8895 | 8852 |
| S_y min | -12,316 | -14550 | -13682 |
| max | 11726 | 14937 | 14065 |
| S_{sig} min | 5503 | 5511 | ----- |
| max | 25728 | 26736 | 26082 |
| S.I. min | 5705 | 5552 | ----- |
| max | 29691 | 30872 | 30111 |
| ----- | | | |
| Nodal Average Coil Stresses | | | |
| S_z max | 6391 | 6414 | 6029 |
| S_x max | 2124 | 2114 | 1944 |
| ----- | | | |
| Force Preload Screws (lbs/radian) | | | |
| Inner center | 67160 | 66820 | 65130 |
| Inner top/bottom | 88160 | 87750 | 87300 |
| Outer center | -38980 | -38880 | -44230 |
| Outer top/bottom | -35540 | -35790 | -40890 |
| ----- | | | |
| U_x (middle of inner wall) | .0161 | .0162 | .0161 |

z = hoop
x = radial
y = axial
SIGE = Von Mises stress
S.I. = stress intensity
----- = not a meaningful comparison as minimum stress exists in
outer support bracket

Coil stress are averaged over the whole coil and are not conductor stresses.

ANSYS
84/ 5/25
11.4444
PLOT NO. 3
POST1
STEP=1
ITER=1
DISPLACEMENT

ORIG SCALING
ZV=1
DIST=6.78
XF=29.9
YF=2.63
DMAX=.0192
DSCA=35.2

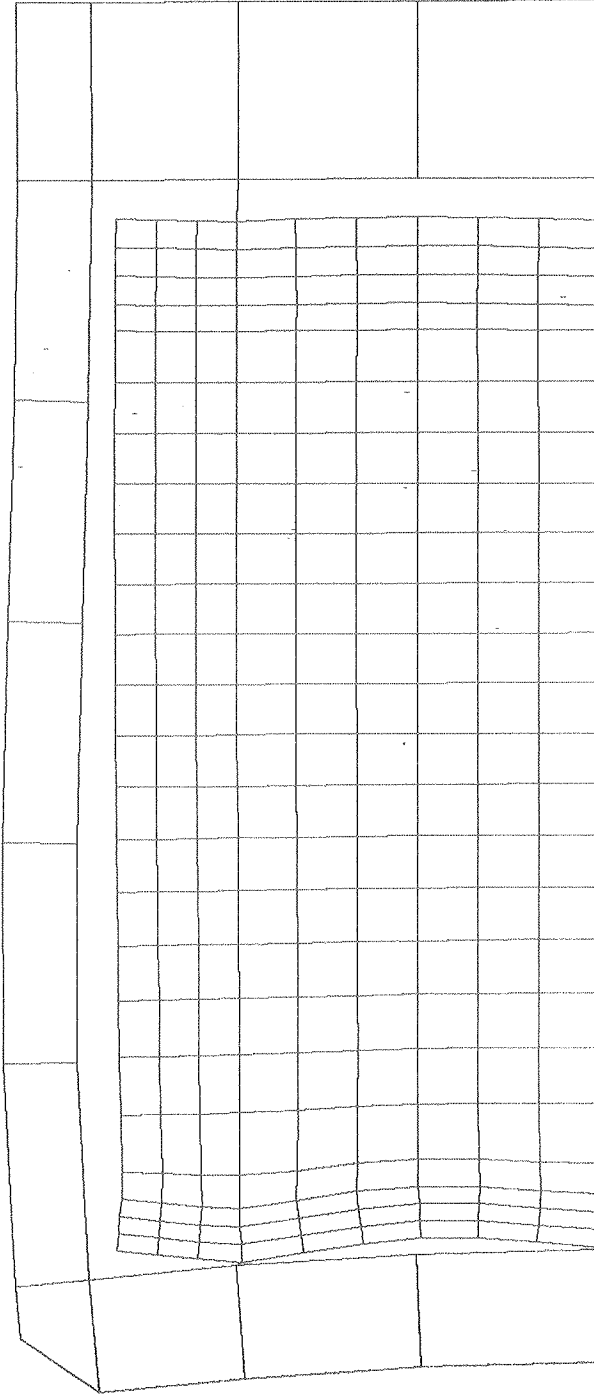


Fig. 10. Course 1/2 Axiymmetric Model

ANSYS
84/ 5/25
11.6100
PLOT NO. 6
POST1
STEP=1
ITER=1
STRESS PLOT
SIDE
ORIG SCALING
ZV=1
DIST=6.78
XF=29.9
YF=2.63
EDGE
DMAX=.0161
MX=25728
MN=5503
INC=1250

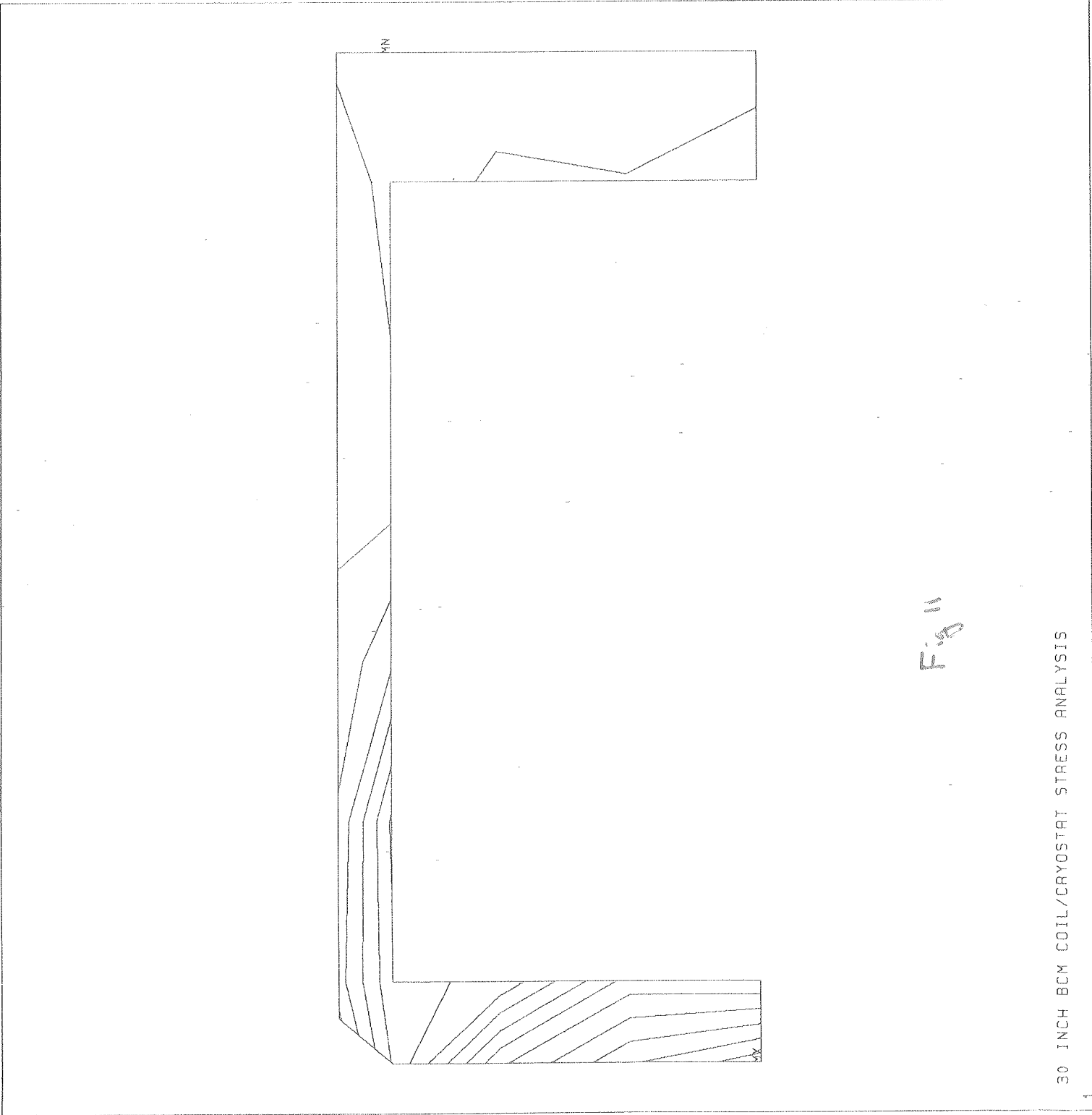


FIG 11

ANSYS

84/ 5/25

11.6100

PLOT NO. 4

POST1

STEP=1

ITER=1

STRESS PLOT

SY

ORIG SCALING

ZV=1

DIST=6.78

XF=29.9

YF=2.63

EDGE

DMAX=.0161

MX=11726

MN=-12316

INC=2000

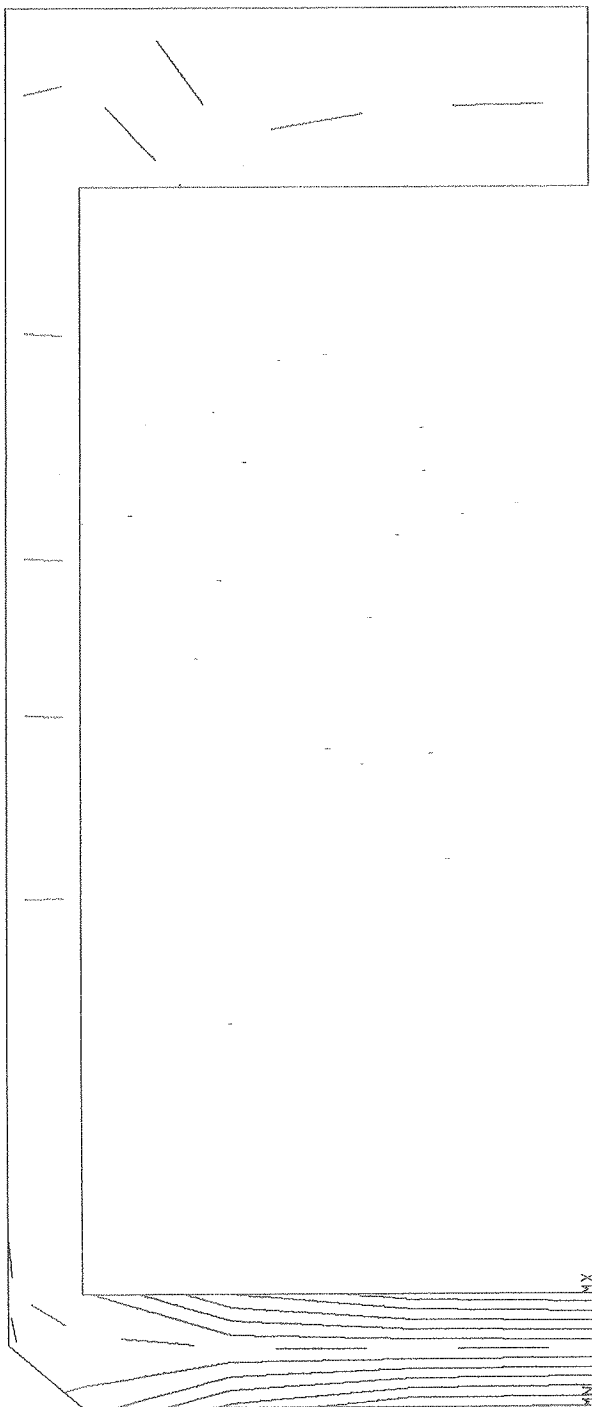


Fig 12

30 INCH BCM COIL/CRYOSTAT STRESS ANALYSIS

ANSYS
84/ 3/22
18.5936
PLOT NO. 3
POST1
STEP=1
ITER=1
DISPLACEMENT
ORIG SCALING
ZV=1
DIST=6.78
XF=29.9
YF=2.63
DMAX=.0193
DSCA=35.1

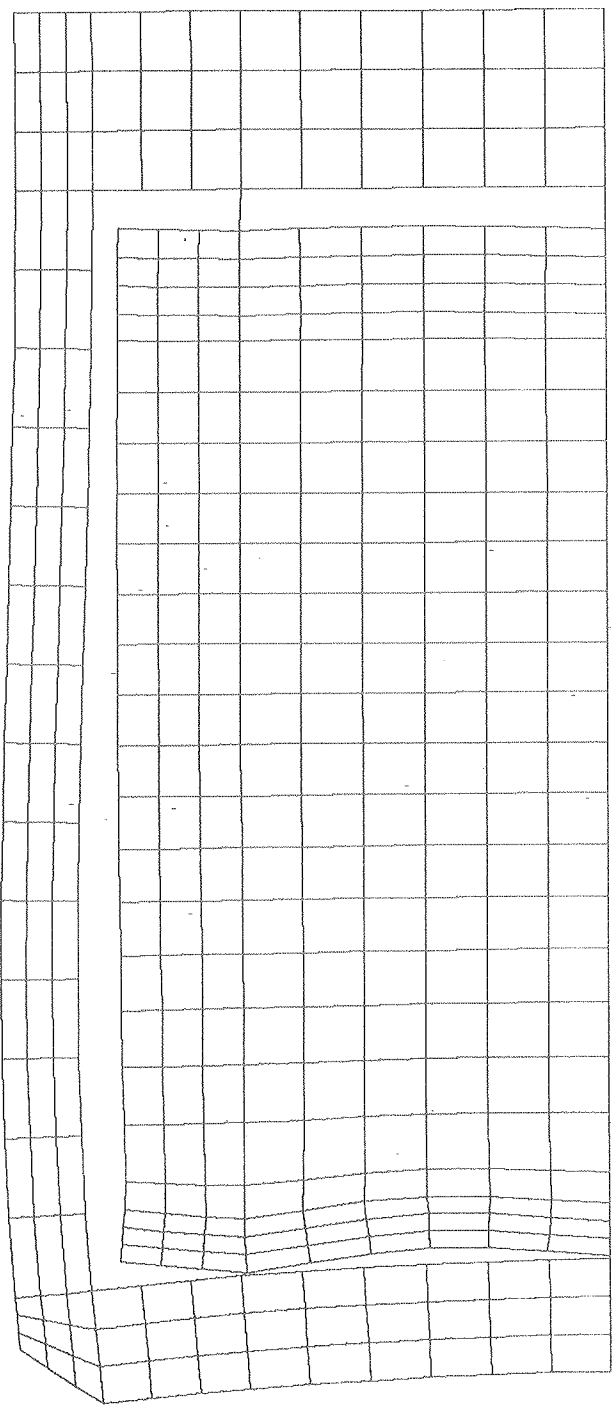


Fig. 13. Refined 1/2 Axisymmetric Model

ANSYS
84/ 4/ 4
14.4083
PLOT NO. 6
POST1
STEP=1
ITER=1
STRESS PLOT
SIGE
ORIG SCALING
ZV=1
DIST=6.78
XF=29.9
YF=2.63
EDGE
DMAX=.0162
MX=26736
MN=5511
INC=1250



Fig 14

ANSYS
84/ 4/ 4
14.4075
PLOT NO. 4
POST1
STEP=1
ITER=1
STRESS PLOT
SY

ORIG SCALING
ZV=1
DIST=6.78
XF=29.9
YF=2.63
EDGE
DMAX=.0162
MX=14937
MN=-14550
INC=2000

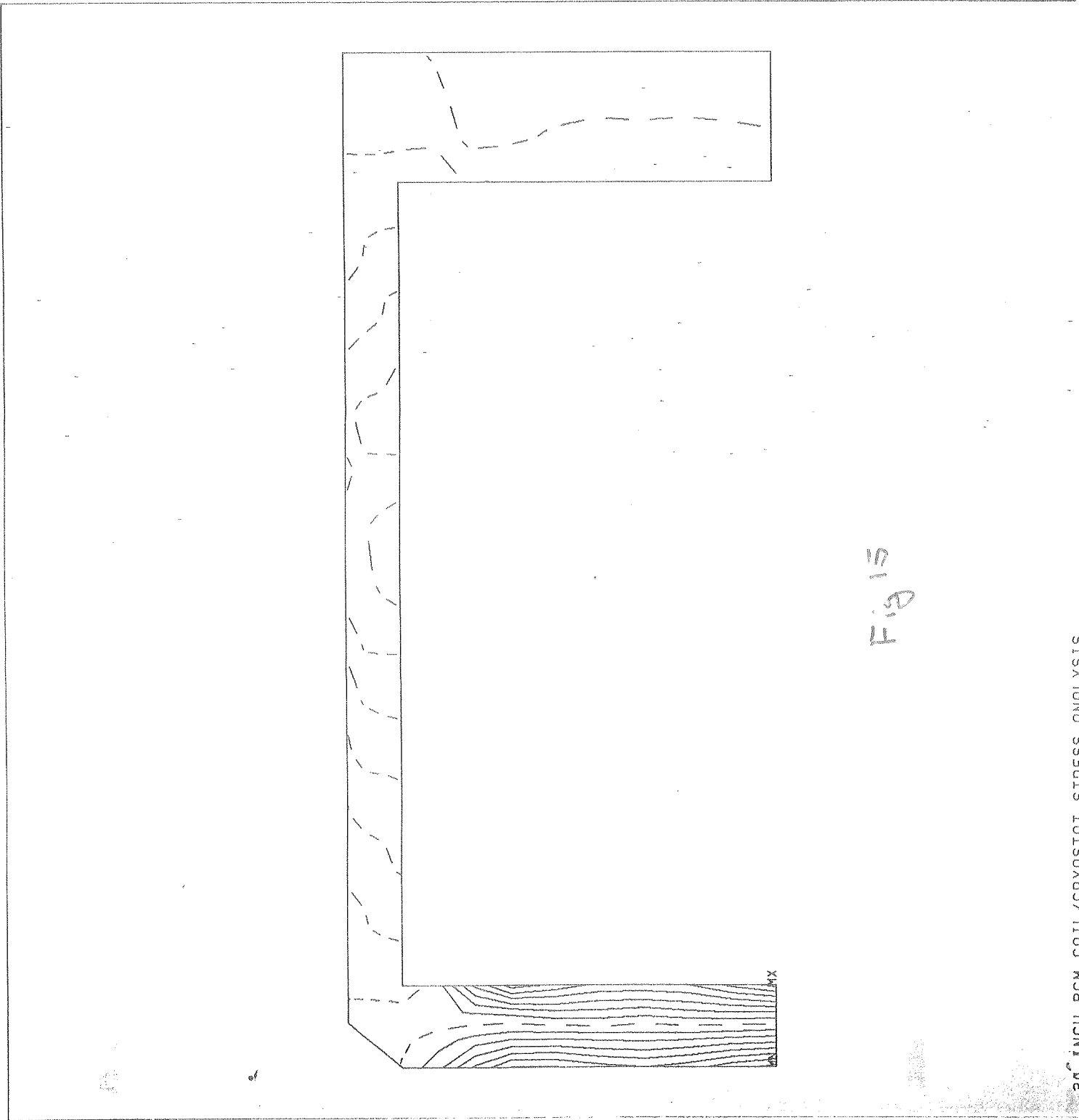


Fig 15

All six load cases are analyzed in the full axisymmetric model. In addition, winding and preloading cases are combined which is the state of the magnet at room temperature. Next all load cases are combined. This is the case of the magnet under full load. Lastly all load cases with the exception of the winding, load are combined for the conductor portion alone. Winding stresses for the conductor must be estimated by other means and added in separately. Table 2 is a summary of the peak stresses found in both the coil and cryostat. Figures 16 to 52 are the model, distortions, and stresses. Note the excessive displacements in some of the plots. This is caused by the very low stiffness assigned to the spar elements during preloading. Coil and cryostat never touch as is shown in some of the plots. Figures 53 to 57 are the stress distributions in the inner push bar after winding and preloading at room temperatures. This is the worse case for either inner or outer bars. Figures 56 to 58 are enlargements of the axial support bracket under combined loading. Figures 65 to 76 are stress plots of the coil.

ANSYS
 84/ 3/22
 17.6461
 PLOT NO. 2
 PREP7 ELEMENTS
 ENUM=1
 TDBC=1
 ORIG SCALING
 ZV=1
 DIST=8.94
 XF=31.9
 YF=.5

| | | | | |
|-----|-----|-----|-----|-----|
| 423 | 424 | 425 | 426 | 427 |
| 418 | 419 | 420 | 421 | 422 |
| 413 | 414 | 415 | 416 | 417 |
| 408 | 409 | 410 | 411 | 412 |
| 403 | 404 | 405 | 406 | 407 |
| 398 | 399 | 400 | 401 | 402 |
| 393 | 394 | 395 | 396 | 397 |
| 388 | 389 | 390 | 391 | 392 |
| 383 | 384 | 385 | 386 | 387 |
| 378 | 379 | 380 | 381 | 382 |
| 373 | 374 | 375 | 376 | 377 |
| 368 | 369 | 370 | 371 | 372 |
| 363 | 364 | 365 | 366 | 367 |
| 358 | 359 | 360 | 361 | 362 |
| 353 | 354 | 355 | 356 | 357 |
| 348 | 349 | 350 | 351 | 352 |
| 343 | 344 | 345 | 346 | 347 |
| 338 | 339 | 340 | 341 | 342 |
| 333 | 334 | 335 | 336 | 337 |
| 328 | 329 | 330 | 331 | 332 |
| 323 | 324 | 325 | 326 | 327 |
| 318 | 319 | 320 | 321 | 322 |
| 313 | 314 | 315 | 316 | 317 |
| 308 | 309 | 310 | 311 | 312 |
| 303 | 304 | 305 | 306 | 307 |
| 298 | 299 | 300 | 301 | 302 |
| 293 | 294 | 295 | 296 | 297 |
| 288 | 289 | 290 | 291 | 292 |
| 283 | 284 | 285 | 286 | 287 |
| 278 | 279 | 280 | 281 | 282 |
| 273 | 274 | 275 | 276 | 277 |
| 268 | 269 | 270 | 271 | 272 |
| 263 | 264 | 265 | 266 | 267 |
| 258 | 259 | 260 | 261 | 262 |
| 253 | 254 | 255 | 256 | 257 |
| 248 | 249 | 250 | 251 | 252 |
| 243 | 244 | 245 | 246 | 247 |
| 238 | 239 | 240 | 241 | 242 |
| 233 | 234 | 235 | 236 | 237 |
| 228 | 229 | 230 | 231 | 232 |
| 223 | 224 | 225 | 226 | 227 |
| 218 | 219 | 220 | 221 | 222 |
| 213 | 214 | 215 | 216 | 217 |
| 208 | 209 | 210 | 211 | 212 |
| 203 | 204 | 205 | 206 | 207 |
| 198 | 199 | 200 | 201 | 202 |
| 193 | 194 | 195 | 196 | 197 |
| 188 | 189 | 190 | 191 | 192 |
| 183 | 184 | 185 | 186 | 187 |
| 178 | 179 | 180 | 181 | 182 |
| 173 | 174 | 175 | 176 | 177 |
| 168 | 169 | 170 | 171 | 172 |
| 163 | 164 | 165 | 166 | 167 |
| 158 | 159 | 160 | 161 | 162 |
| 153 | 154 | 155 | 156 | 157 |
| 148 | 149 | 150 | 151 | 152 |
| 143 | 144 | 145 | 146 | 147 |
| 138 | 139 | 140 | 141 | 142 |
| 133 | 134 | 135 | 136 | 137 |
| 128 | 129 | 130 | 131 | 132 |
| 123 | 124 | 125 | 126 | 127 |
| 118 | 119 | 120 | 121 | 122 |
| 113 | 114 | 115 | 116 | 117 |
| 108 | 109 | 110 | 111 | 112 |
| 103 | 104 | 105 | 106 | 107 |
| 98 | 99 | 100 | 101 | 102 |
| 93 | 94 | 95 | 96 | 97 |
| 88 | 89 | 90 | 91 | 92 |
| 83 | 84 | 85 | 86 | 87 |
| 78 | 79 | 80 | 81 | 82 |
| 73 | 74 | 75 | 76 | 77 |
| 68 | 69 | 70 | 71 | 72 |
| 63 | 64 | 65 | 66 | 67 |
| 58 | 59 | 60 | 61 | 62 |
| 53 | 54 | 55 | 56 | 57 |
| 48 | 49 | 50 | 51 | 52 |
| 43 | 44 | 45 | 46 | 47 |
| 38 | 39 | 40 | 41 | 42 |
| 33 | 34 | 35 | 36 | 37 |
| 28 | 29 | 30 | 31 | 32 |
| 23 | 24 | 25 | 26 | 27 |
| 18 | 19 | 20 | 21 | 22 |
| 13 | 14 | 15 | 16 | 17 |
| 8 | 9 | 10 | 11 | 12 |
| 3 | 4 | 5 | 6 | 7 |
| 1 | 2 | 3 | 4 | 5 |

Fig. 16. Full Axisymmetric ANSYS Model

ANSYS

84/ 3/22

17.6475

PLOT NO. 3

PREP7 ELEMENTS

MNUM=1

T0BC=1

ORIG SCALING

ZV=1

DIST=8.94

XF=31.9

YF=.5

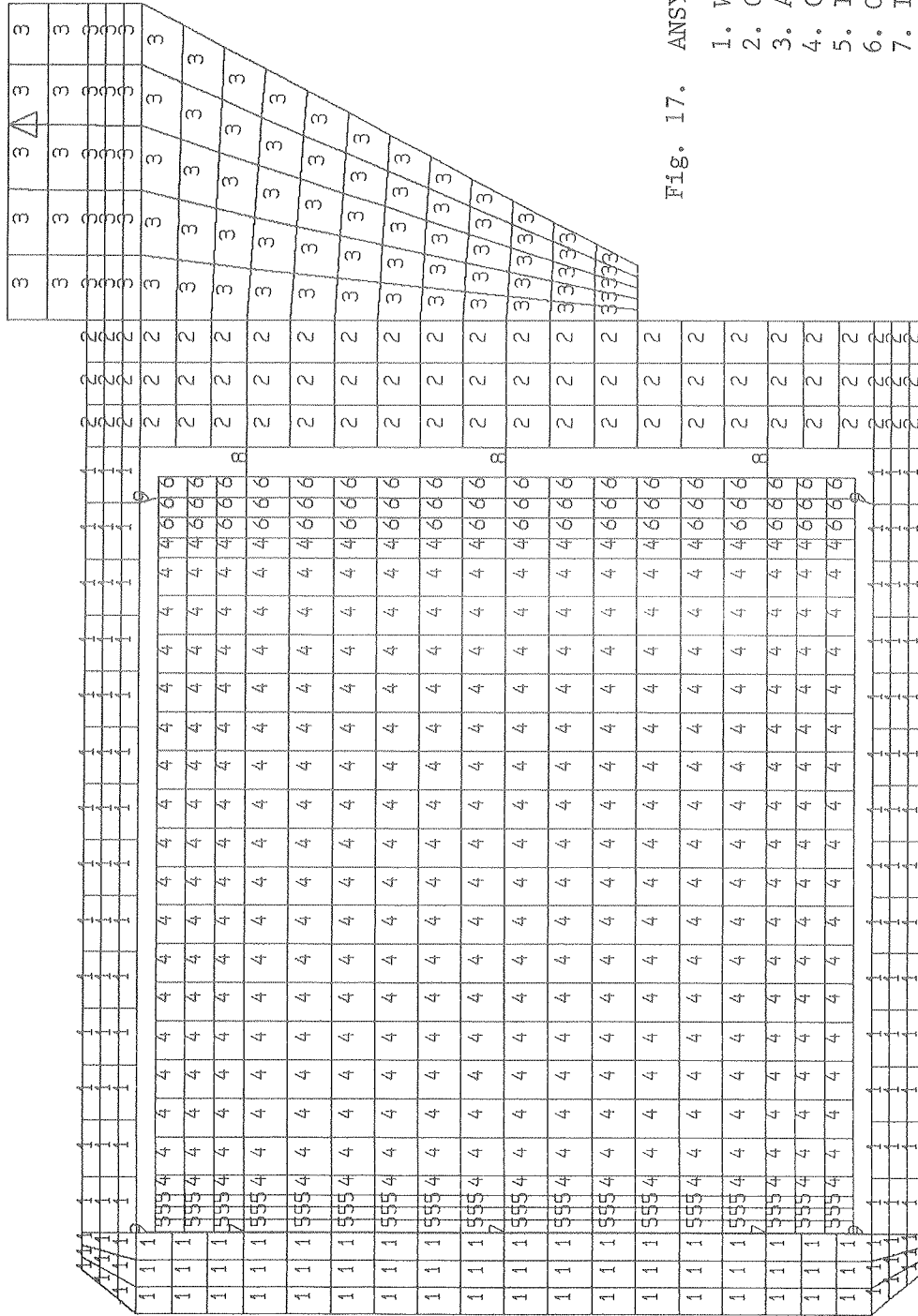


Fig. 17. ANSYS Model by Material Type

1. Winding Bobbin
2. Outer Wall
3. Axial Support Bracket
4. Coil
5. Inner Push Bar
6. Outer Push Bar
7. Inner Preload Screw
8. Outer Preload Screw

ANSYS
84/ 3/22
19.6894
PLOT NO. 5
POST1
STEP=1
ITER=1
DISPLACEMENT
ORIG SCALING
ZV=1
DIST=8.94
XF=31.9
YF=.5
DMAX=.0101
OSCA=88.5

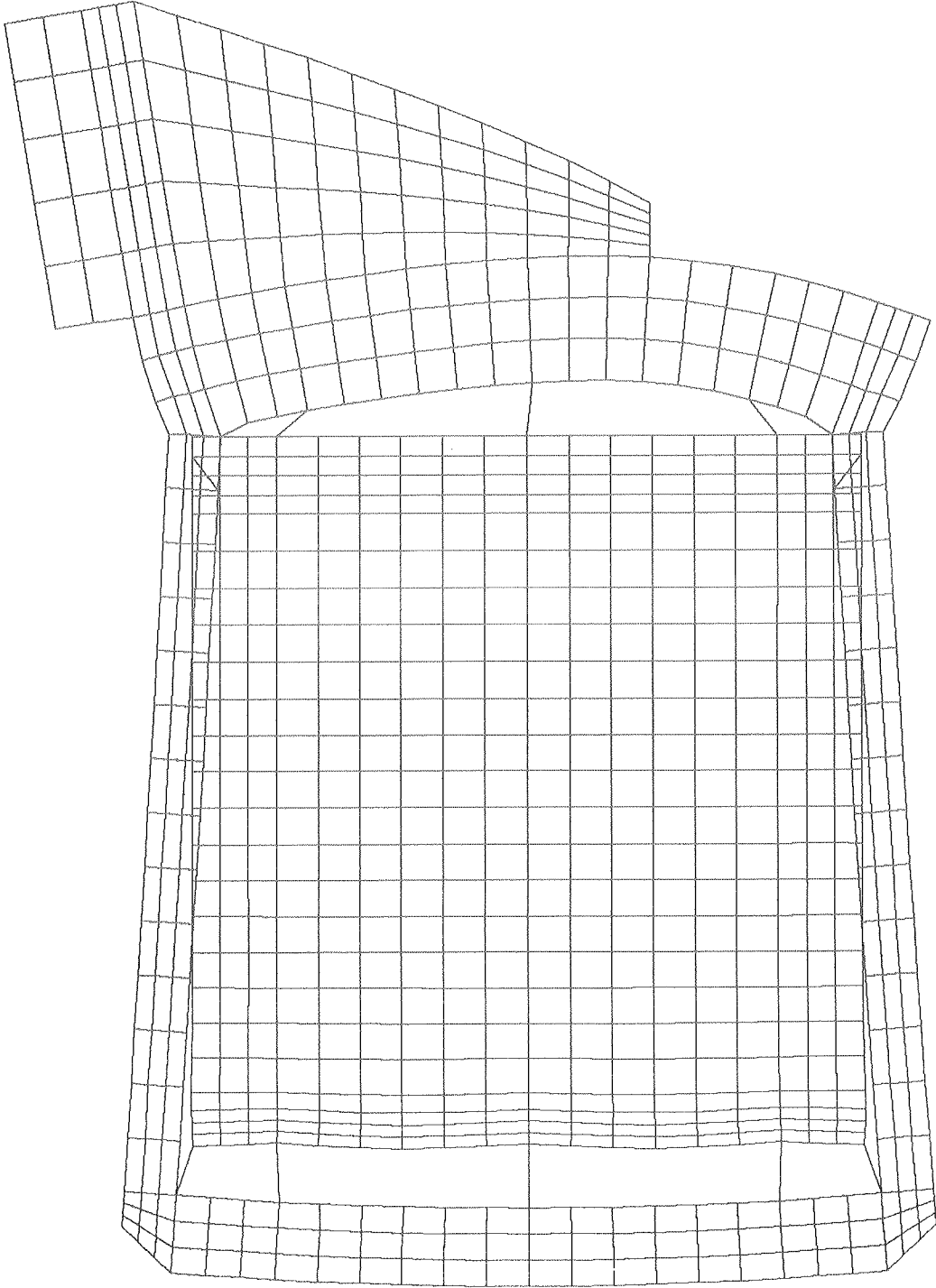


Fig 18

ANSYS
84/ 3/22
19.6933
PLOT NO. 6
POST1
STEP=2
ITER=1
DISPLACEMENT
ORIG SCALING
ZV=1
DIST=8.94
XF=31.9
YF=.5
DMAX=.0187
DSCA=47.8

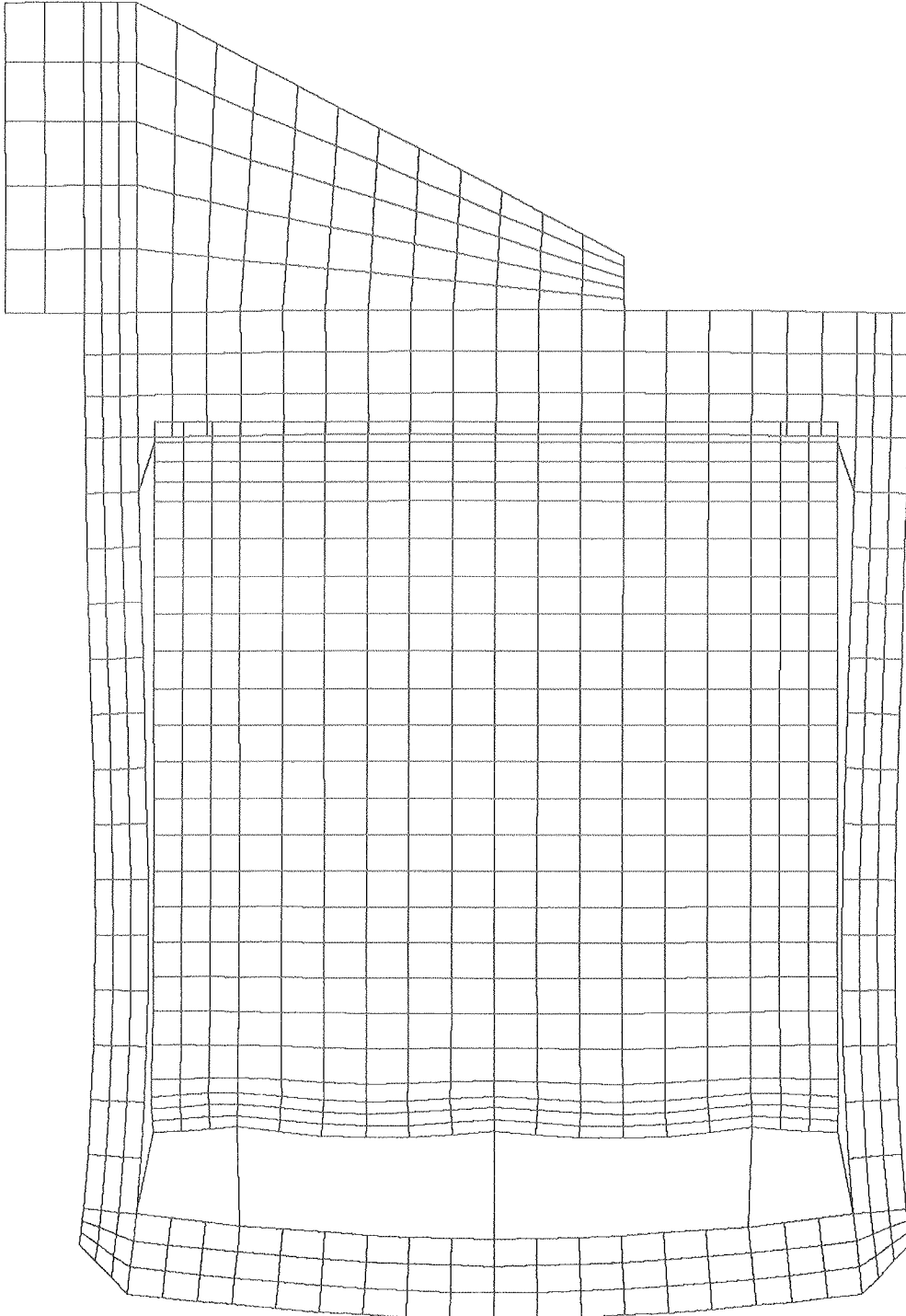


Fig 19

ANSYS
84/ 3/22
19.6978
PLOT NO. 7
POST1
STEP=3
ITER=1
DISPLACEMENT
ORIG SCALING
ZV=1
DIST=8.94
XF=31.9
YF=.5
DMAX=.0106
DSCA=84.1

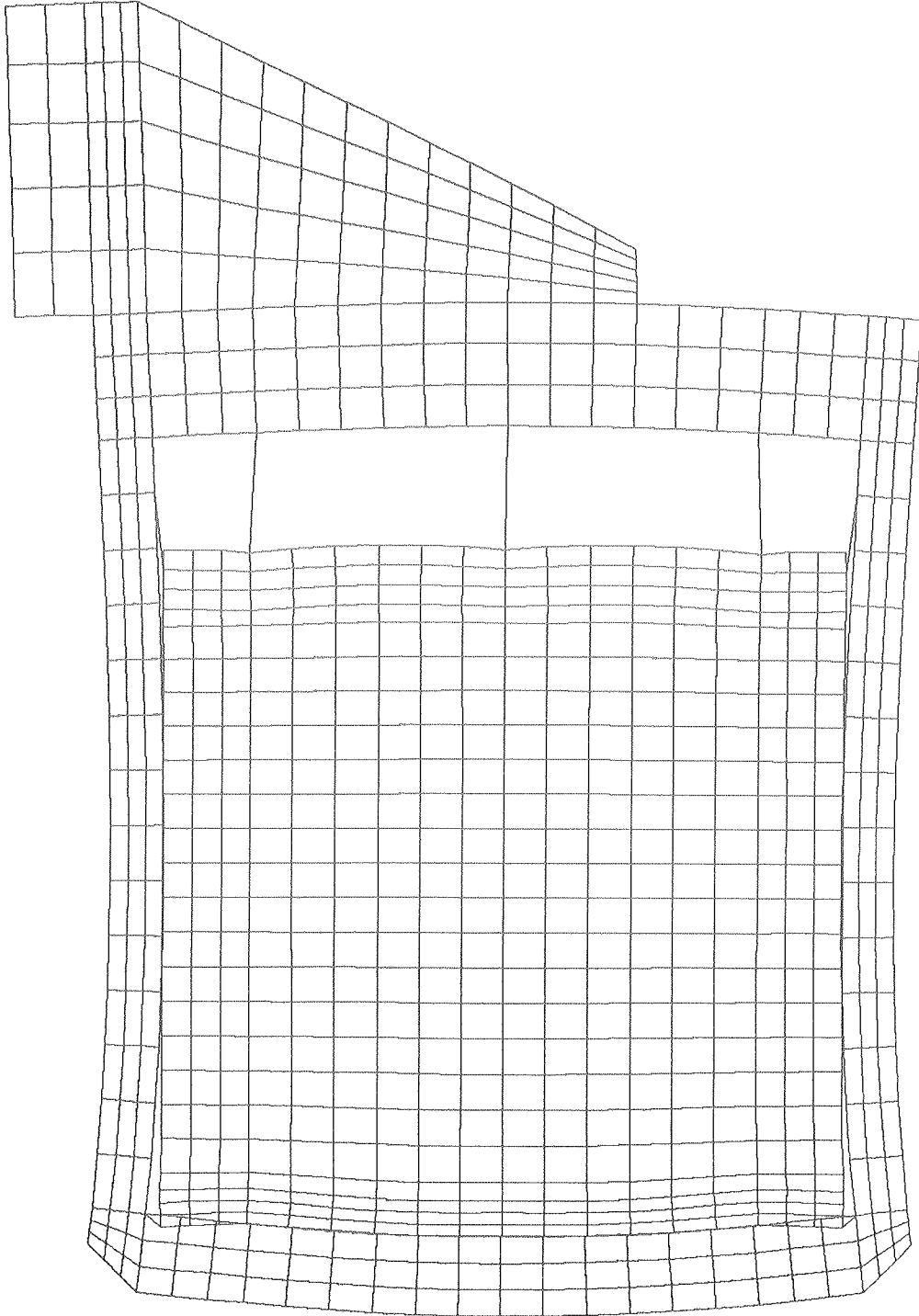


Fig 20

ANSYS
84/ 3/22
19.7017
PLOT NO. 8
POST1
STEP=4
ITER=1
DISPLACEMENT
ORIG SCALING
ZV=1
DIST=8.94
XF=31.9
YF=.5
DMAX=.123
DSCA=7.29

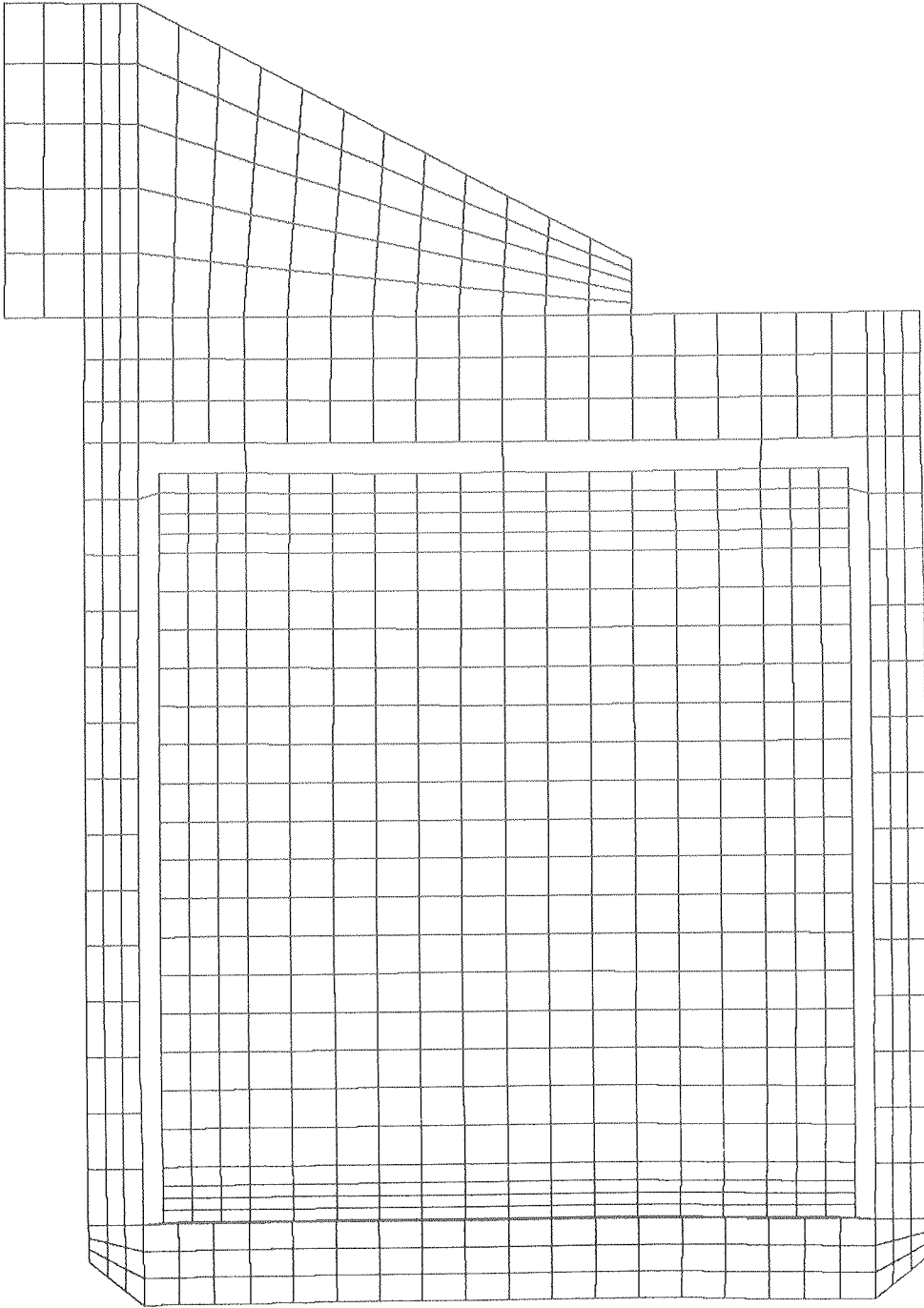


Fig. 21

ANSYS
84/ 3/22
19.7064
PLOT NO. 9
POST1
STEP=5
ITER=1
DISPLACEMENT
ORIG SCALING
ZV=1
DIST=8.94
XF=31.9
YF=.5
OMAX=.0191
OSCA=46.7

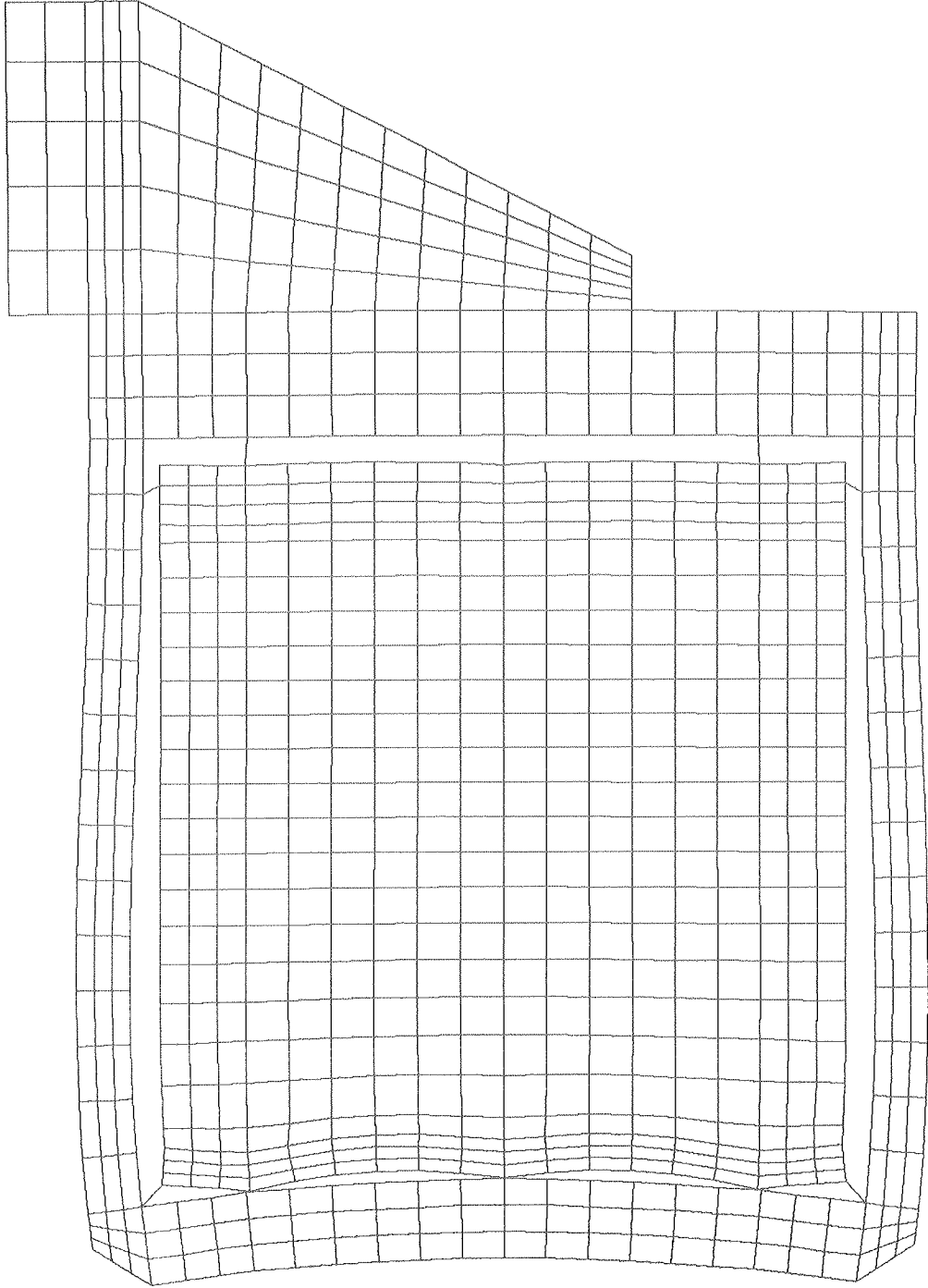


Fig 22

ANSYS
84/ 3/22
19.7106
PLOT NO. 10
POST1
STEP=6
ITER=1
DISPLACEMENT
ORIG SCALING
ZV=1
DIST=8.94
XF=31.9
YF=.5
DMAX=.0292
OSCA=30.6

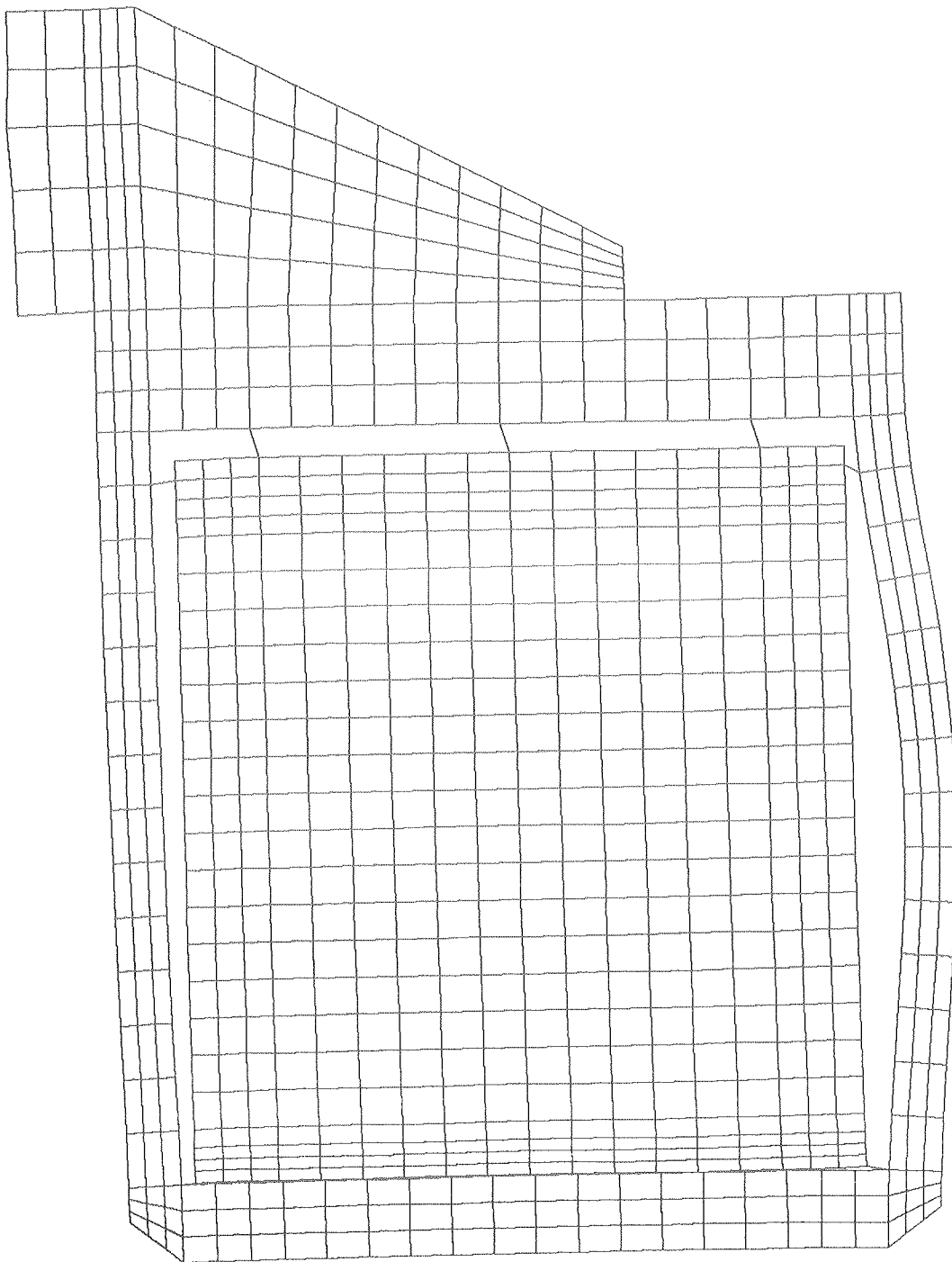


Fig 23

ANSYS
84/ 4/ 5
16.0831
PLOT NO. 41
POST1
STEP=9999
ITER=1
DISPLACEMENT
ORIG SCALING
ZV=1
DIST=8.94
XF=31.9
YF=.5
DMAX=.0246
DSCA=36.3

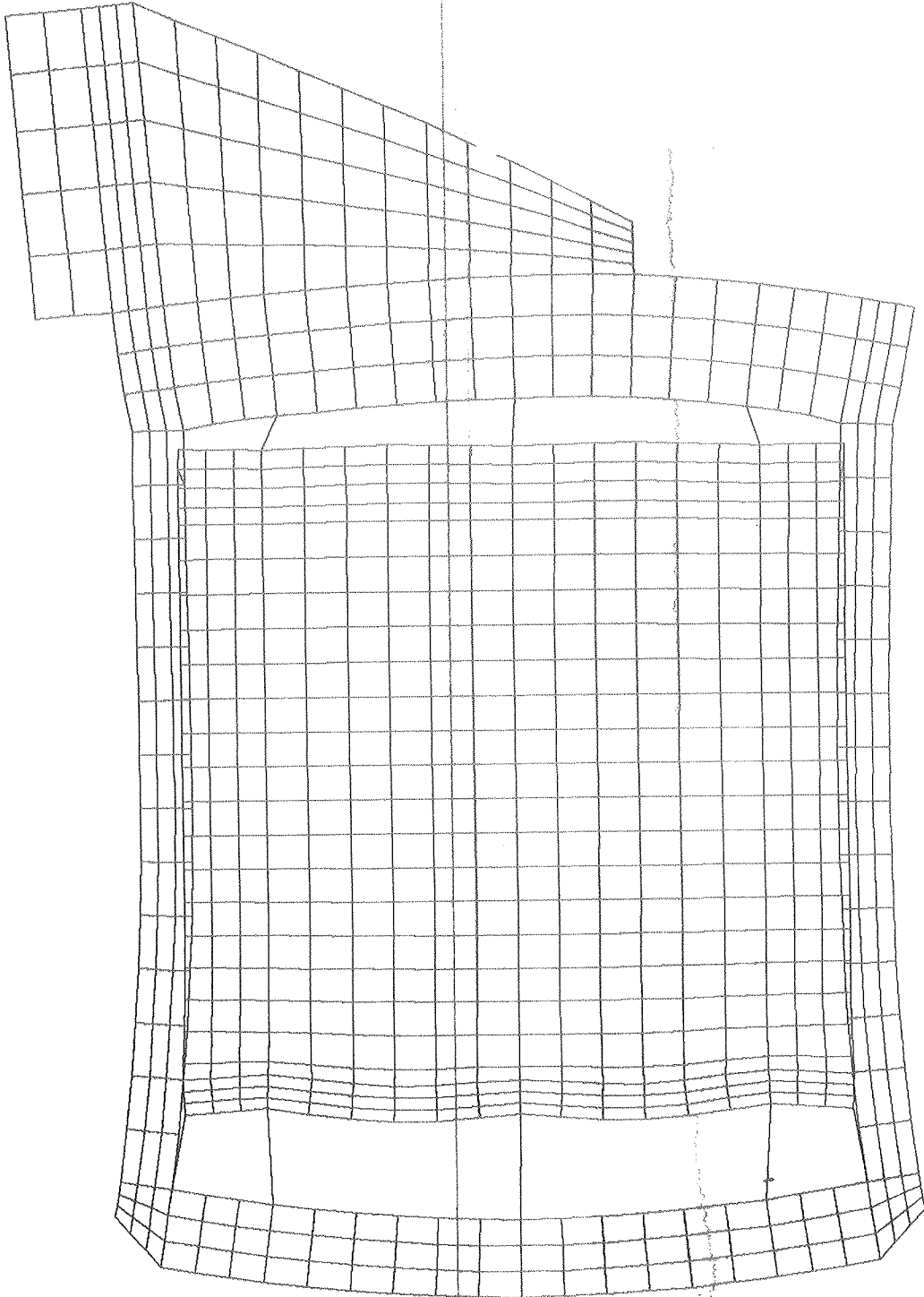


Fig 24

24

ANSYS
84/ 4/ 5
16.1153
PLOT NO. 46
POST1
STEP=9999
ITER=1
DISPLACEMENT
*
ORIG SCALING
ZV=1
DIST=8.94
XF=31.9
YF=.5
DMAX=.125
DSCA=7.13

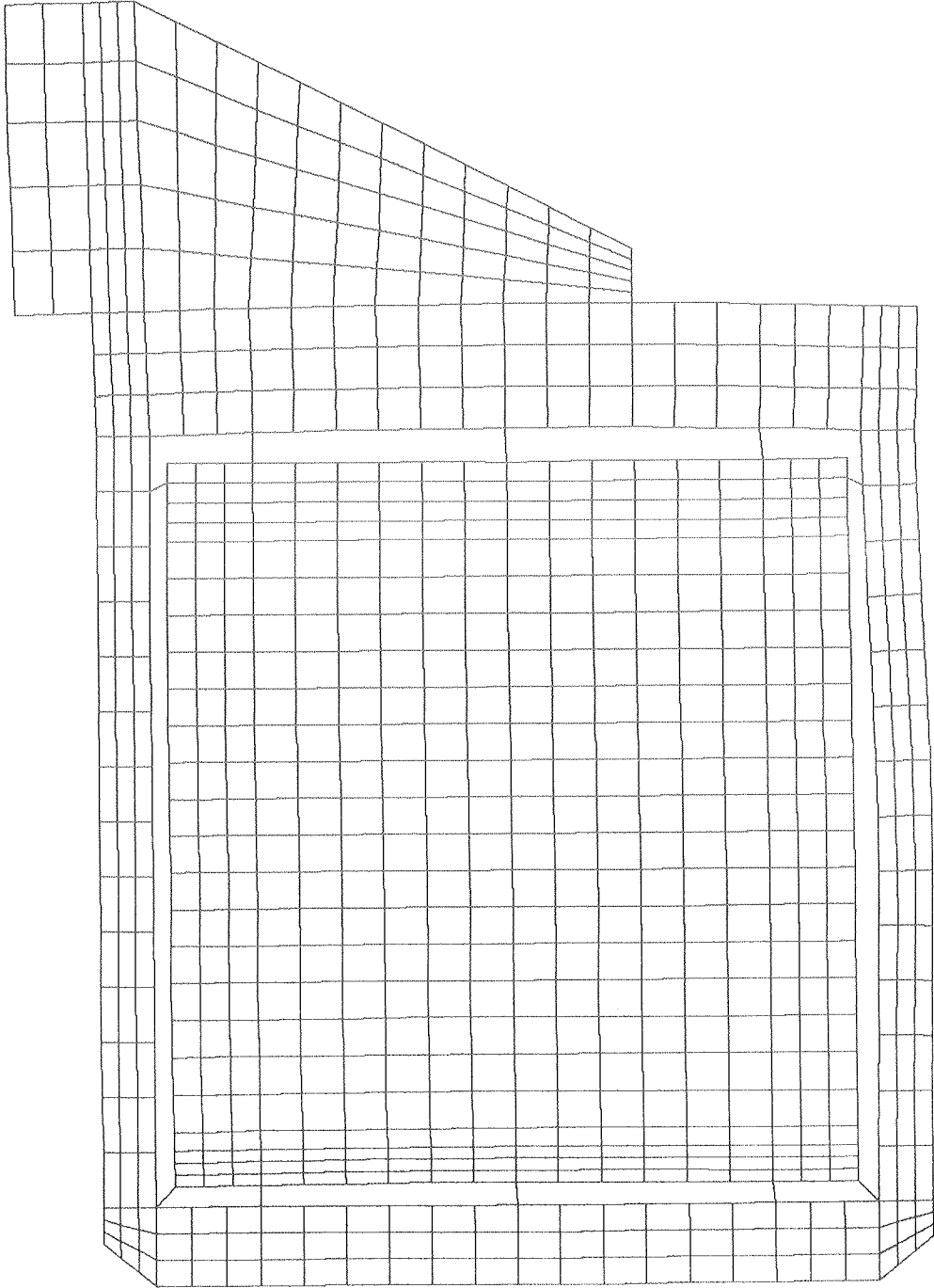


Fig 25

ANSYS
84/ 4/ 5
15.9178
PLOT NO. 2
POST1
STEP=1
ITER=1
STRESS PLOT
SZ
ORIG SCALING
ZV=1
C1S1=5.91
XF=29.1
EDGE
CMAX=.0101
MX=-749
MN=-6154
INC=400

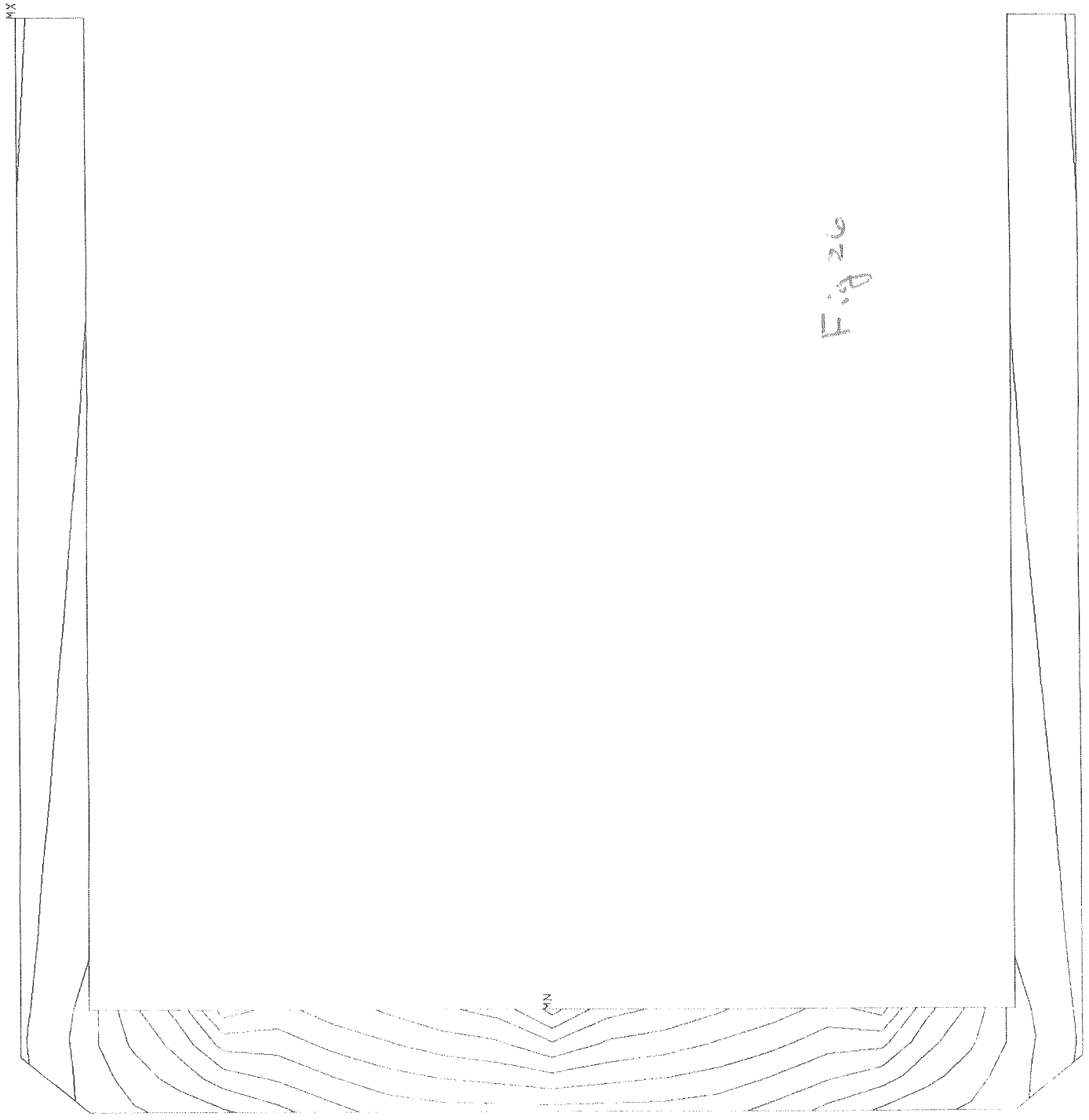


Fig 26

ANSYS
84/ 4/ 5
15.9181
PLOT NO. 3
POST1
STEP=1
ITER=1
STRESS PLOT
5X
ORIG SCALING
ZV=1
DIST=5.91
XF=29.1
EDGE
DMAX=.0101
MX=712
MN=-1653
INC=200

71

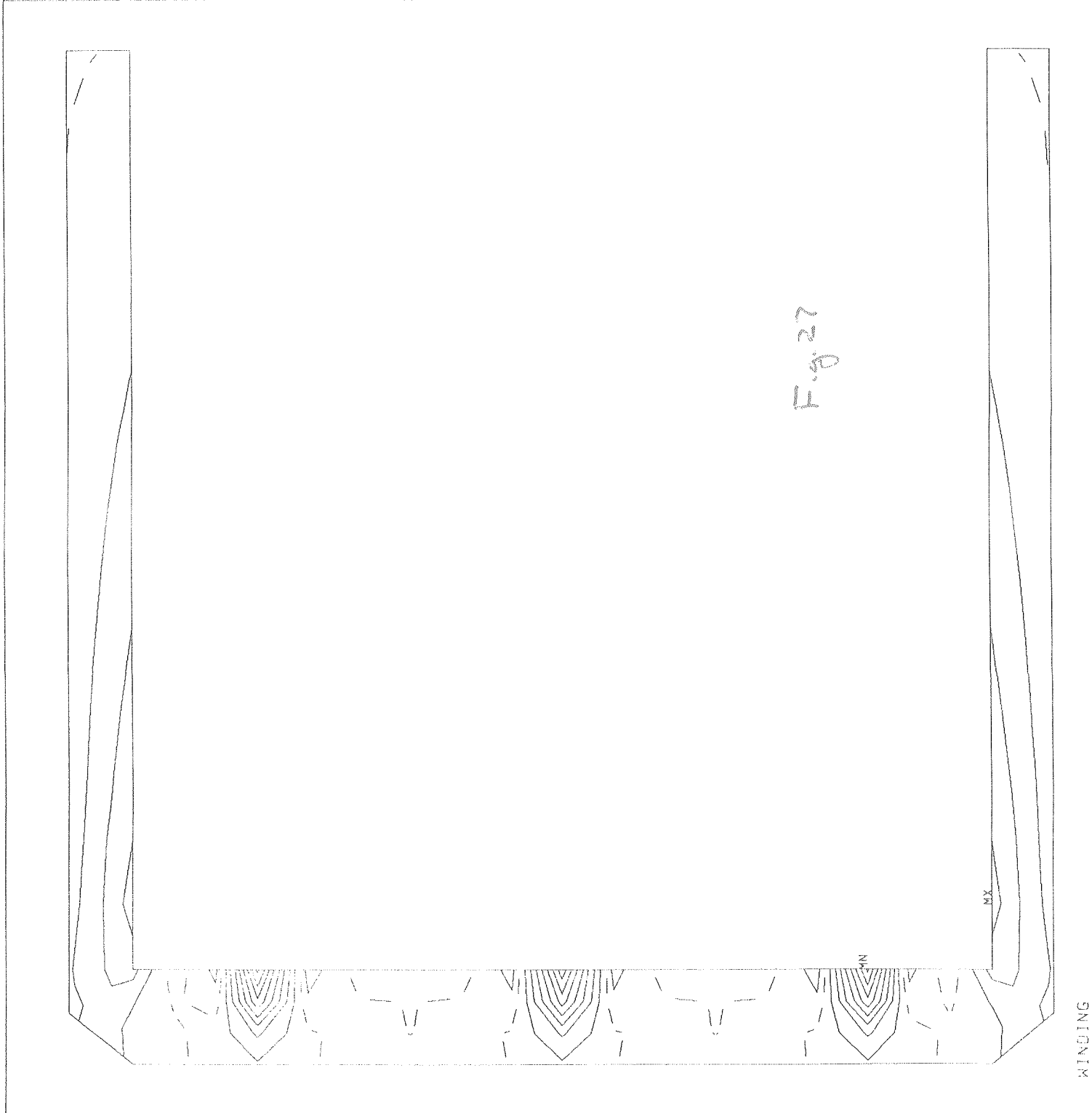


Fig. 27

RNSYS
84/ 4/ 5
15.9183
PLOT NO. 4
POST1
STEP=1
ITER=1
STRESS PLOT
SY
ORIG SCALING
ZV=1
DIST=5.91
XF=29.1
EDGE
DMAX=.0101
MX=4128
MN=-4285
INC=500

23

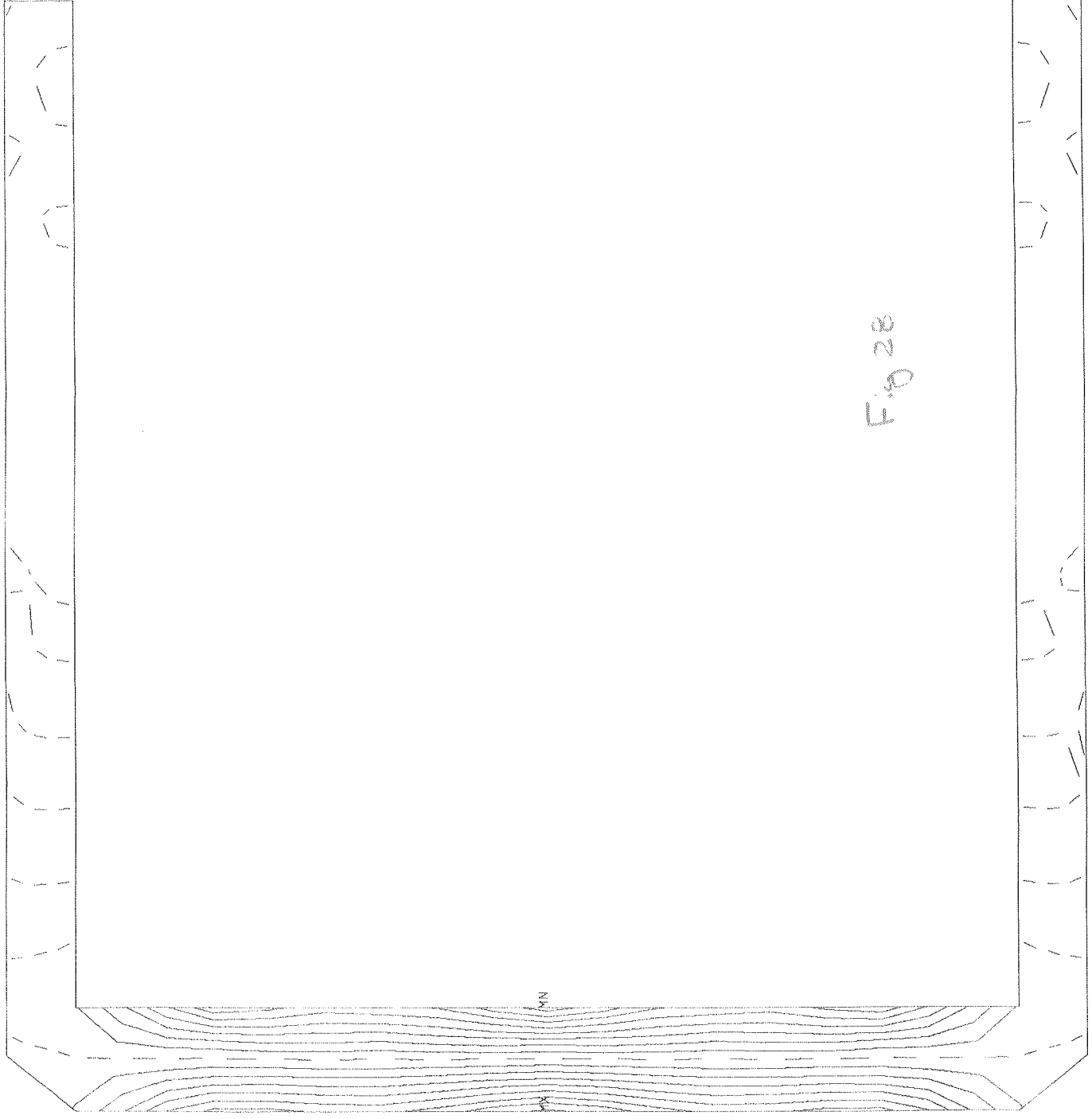


Fig 28

WINDING

ANSYS
84/ 4/ 5
15.9281
PLOT NO. 6
POST1
STEP=2
ITER=1
STRESS PLOT
SZ
ORIG SCALING
ZV=1
DIST=8.94
XF=31.9
YF=.5
EDGE
DMAX=.0106
MX=-.0438
MN=-18441
INC=1250

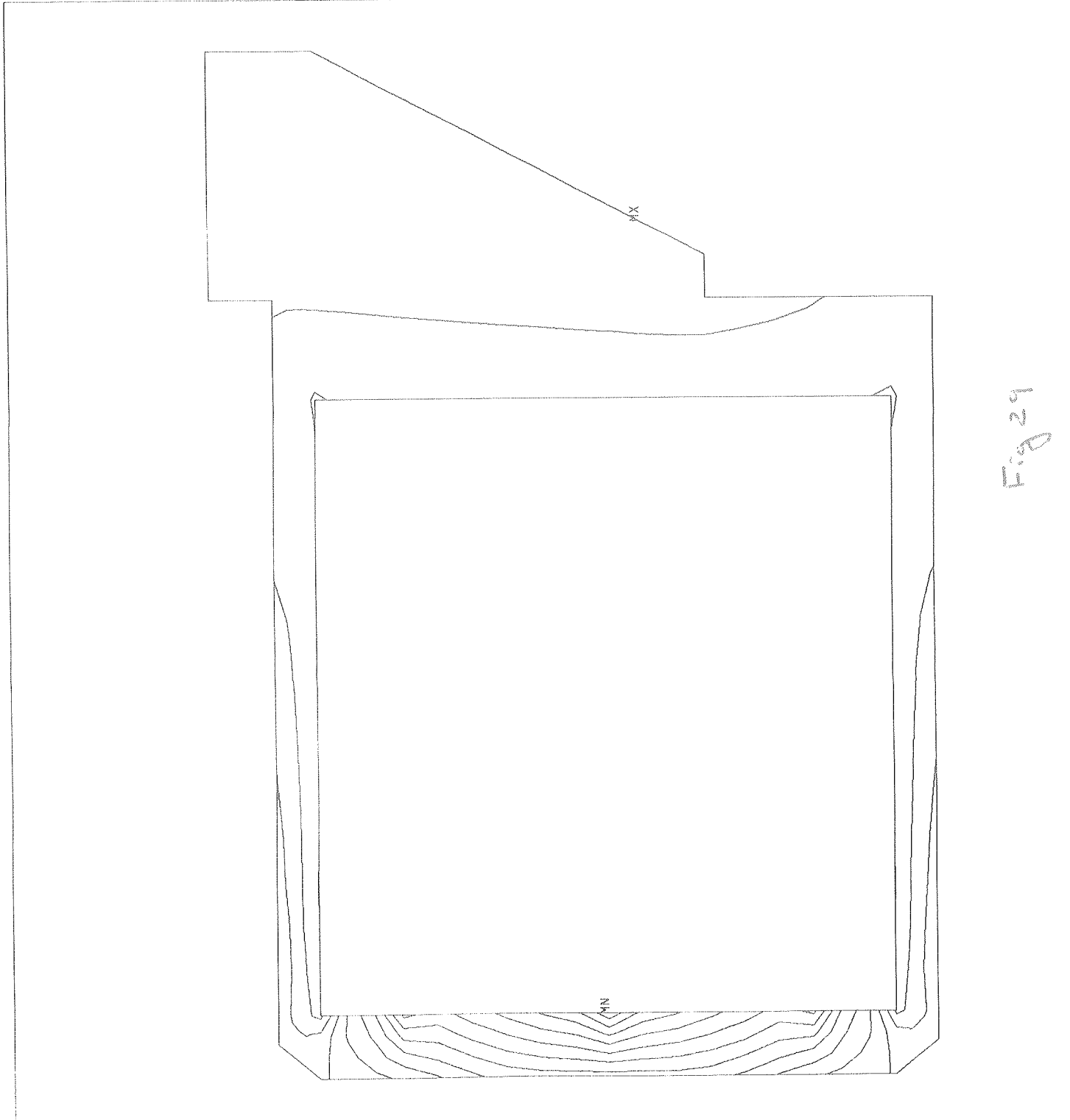


Fig 29
B

ANSYS
 84/ 4/ 5
 15.9294
 PLOT NO. 7
 POST1
 STEP=2
 ITER=1
 STRESS PLOT
 SX
 ORIG SCALING
 ZV=1
 DIST=8.94
 XF=31.9
 YF=.5
 EDGE
 DMAX=.0106
 MX=10355
 MN=-6442
 INC=1000

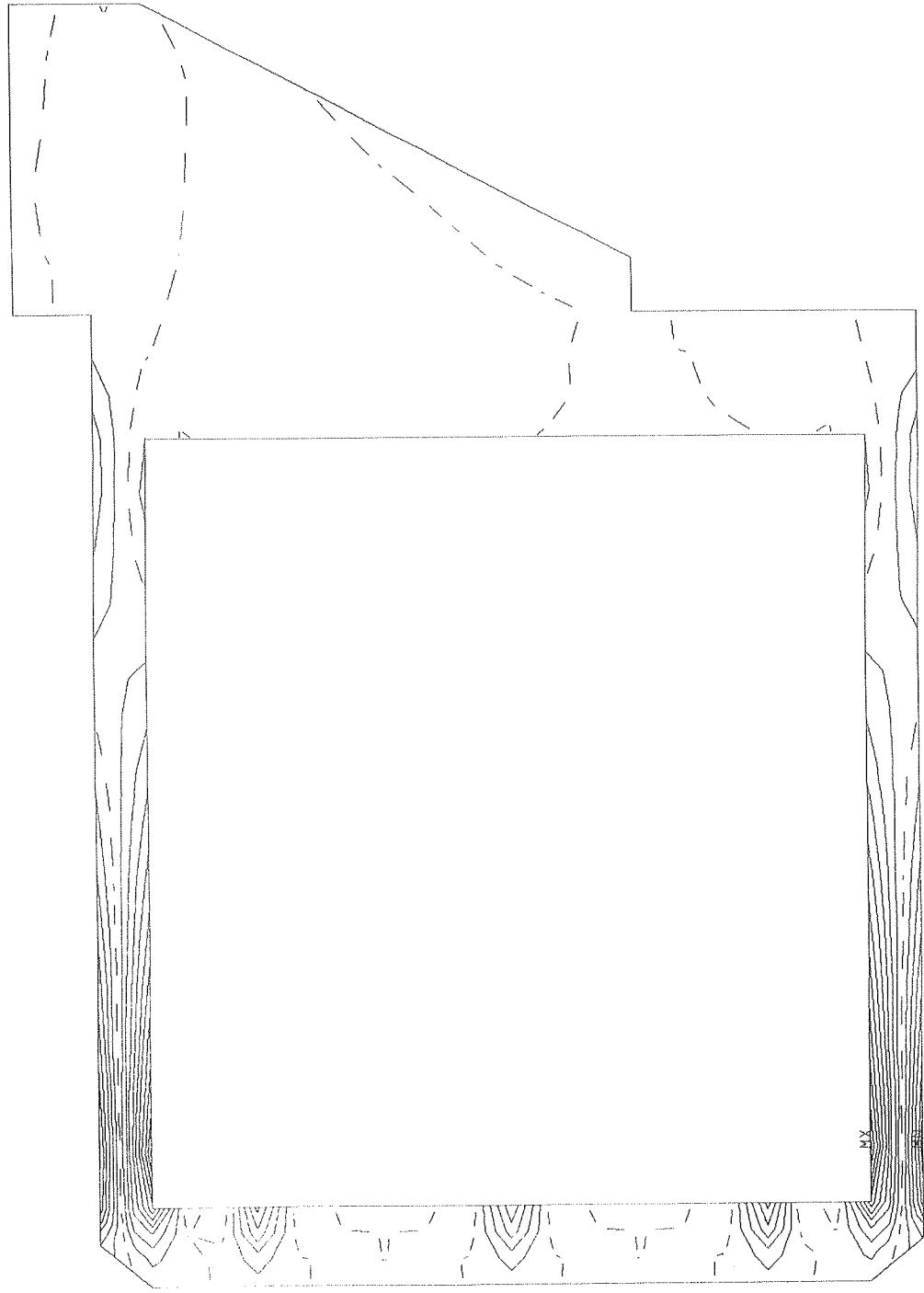


Fig 30

ANSYS
84/ 4/ 5
15.9300
PLOT NO. 8
POST1
STEP=2
ITER=1
STRESS PLOT
SY
ORIG SCALING
ZV=1
DIST=8.94
XF=31.9
YF=.5
EDGE
DMAX=.0106
MX=13668
MN=-13967
INC=2000

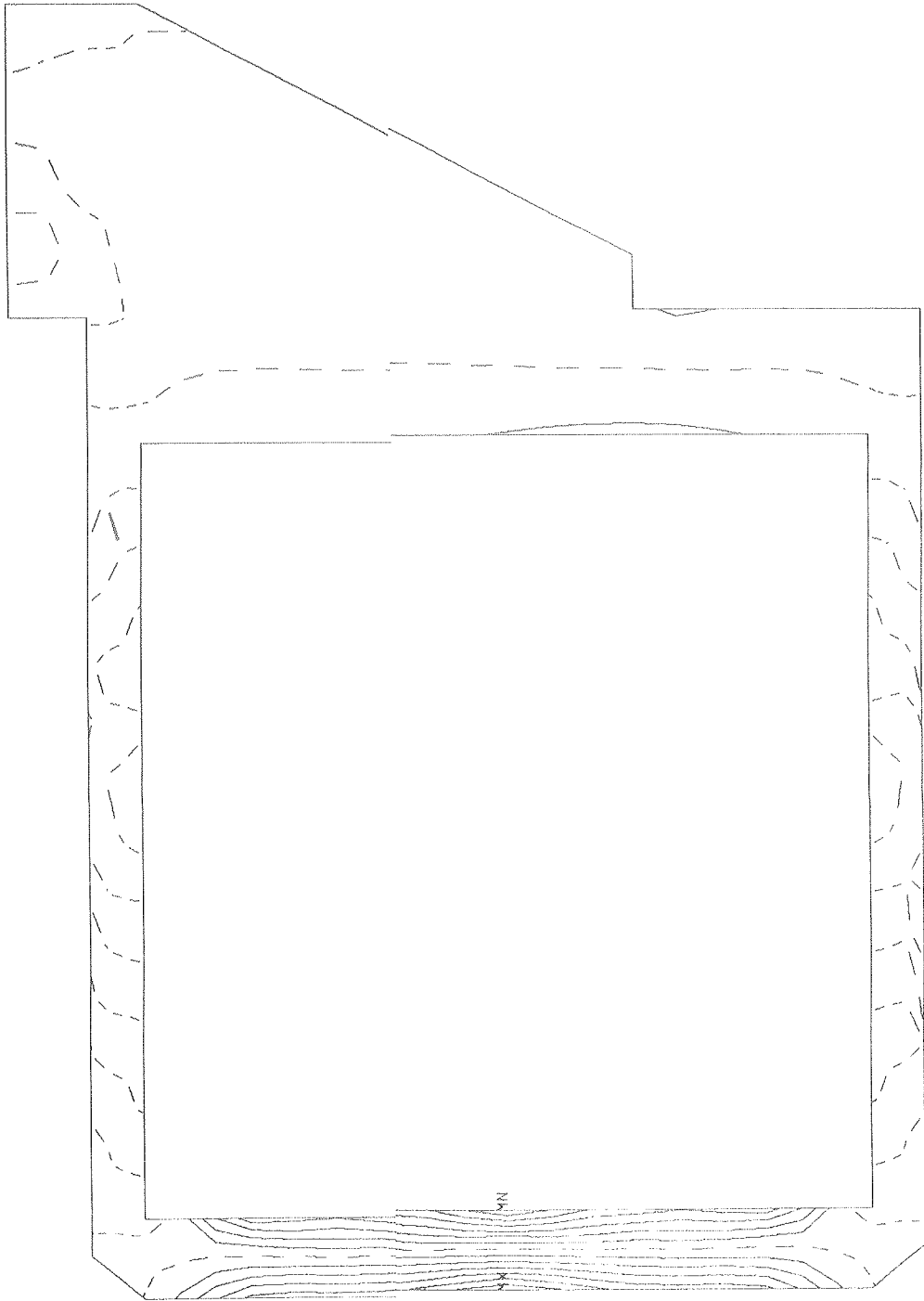


Fig 21

ANSYS
84/ 4/ 5
15.2511
PLOT NO. 12
POST1
STEP=3
ITER=1
STRESS PLOT
SZ
ORIG SCALING
ZV=1
DIST=8.94
XF=31.9
YF=.5
EDGE
DMAX=.00438
MX=4657
MN=-4598
INC=800

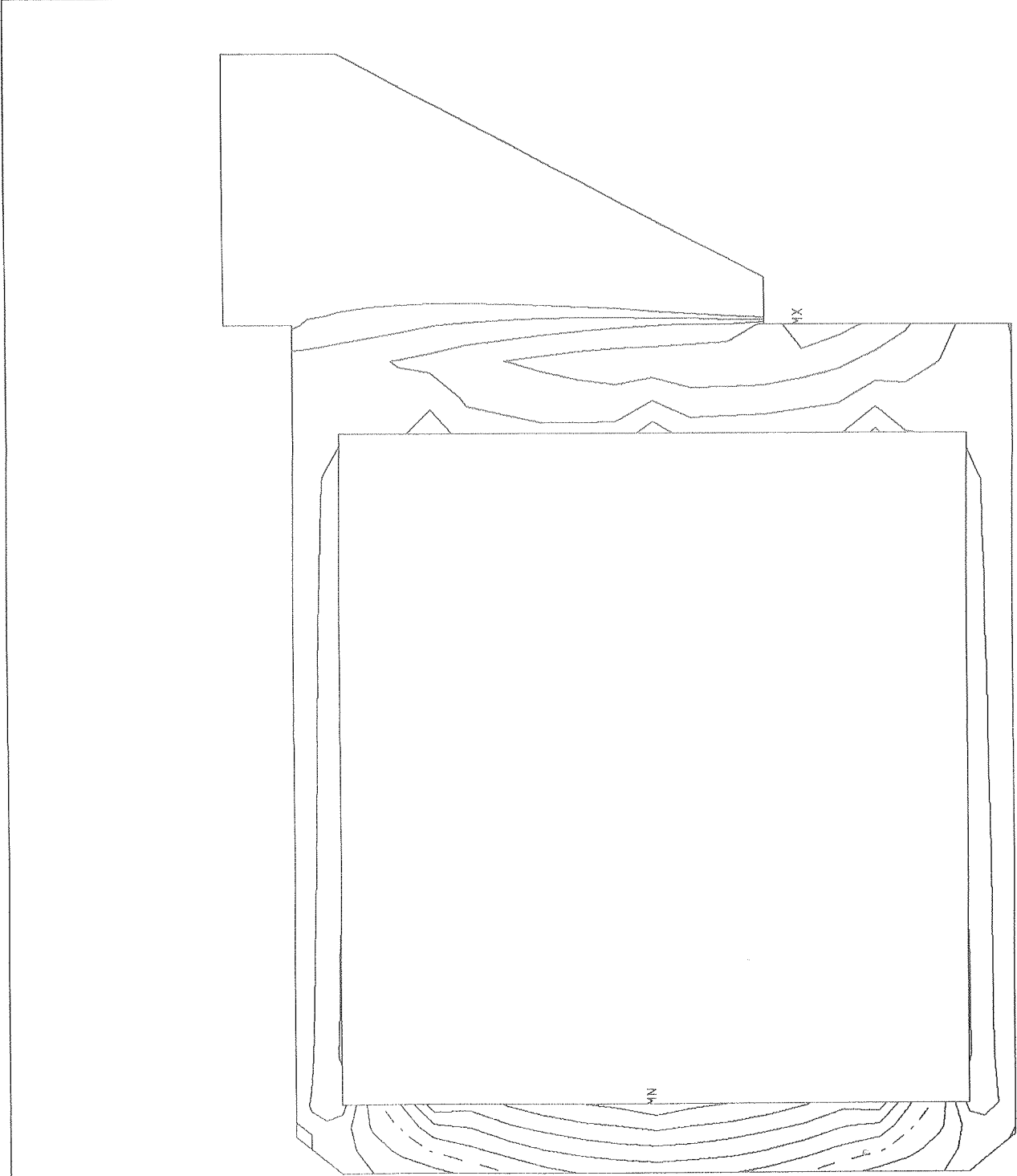


Fig 32

ANSYS
84/ 4/ 5
15.9519
PLOT NO. 13
POST1
STEP=3
ITER=1
STRESS PLOT
SX
ORIG SCALING
ZV=1
DIST=8.94
XF=31.9
YF=.5
EDGE
DMAX=.00438
MX=5410
MN=-2575
INC=500

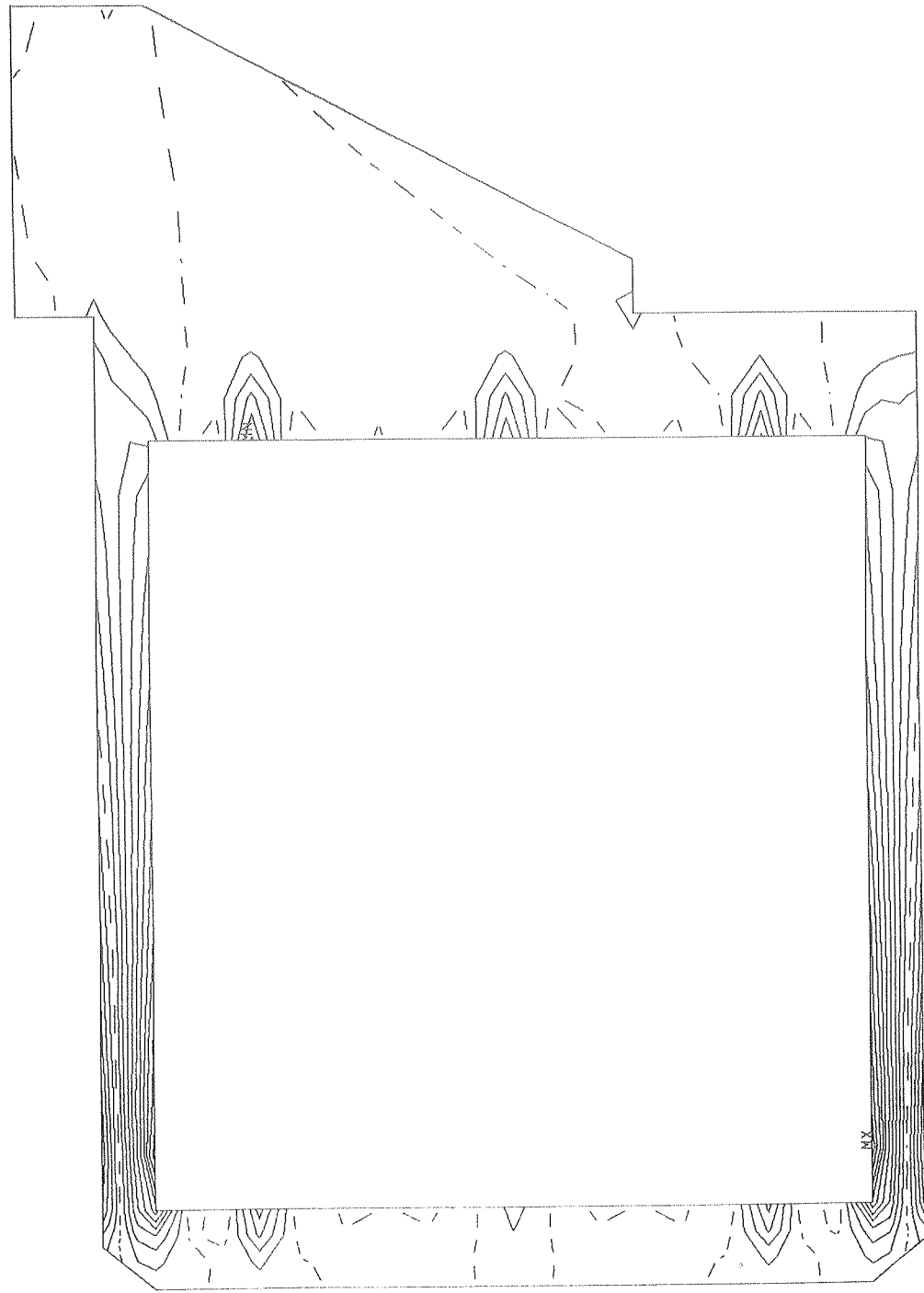


FIG 33

ANSYS
84/ 4/ 5
15.9525
PLOT NO. 14
POST1
STEP=3
ITER=1
STRESS PLOT
SY
ORIG SCALING
ZV=1
DIST=8.94
XF=31.9
YF=.5
EDGE
DMAX=.00438
MX=5914
MN=-5874
INC=800

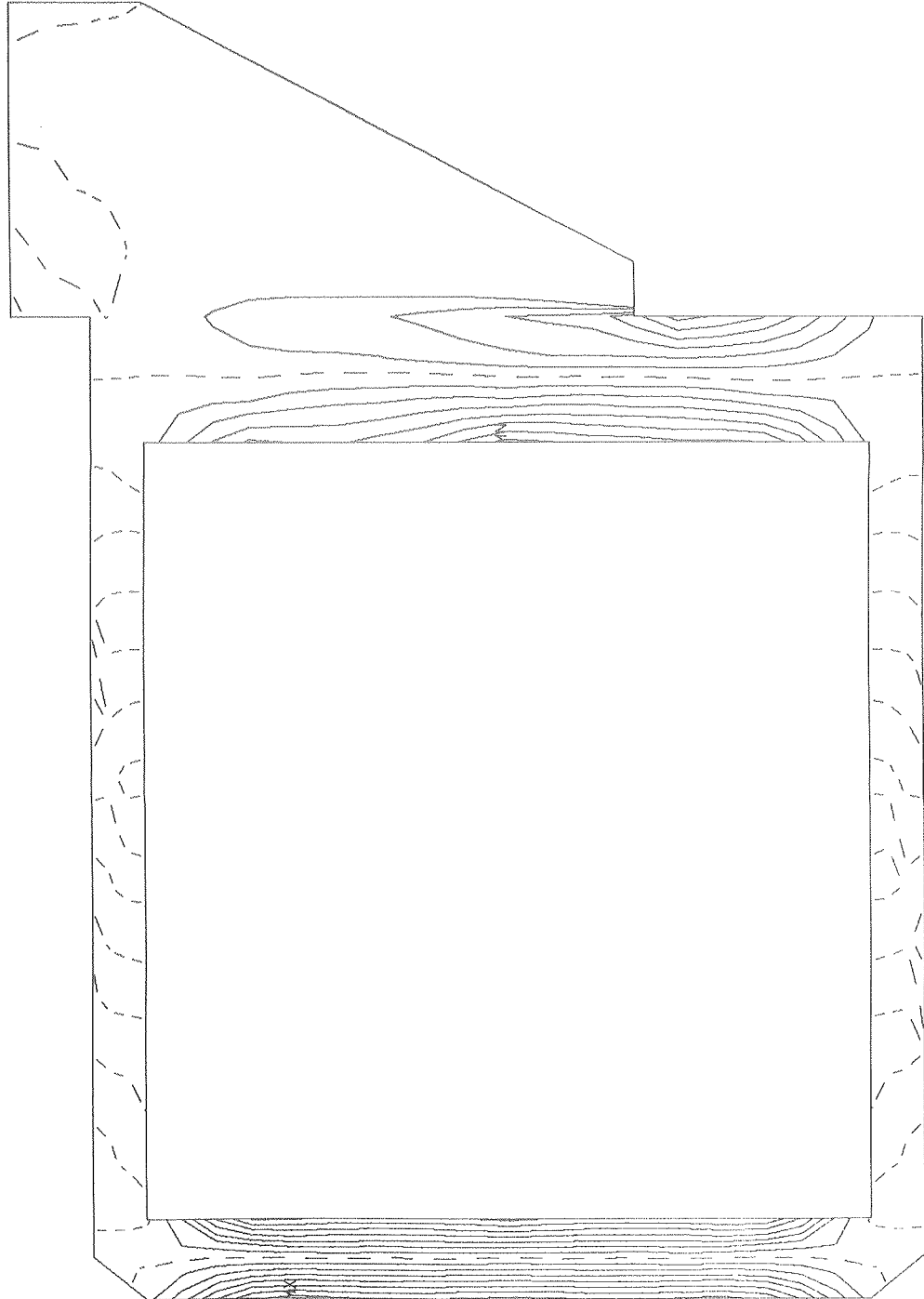


Fig. 34

ANSYS
84/ 4/ 5
15.9744
PLOT NO. 18
POST1
STEP=4
ITER=1
STRESS PLOT
SZ
ORIG SCALING
ZV=1
DIST=8.94
XF=31.9
YF=.5
EDGE
DMAX=.123
MX=3932
MN=-4679
INC=500

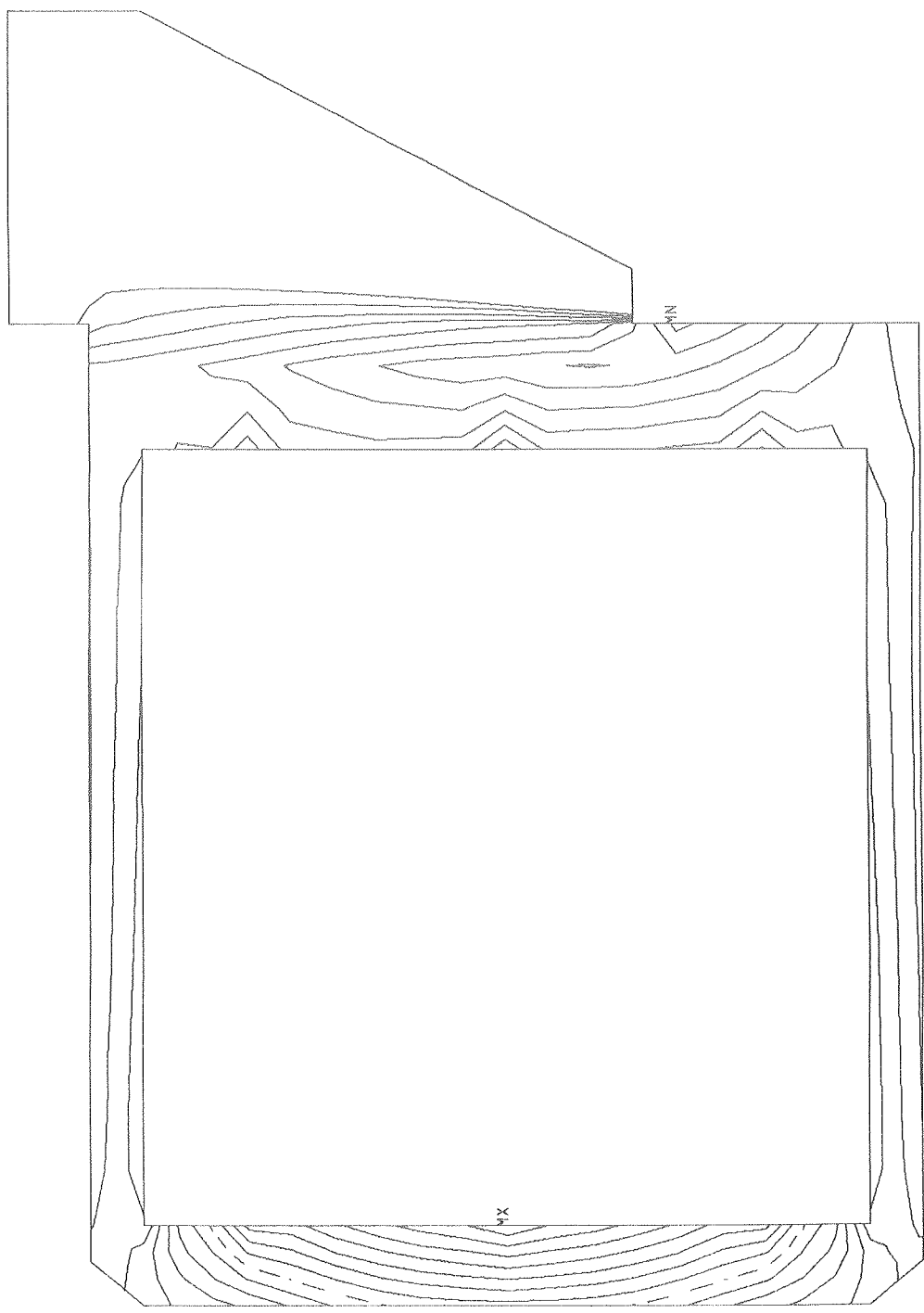


Fig 35

ANSYS
84/ 4/ 5
15.9753
PLOT NO. 19
POST1
STEP=4
ITER=1
STRESS PLOT
SX
ORIG SCALING
ZV=1
DIST=8.94
XF=31.9
YF=.5
EDGE
DMAX=.123
MX=2665
MN=-4566
INC=500

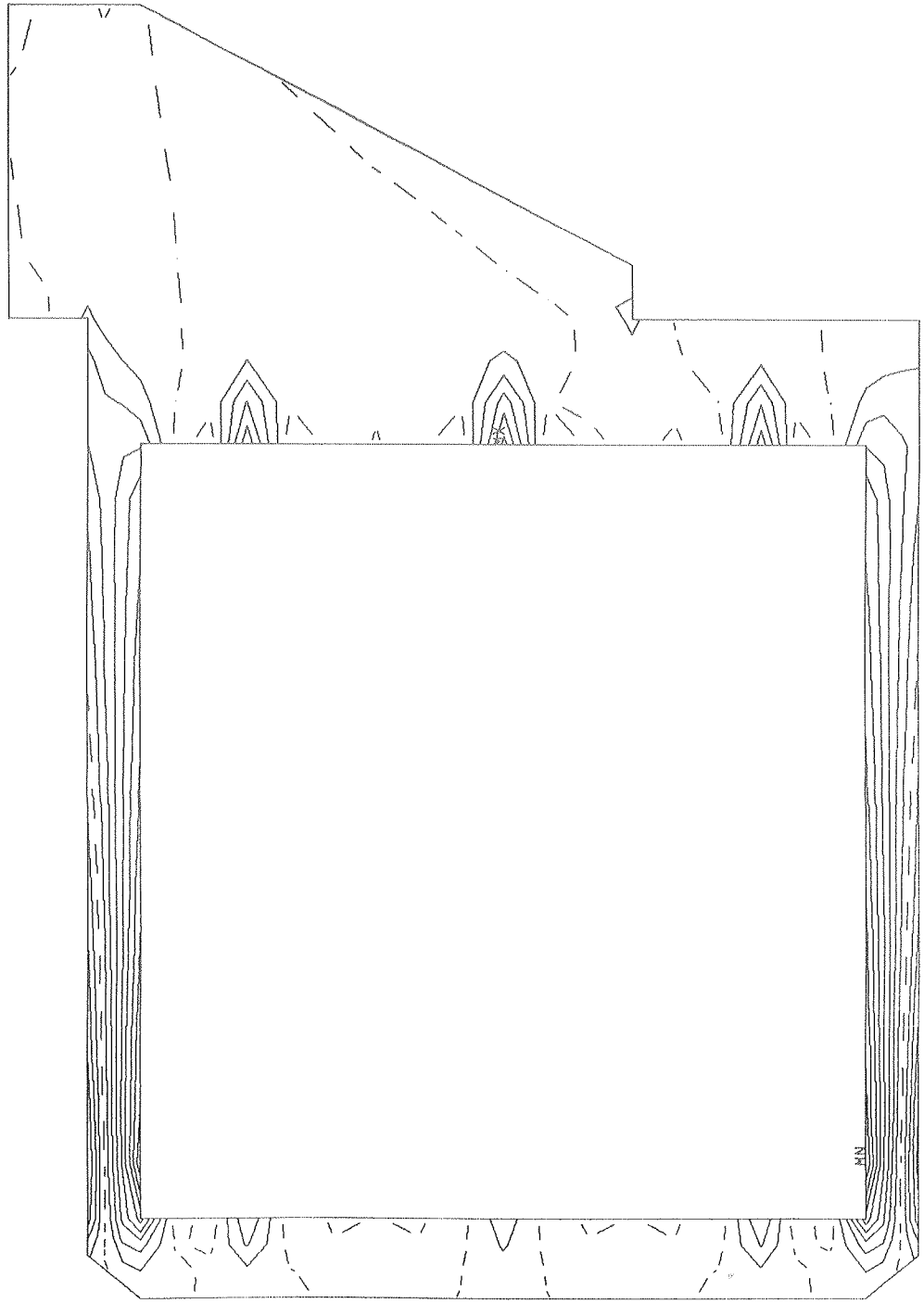


Fig 36

ANSYS
84/ 4/ 5
15.9758
PLOT NO. 20
POST1
STEP=4
ITER=1
STRESS PLOT
SY
ORIG SCALING
ZV=1
DIST=8.94
XF=31.9
YF=.5
EDGE
DMAX=.123
MX=5972
MN=-5818
INC=800

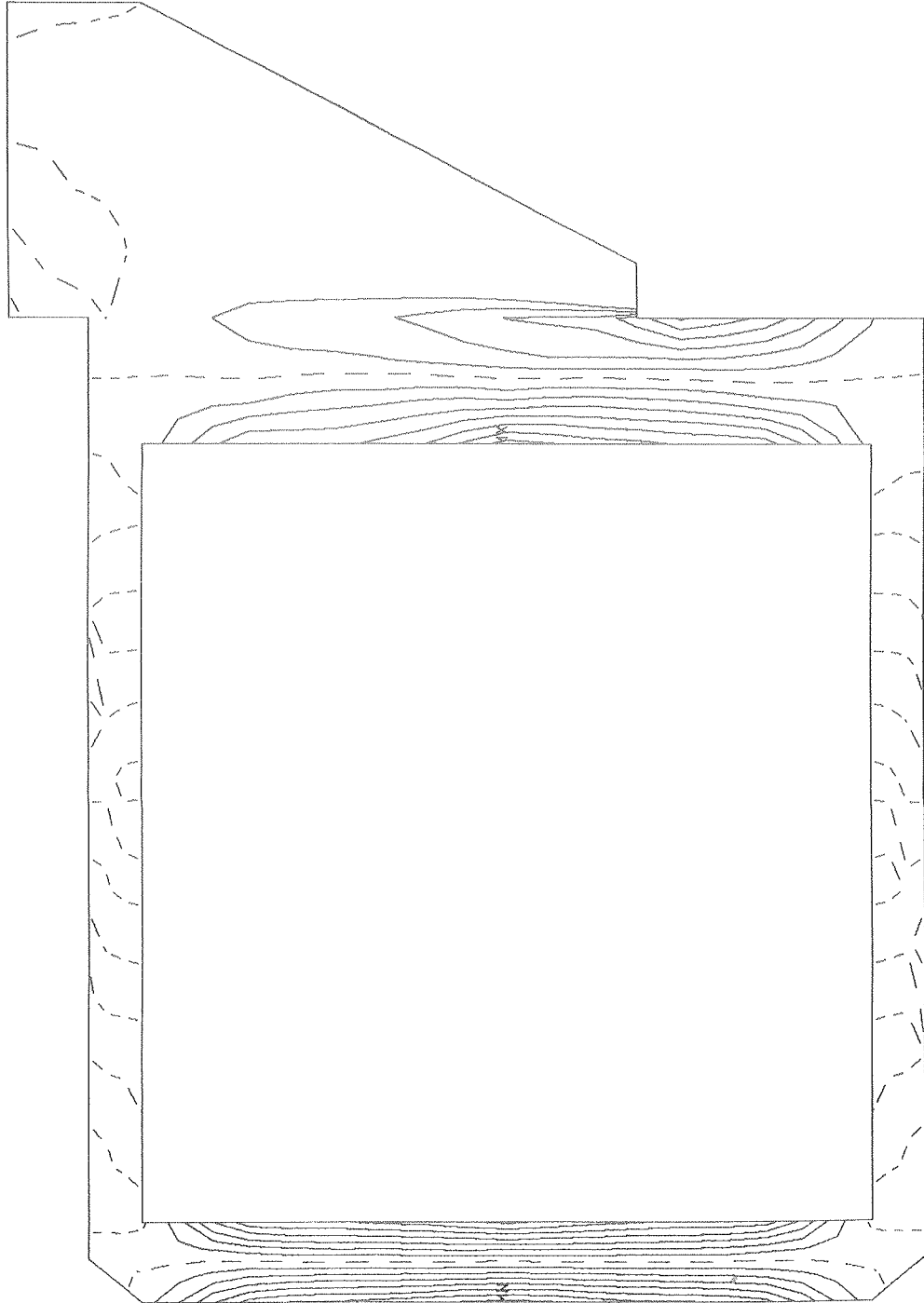


Fig 37

ANSYS
84/ 4/ 5
16.0042
PLOT NO. 24
POST1
STEP=5
ITER=1
STRESS PLOT
SZ
ORIG SCALING
ZV=1
DIST=8.94
XF=31.9
YF=.5
EDGE
DMAX=.0161
MX=25398
MN=.17
INC=2000

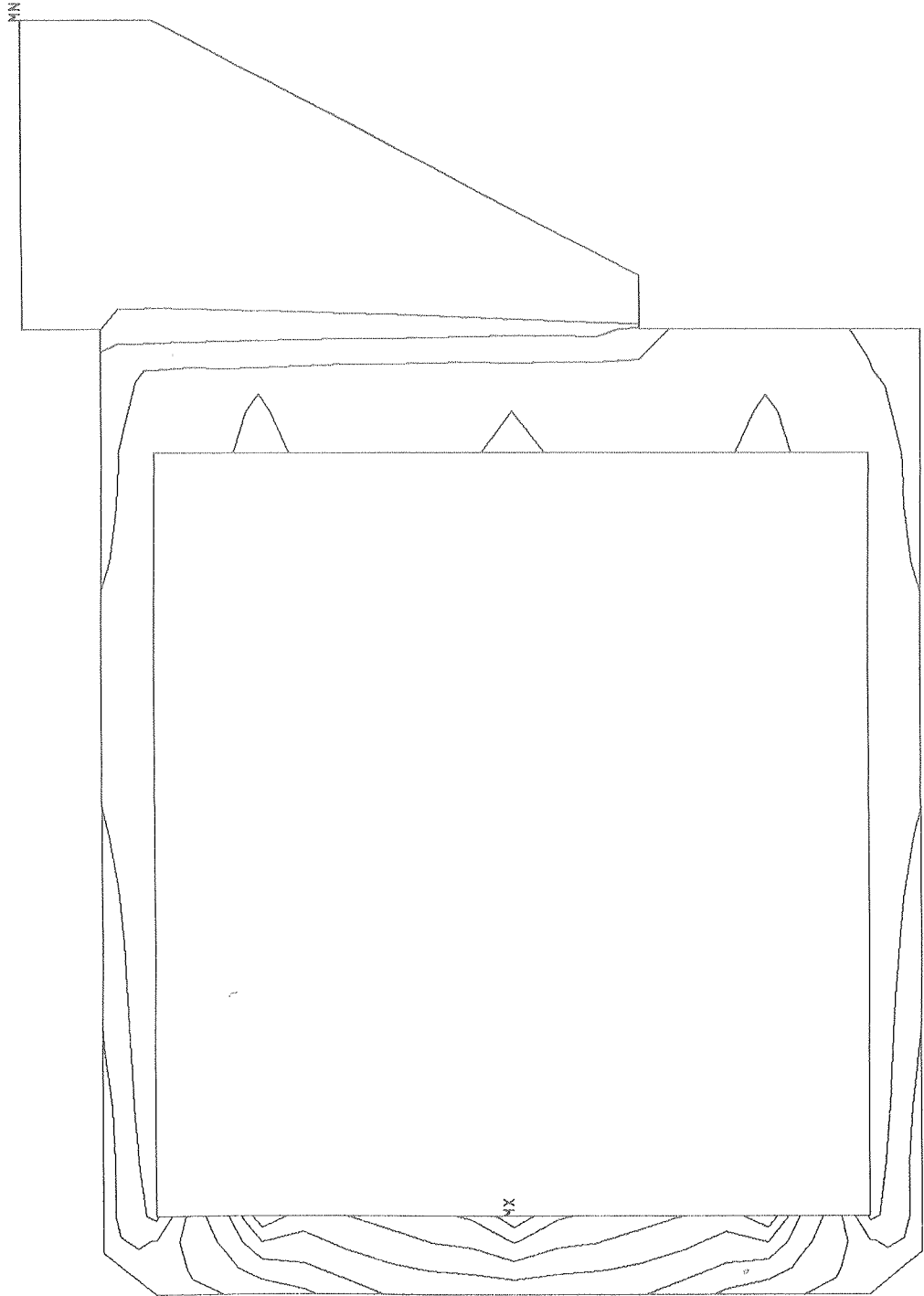


Fig 32

ANSYS
84/ 4/ 5
16.0050
PLOT NO. 25
POST1
STEP=5
ITER=1
STRESS PLOT
SX
ORIG SCALING
ZV=1
DIST=8.94
XF=31.9
YF=.5
EDGE
DMAX=.0161
MX=8852
MN=-12745
INC=2000

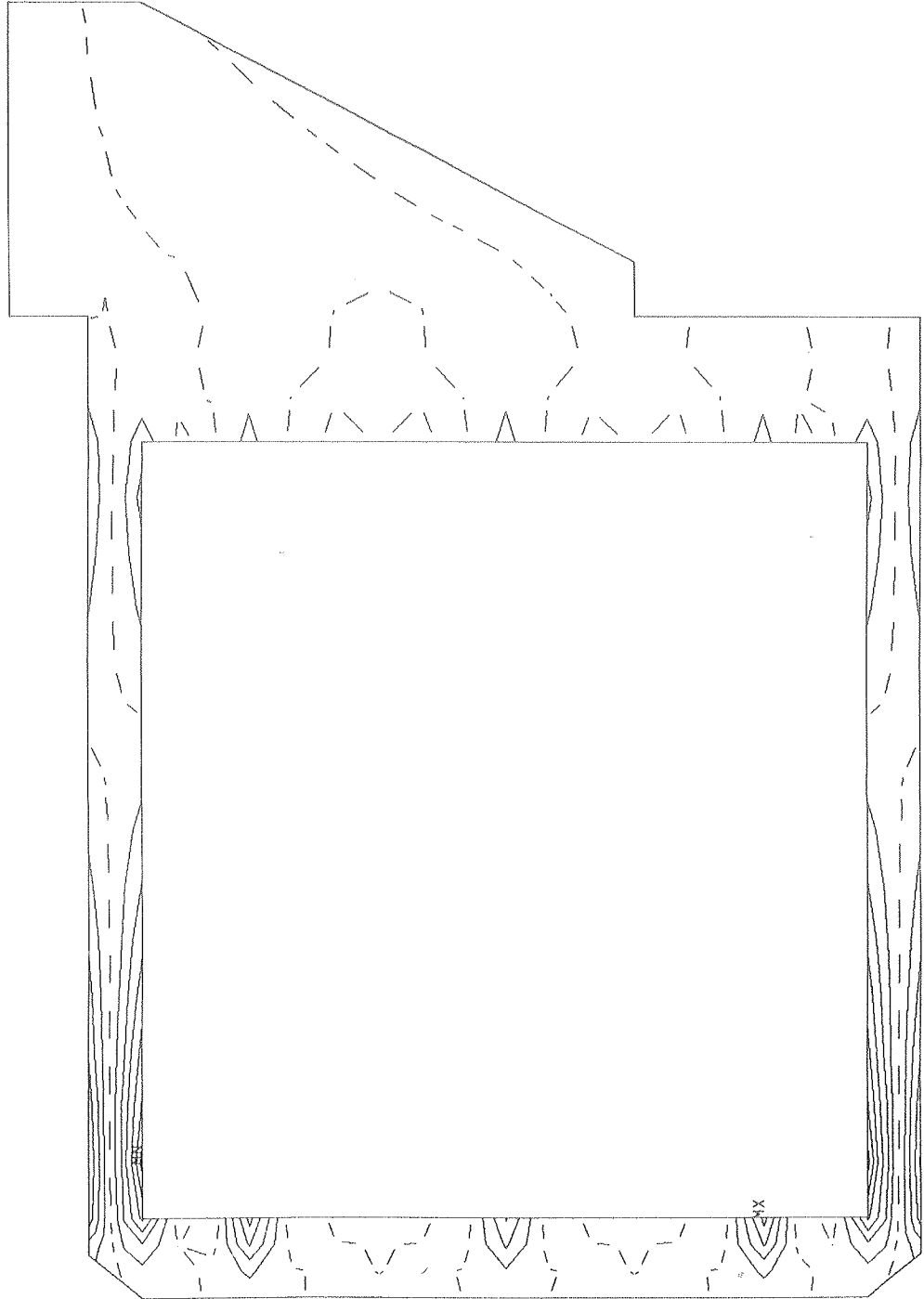


Fig 39

ANSYS
84/ 4/ 5
16.0058
PLOT NO. 26
POST1
STEP=5
ITER=1
STRESS PLOT
SY
ORIG SCALING
ZV=1
DIST=8.94
XF=31.9
YF=.5
EDGE
DMAX=.0161
MX=14065
MN=-13682
INC=2000

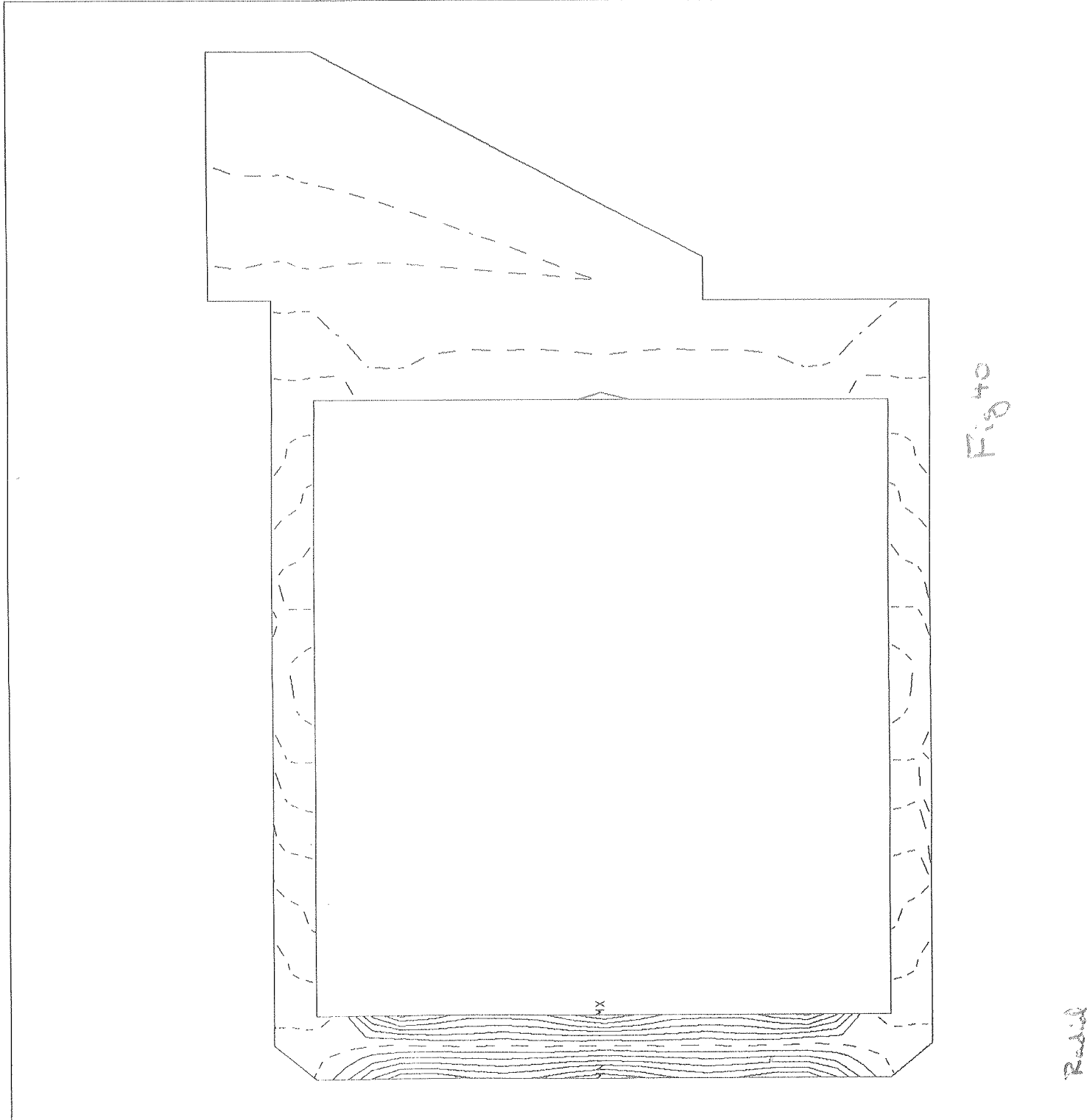


Fig 40

Radial
DISTANCE

ANSYS
84/ 4/ 5
16.0283
PLOT NO. 30
POST1
STEP=6
ITER=1
STRESS PLOT
SZ
ORIG SCALING
ZV=1
DIST=8.94
XF=31.9
YF=.5
EDGE
DMAX=.0292
MX=12314
MN=-6506
INC=1250

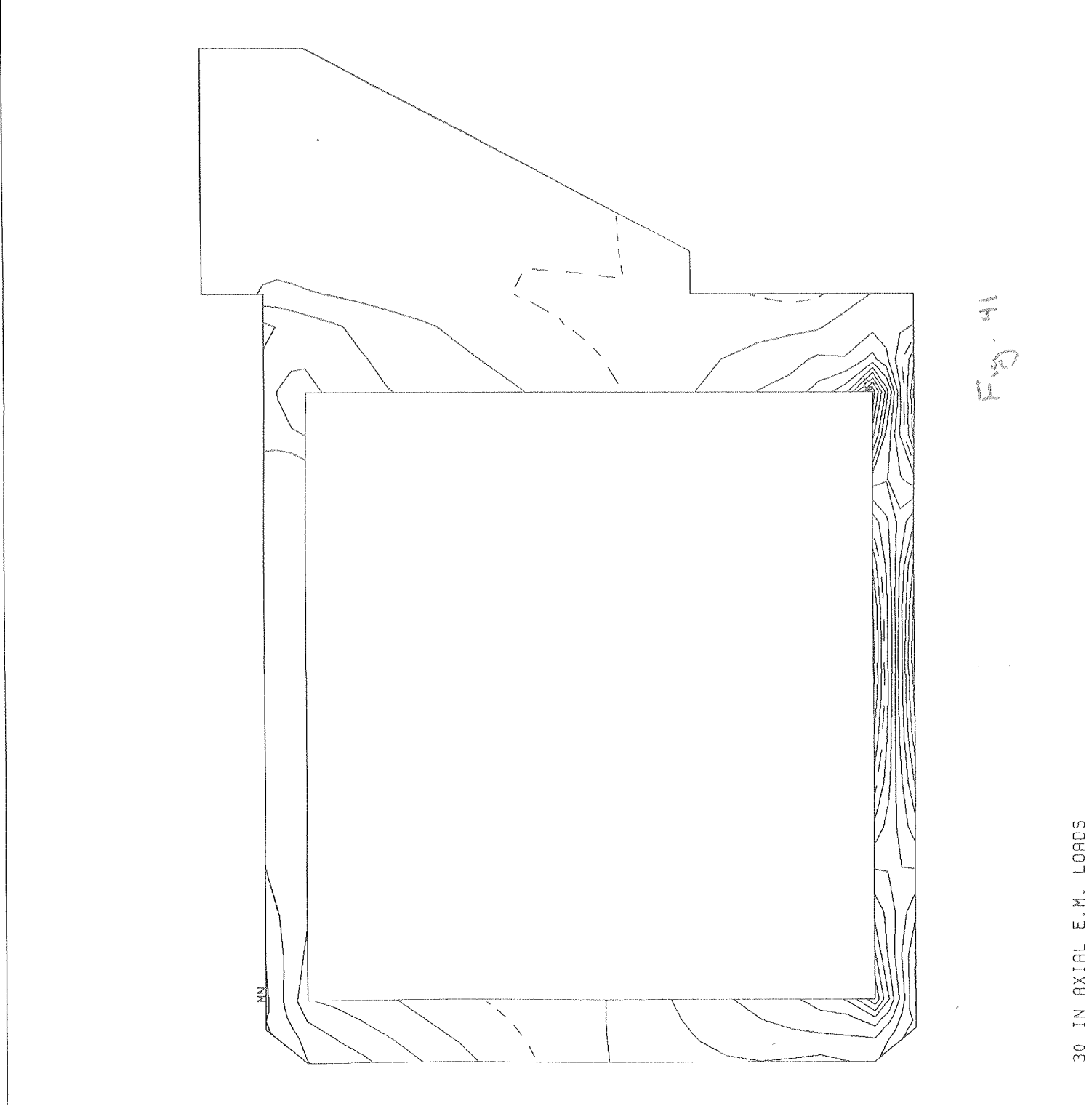


Fig. 4

RNSYS
84/ 4/ 5
16.0289
PLOT NO. 31
POST1
STEP=6
ITER=1
STRESS PLOT
SX
ORIG SCALING
ZV=1
DIST=8.94
XF=31.9
YF=.5
EDGE
DMAX=.0292
MX=28961
MN=-27533
INC=4000

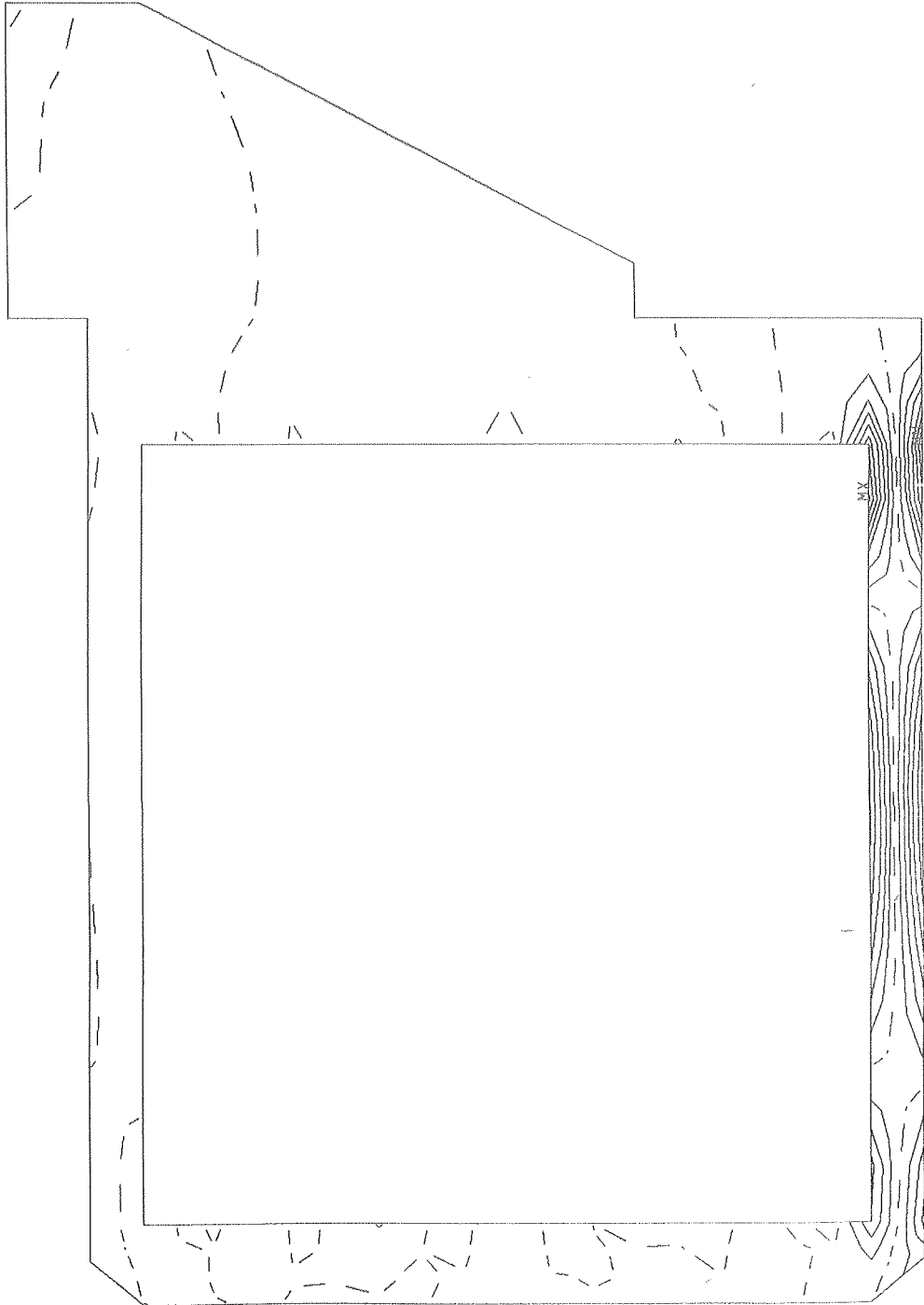


Fig 42

Axis

ANSYS
84/ 4/ 5
16.0294
PLOT NO. 32
POST1
STEP=6
ITER=1
STRESS PLOT
SY
ORIG SCALING
ZV=1
DIST=8.94
XF=31.9
YF=.5
EDGE
DMAX=.0292
MX=13952
MN=-5893
INC=1250

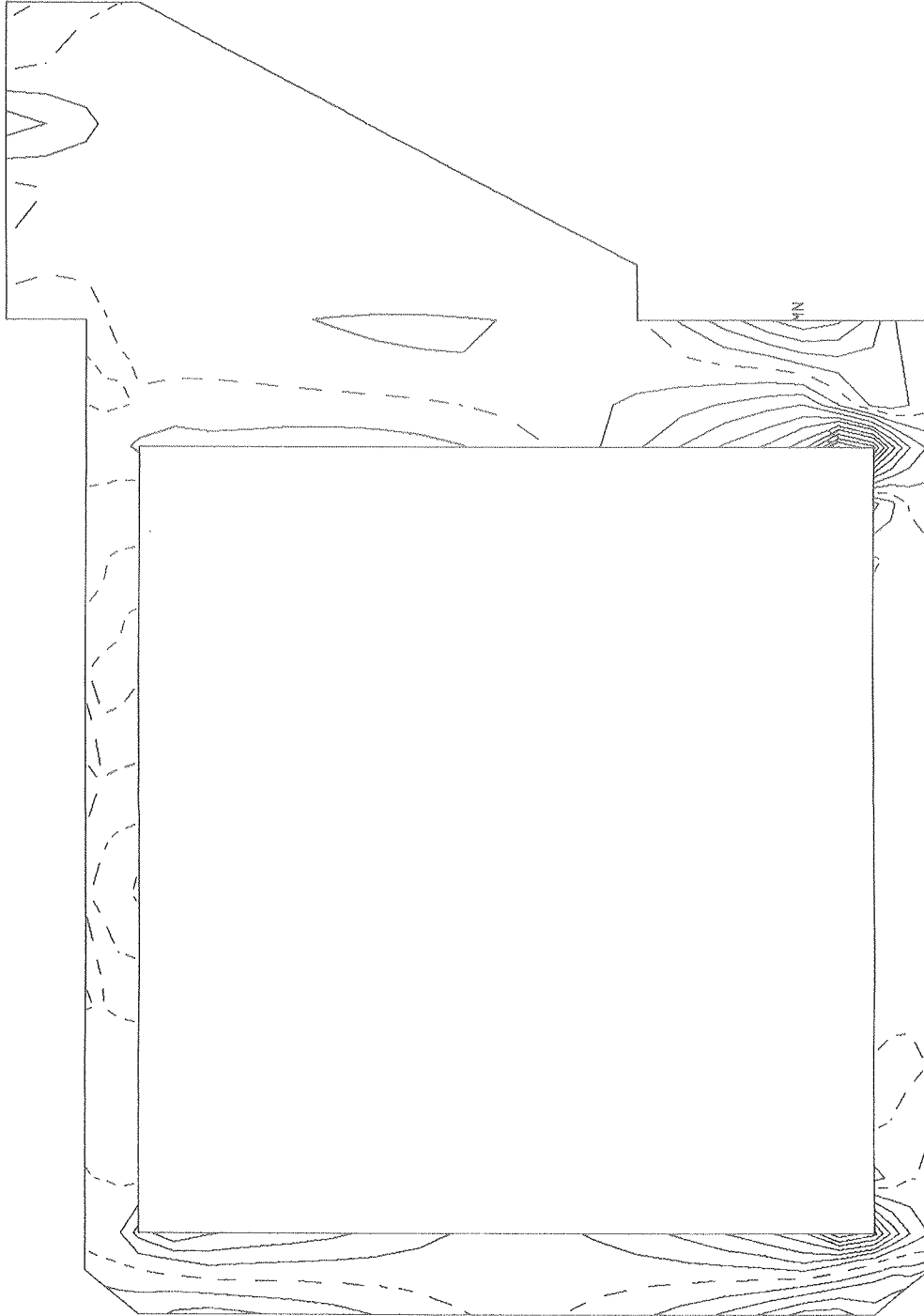


Fig 43

ANSYS
84/ 4/ 5
16.0869
PLOT NO. 42
POST1
STEP=9999
ITER=1
STRESS PLOT
SZ
ORIG SCALING
ZV=1
DIST=8.94
XF=31.9
YF=.5
EDGE
DMAX=.017
MX=3874
MN=-29193
INC=2000

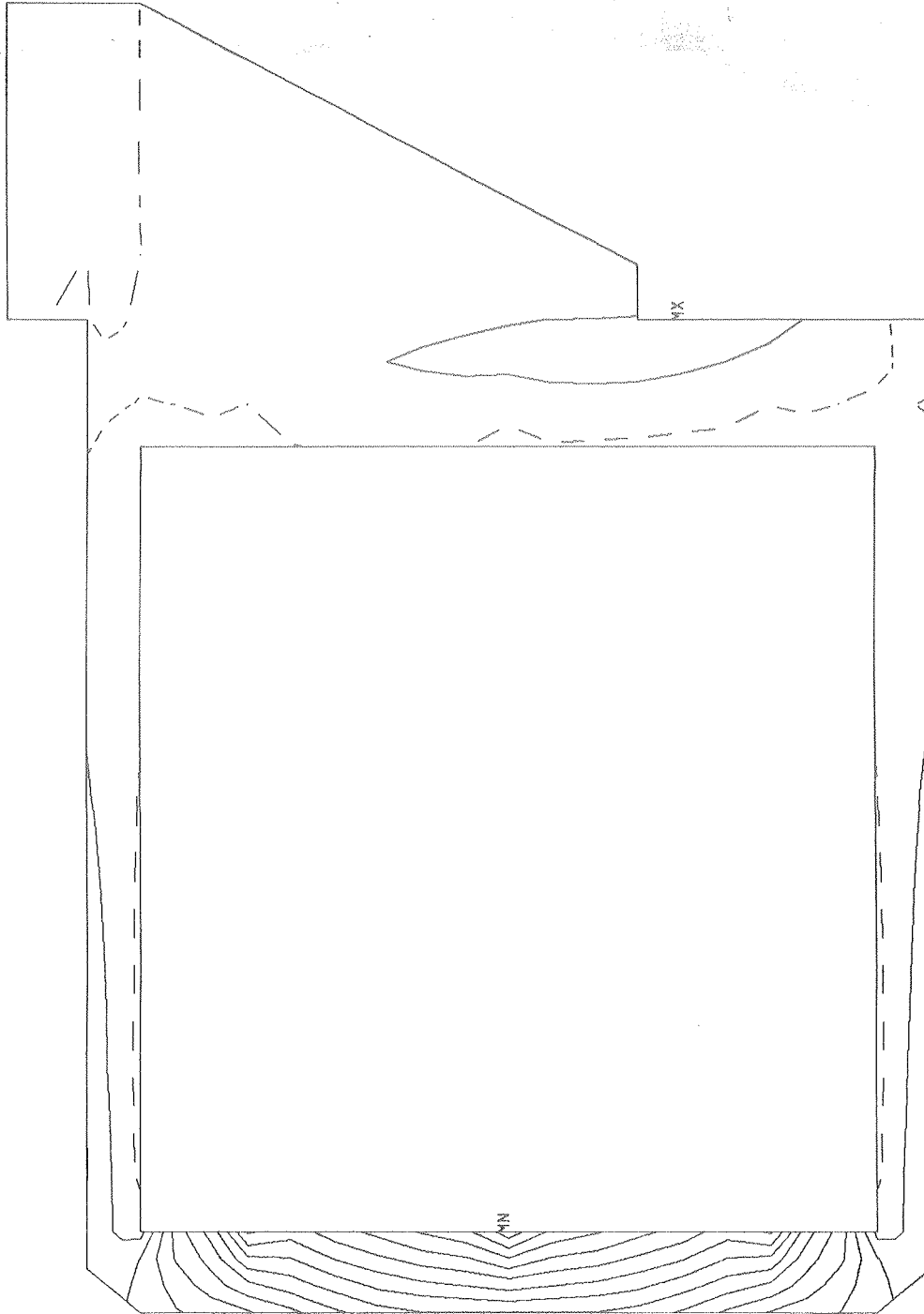


Fig 44

ANSYS
84/ 4/ 5
16.0881
PLOT NO. 43
POST1
STEP=9999
ITER=1
STRESS PLOT
SX
ORIG SCALING
ZV=1
DIST=8.94
XF=91.9
YF=.5
EDGE
DMAX=-.017
MX=16477
MN=-9236
INC=2000

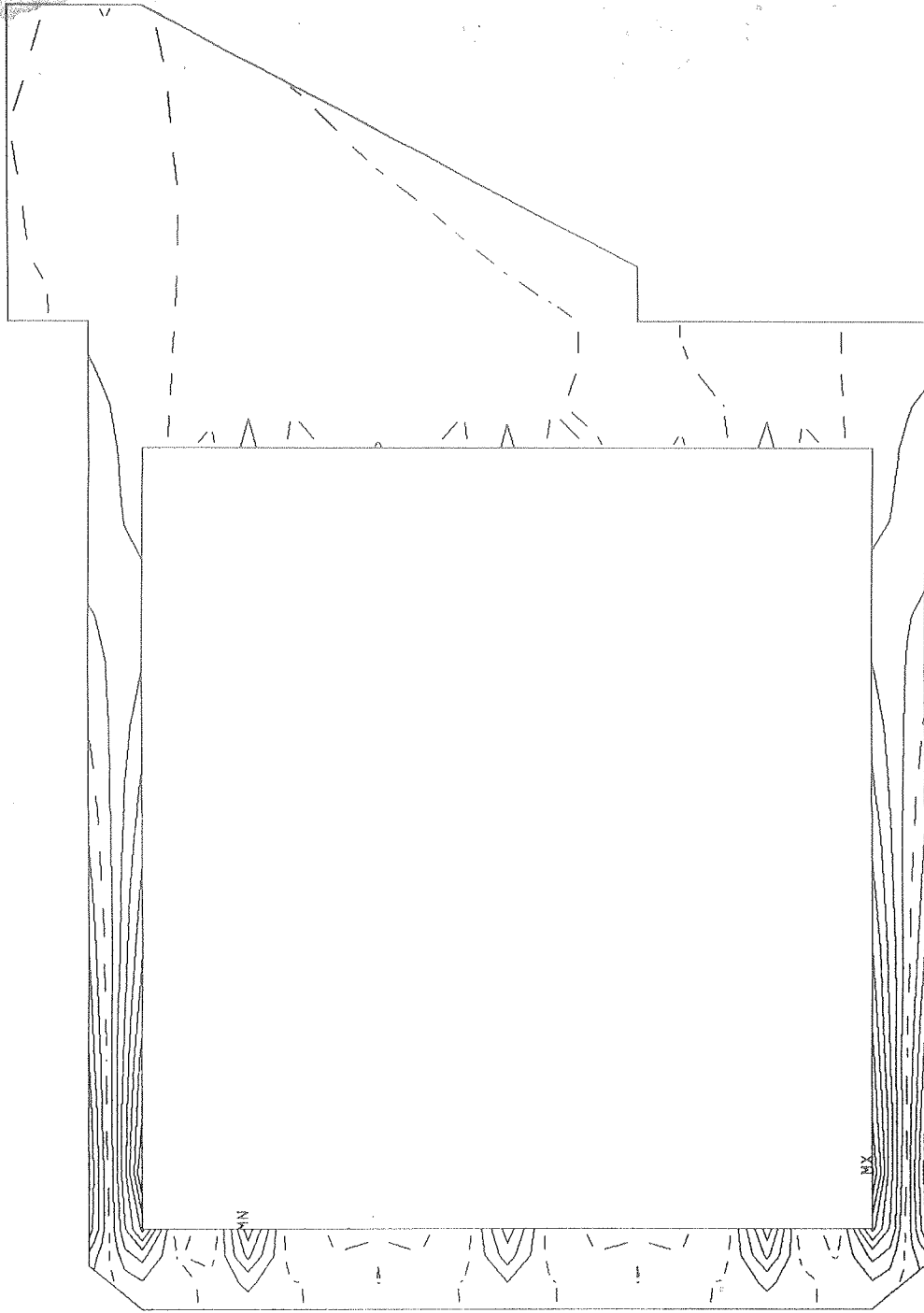


Fig 45

ANSYS
84/ 4/ 5
16.0886
PLOT NO. 44
POST1
STEP=9999
ITER=1
STRESS PLOT
SY
ORIG SCALING
ZV=1
DIST=8.94
XF=31.9
YF=.5
EDGE
DMAX=.017
MX=23661
MN=-24061
INC=4000

4/8

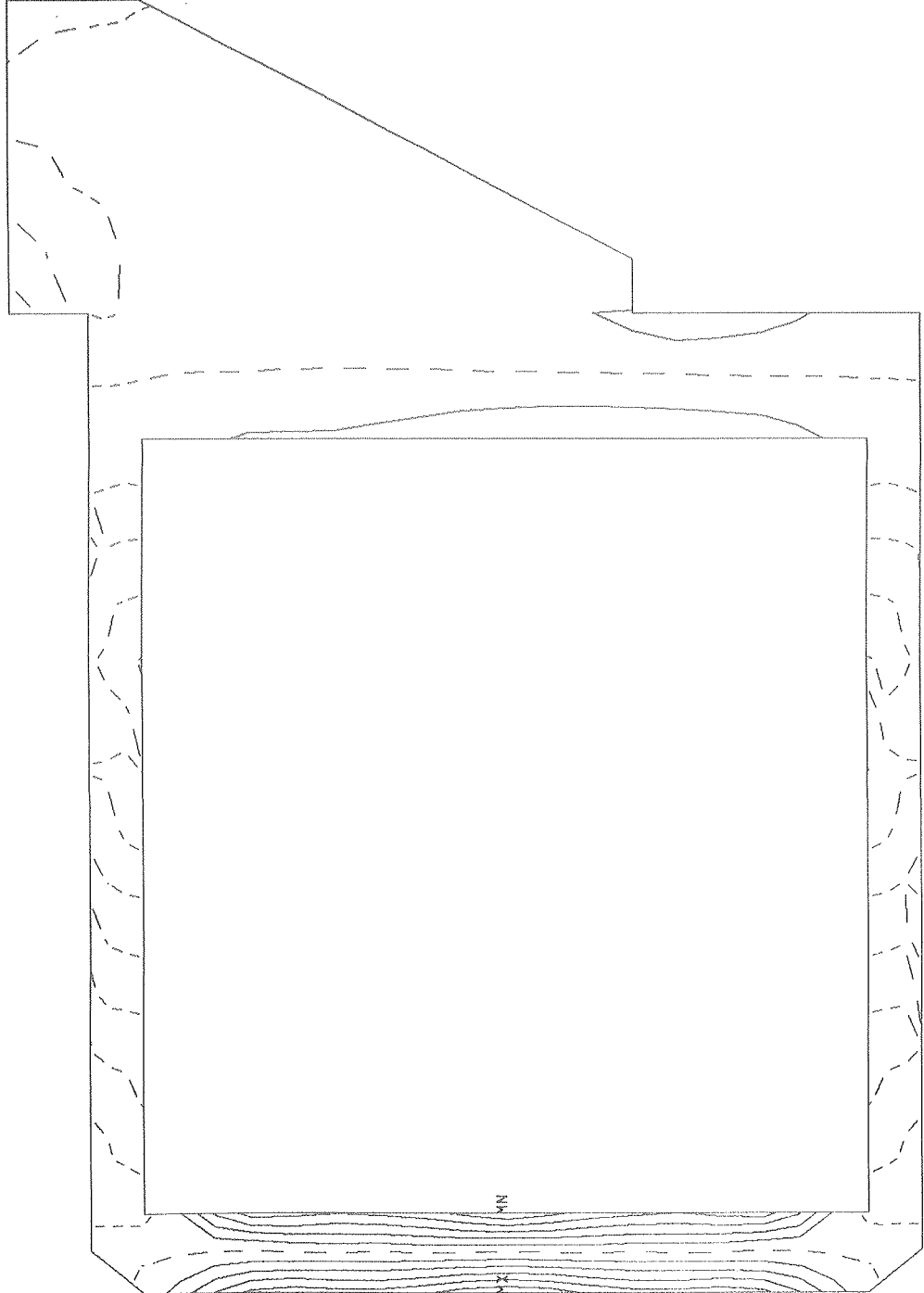


Fig 2

RNSYS
84/ 4/ 5
16.0894
PLOT NO. 45
POST1
STEP=9999
ITER=1
STRESS PLOT
SIGE
ORIG SCALING
ZV=1
DIST=8.94
XF=31.9
YF=.5
EDGE
DMAX=.017
MX=33071
MN=2.45
INC=2000

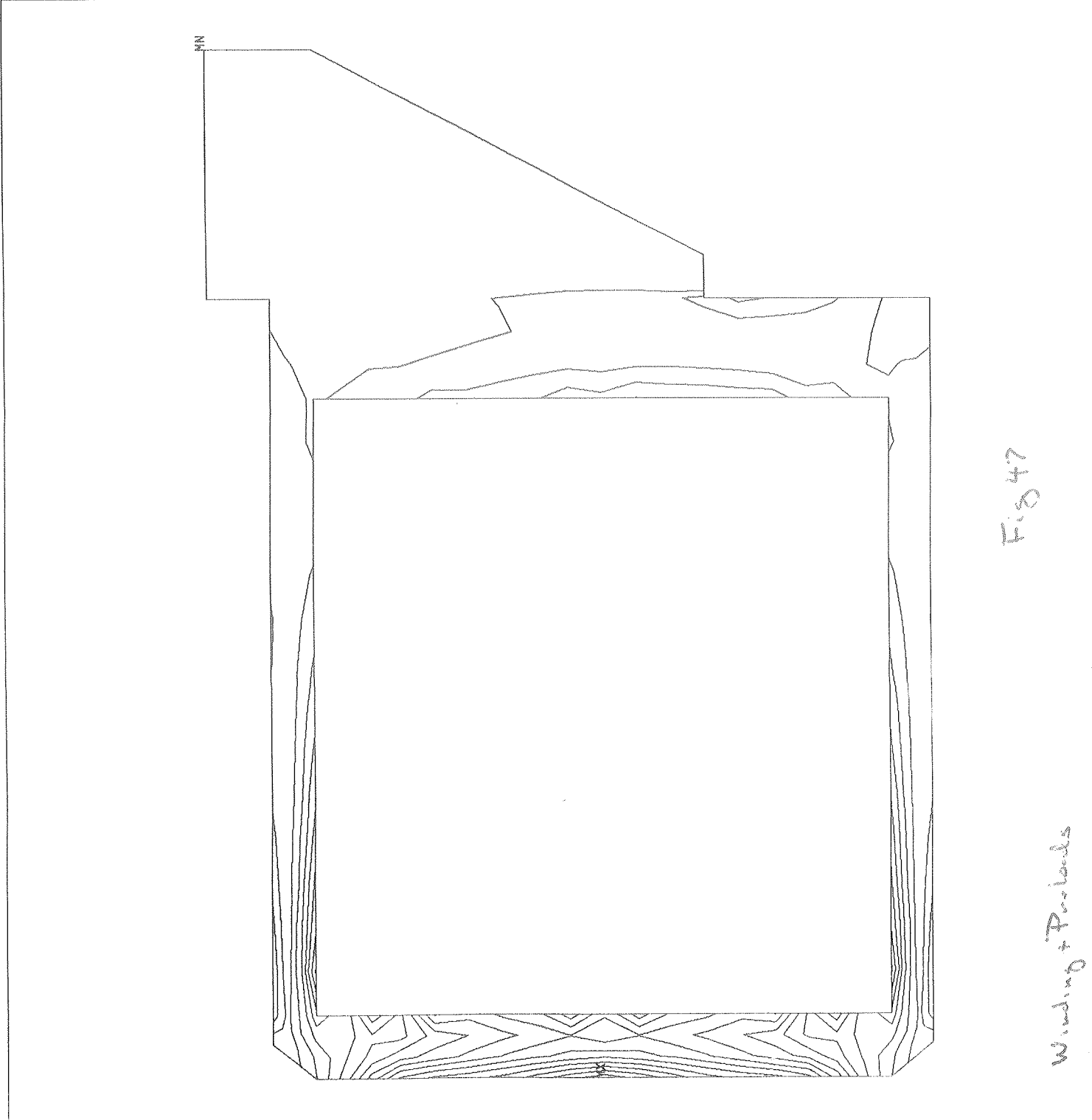


Fig 47

Winding + Poissons

ANSYS
84/ 4/ 5
16.1197
PLOT NO. 50
POST1
STEP=9999
ITER=1
STRESS PLOT
SZ
ORIG SCALING
ZV=1
DIST=8.94
XF=31.9
YF=.5
EDGE
DMAX=.125
MX=16558
MN=-1590
INC=1250

59

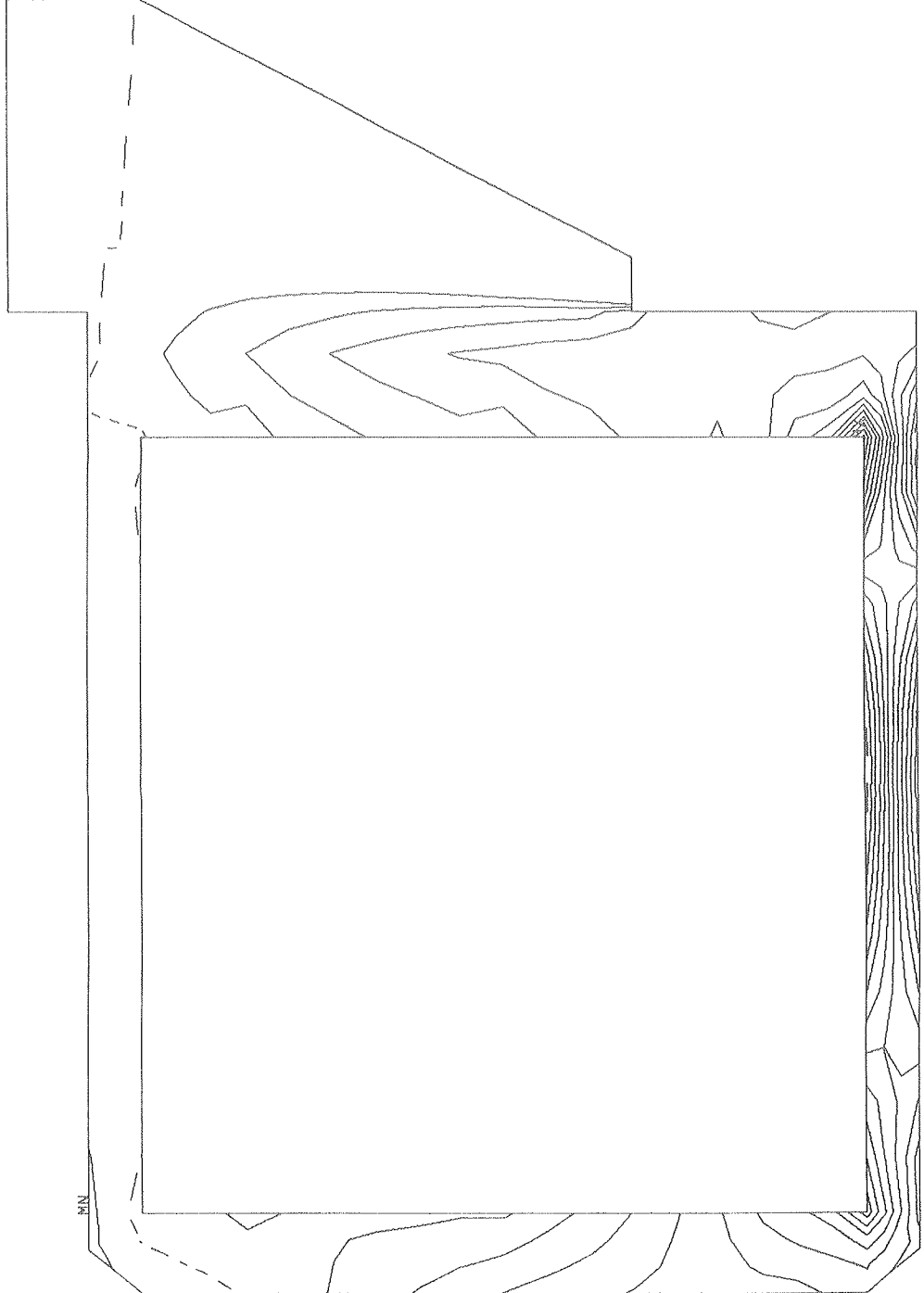


Fig 48

ANSYS
84/ 4/ 5
16.1206
PLOT NO. 51
POST1
STEP=9999
ITER=1
STRESS PLOT
SX
ORIG SCALING
ZV=1
DIST=8.94
XF=31.9
YF=.5
EDGE
DMAX=.125
MX=32421
MN=-28071
INC=4000

60

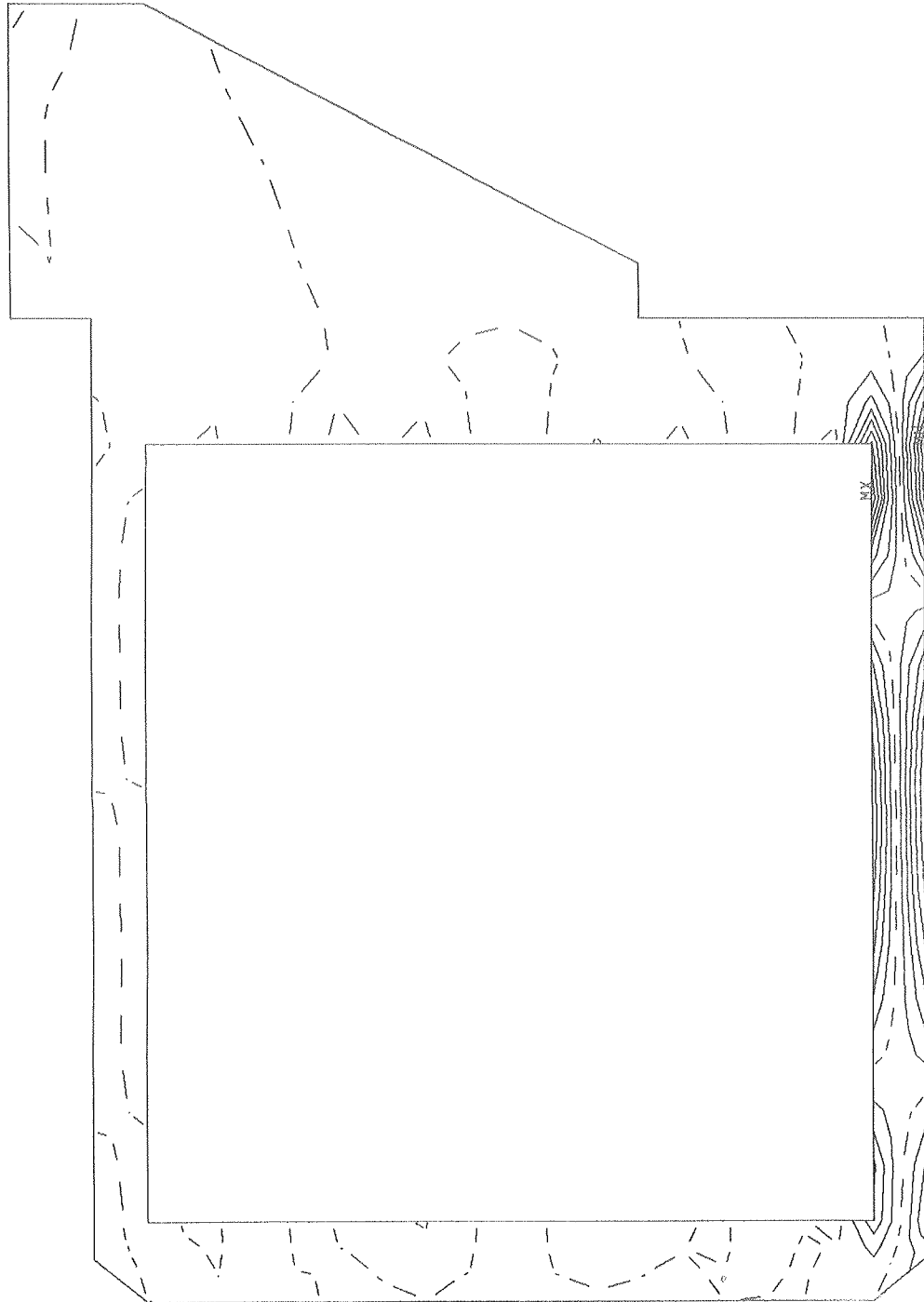


Fig 49

ANSYS
84/ 4/ 5
16.1214
PLOT NO. 52
POST1
STEP=9999
ITER=1
STRESS PLOT
SY
ORIG SCALING
ZV=1
DIST=8.94
XF=31.9
YF=.5
EDGE
DMAX=.125
MX=12922
MN=-5205
INC=1250

50

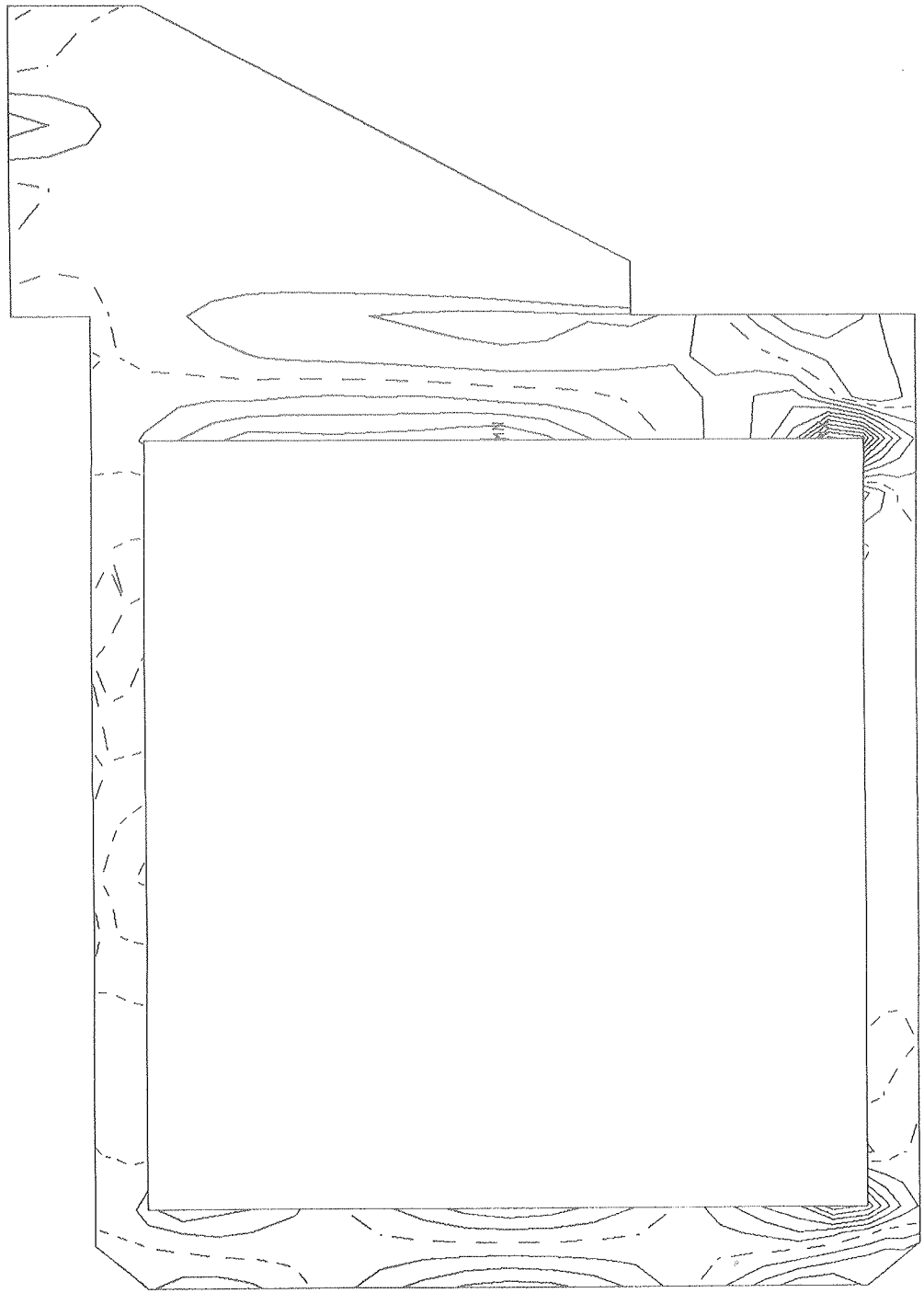
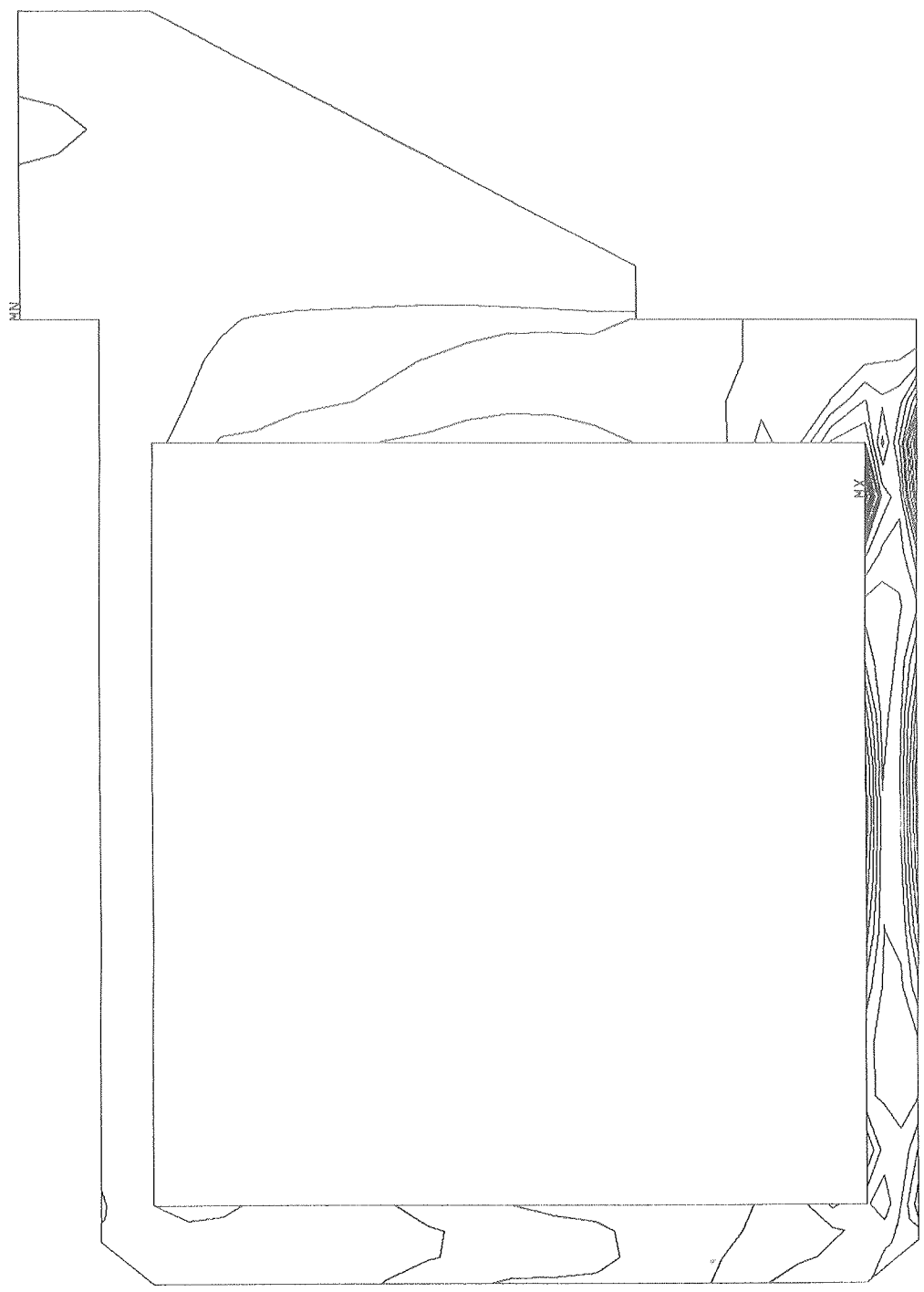


Fig 50

ANSYS
84/ 4/ 5
16.1219
PLOT NO. 53
POST1
STEP=9999
ITER=1
STRESS PLOT
SIGE
ORIG SCALING
ZV=1
DIST=8.94
XF=31.9
YF=.5
EDGE
DMAX=.125
MX=31270
MN=100
INC=2000



15.8.51

All Loads

ANSYS
84/ 4/ 5
16.1228
PLOT NO. 54
POST1
STEP=9999
ITER=1
STRESS PLOT
SI
ORIG SCALING
ZV=1
DIST=8.94
XF=31.9
YF=.5
EDGE
DMAX=.125
MX=35927
MN=114
INC=2000

52

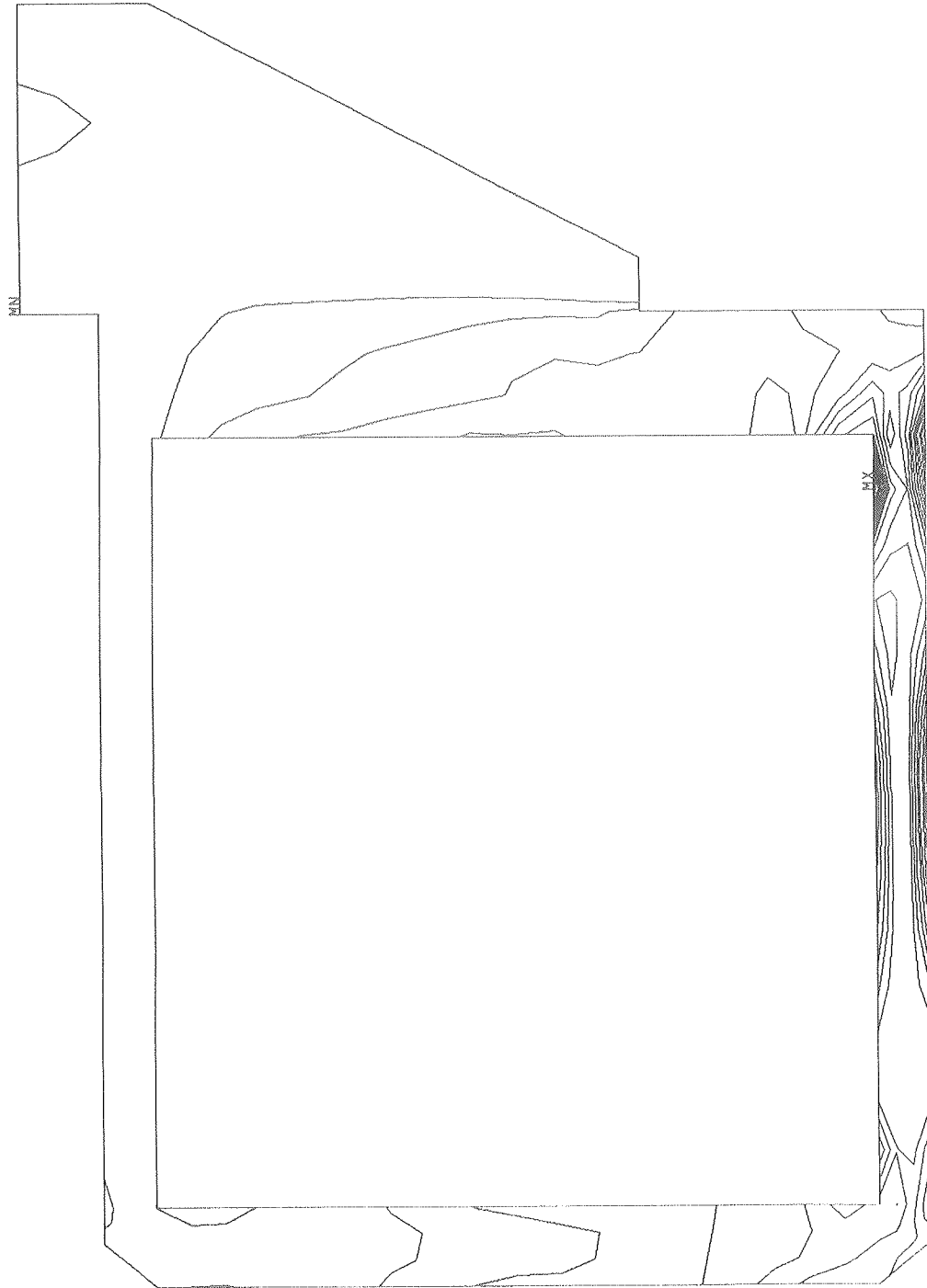


Fig 52

ANSYS
84/ 5/30
14.9244
PLOT NO. 1
POST1
STEP=9999
ITER=1
STRESS PLOT
SX

ORIG SCALING
ZV=1
DIST=4.78
XF=25
EDGE
DMAX=.0246
MX=2387
MN=-11344
INC=800

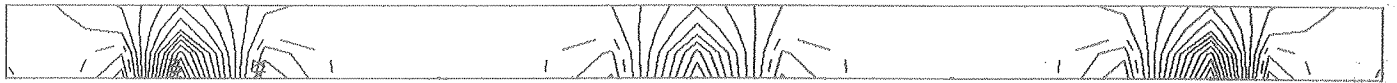
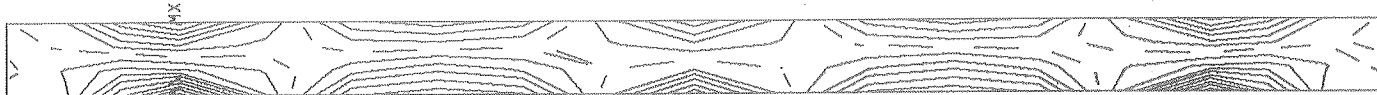


Fig. 53. Inner Push Bar

ANSYS
84/ 5/30
14.9250
PLOT NO. 2
POST1
STEP=9999
ITER=1
STRESS PLOT
SY
ORIG SCALING
ZV=1
DIST=4.78
XF=25
EDGE
DMAX=.0246
MX=8111
MN=-12020
INC=1250



HSB.F

ANSYS
84/ 5/30
14.9250
PLOT NO. 3
POST1
STEP=9999
ITER=1
STRESS PLOT
SIGE

ORIG SCALING
ZV=1
DIST=4.78
XF=25
EDGE
DMAX=.0246
MX=13074
MN=531
INC=800

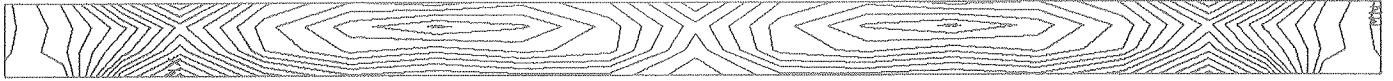


Fig. 55

55

```

ANSYS
84/ 6/ 6
14.2322
PLOT NO. 6
POST1
STEP=9999
ITER=1
STRESS PLOT
SY
ORIG SCALING
ZV=1
DIST=4.33
XF=38
YF=2.31
DMAX=.125
OSCA=3.46
MX=3221
MN=-469
INC=250

```

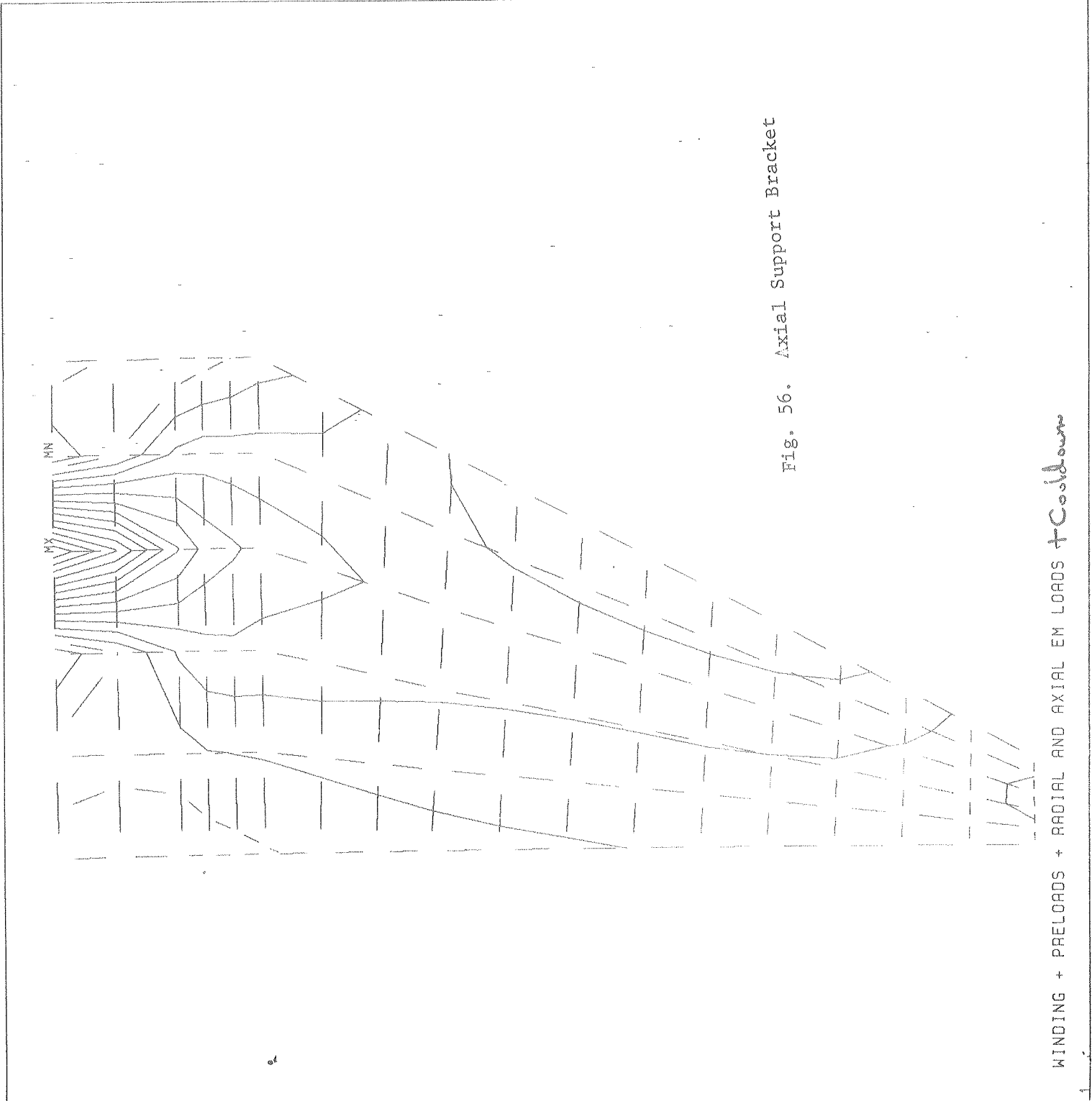


Fig. 56. Axial Support Bracket

53

54

ANSYS
 84/ 6/ 6
 14.2325
 PLOT NO. 7
 POST1
 STEP=9999
 ITER=1
 STRESS PLOT
 SX
 ORIG SCALING
 ZV=1
 DIST=4.33
 XF=38
 YF=2.31
 DMAX=.125
 DSCA=3.46
 MX=1376
 MN=-747
 INC=125

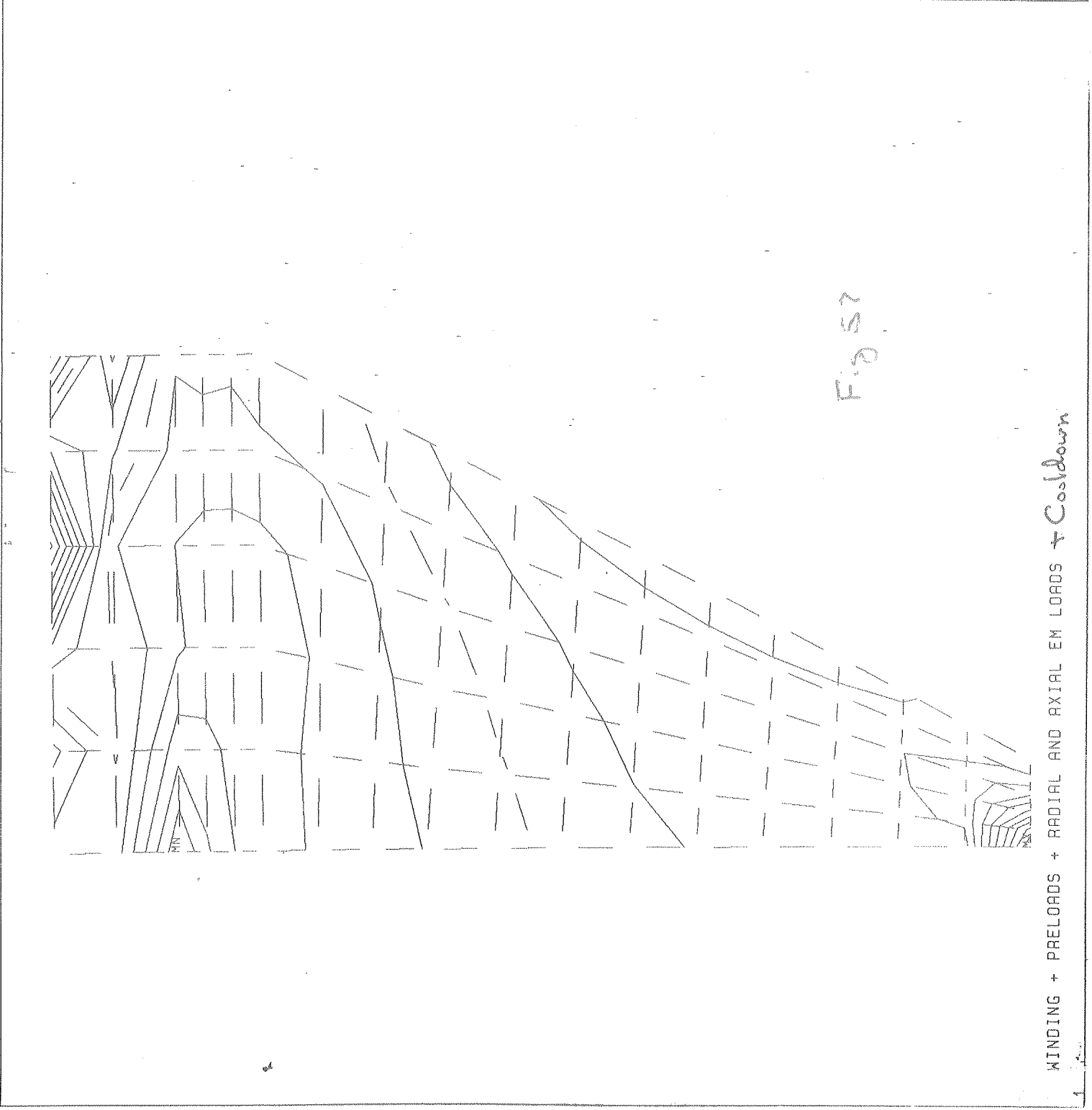


Fig 57

WINDING + PRELOADS + RADIAL AND AXIAL EM LOADS + Cosdown

ANSYS
84/ 6/ 6
14.2328
PLOT NO. 8
POST1
STEP=9999
ITER=1
STRESS PLOT
SIGE
ORIG SCALING
ZV=1
DIST=4.93
XF=38
YF=2.31
DMAX=.125
DSCA=3.46
MX=3093
MN=100
INC=200

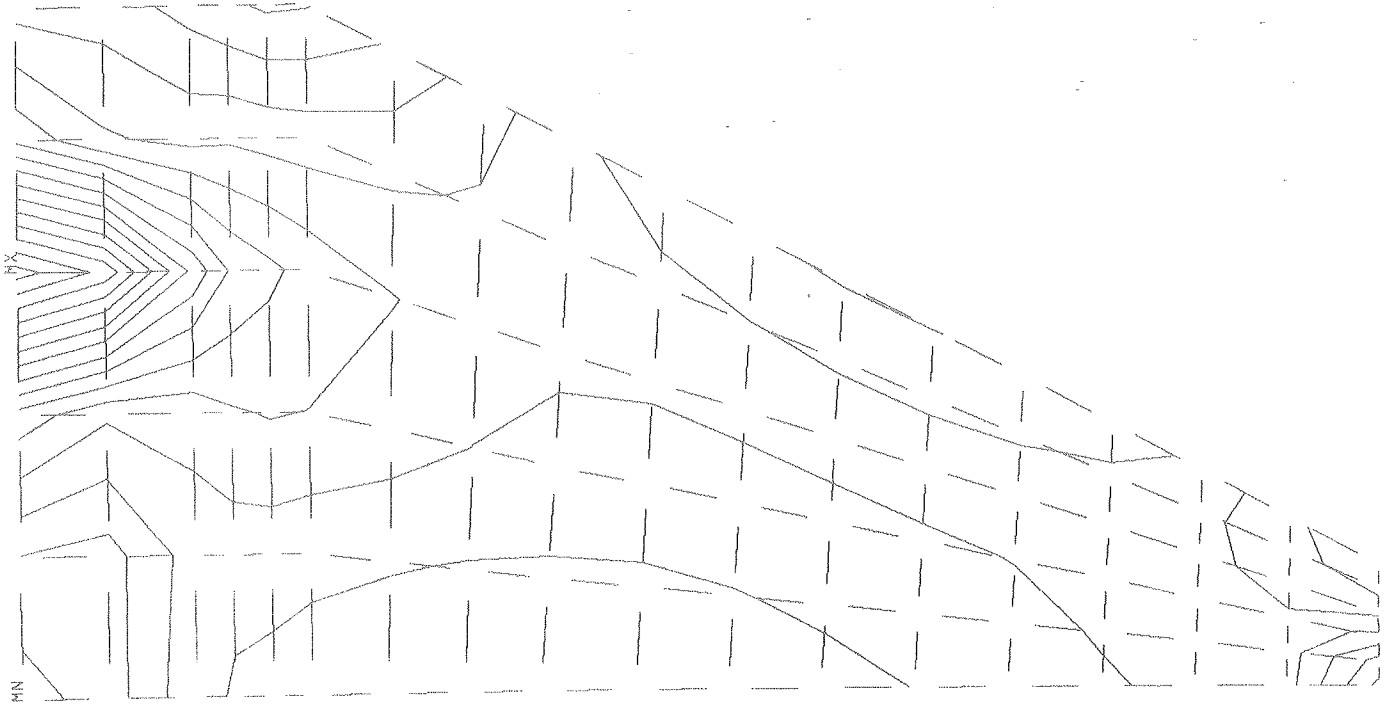


Fig 58

WINDING + PRELOADS + RADIAL AND AXIAL EM LOADS + Cooledown

Discussion of Stresses and Deflections:

The full axisymmetric model is rather unusual in that widely varying moduli are used in different load steps. Care must be taken in interpreting stresses and deflections especially for the combined load cases. For example relatively large deformations occur in the outer wall and axial support bracket during winding due to their low modulus. In fact they experience zero deformation because they are not physically welded to the bobbin at this point. Deflections are essentially unimportant to us and will not be discussed further.

All peak stresses given in Table 2 are averaged nodel stresses from connecting elements. These are found in the post processing. The maximum Von Mises stress in the cryostat is 38 Ksi and occurs in the inner wall after preloading. Stresses in the coil, preload bars, and axial support bracket require additional explanation. When considering all load cases except winding the following maximum conductor stresses are found.

$$\begin{aligned}\sigma_{\theta}(\text{conductor}) &= \sigma_{\theta}(\text{coil}) \frac{A_{\text{coil}}}{A_{\text{conductor}}} = \sigma_{\theta}(\text{coil}) \frac{70.79}{.0167 \times 2840} \\ &= 1.49 \sigma_{\theta}(\text{coil})\end{aligned}$$

based on a conductor area of .0167 in²

Thus excluding winding stresses the maximum hoop stress in the conductor is 1.49 x 11483 = 17,100 psi or 286 lbs of tension. This occurs in the first layer.

$$\sigma_r(\text{conductor}) = \sigma_r(\text{coil}) \times \frac{2 \pi r}{\text{Total G-10 width}} = \sigma_r(\text{coil}) \times \frac{2 \pi r}{60 \times .75}$$

The largest radial compressive coil stress is at r = 30.25. The maximum bearing pressure on the conductor is then given by -831 x 4.22 = -3510 psi.

Stresses given for the preload screws, push bars, and axial support bracket must be further analyzed to find the true stress since these are discontinuous structures modeled as continuous axisymmetric elements.

Preload Screws:

Maximum load on inner screws = 91800 lbs/radian
(after winding & preloads)

Maximum load on inner screws = -54280 lbs/radian
(all loads combined)

Table 2

Peak Stresses in Cryostat and Coil

| | Cryostat Stresses | | | S.I. | Avg. Coil Stresses | | | Force in Preload Screws (lbs/radian) | | | |
|--------------------------|--------------------|--------------------|--------------------|-------|--------------------|--------------------|--------------------|--------------------------------------|------------------|-------------------|------------------|
| | S _z max | S _x max | S _y max | | SIGE | S _z max | S _x max | S _y max | Inner Top/Bottom | Inner Center | Outer Top/Bottom |
| Winding | -6154 | -1653 | -4285 | 6578 | 7571 | --- | --- | -16500 | -16500 | 0 | 0 |
| Inner Preload | -18441 | 10355 | -13967 | 20223 | 23140 | 3961 | -1279 | -53100 | -53100 | 0 | 0 |
| Outer Preload | 4657 | 5410 | 5914 | 6987 | 7679 | -1682 | -560 | -22200 | -7420 | -40000 | -40000 |
| Cooldown | -4679 | -4566 | 5972 | 7094 | 7811 | 2130 | 588 | 14780 | 8590 | 35750 | 44050 |
| Radial E.M. | 25398 | -12745 | 14065 | 26082 | 30110 | 6029 | 1944 | 87300 | 65130 | -40890 | -44231 |
| Axial E.M. | 12314 | 28961 | 13952 | 28371 | 32400 | 1365 | -158 | -2060 | -5870 | 4540 T -9140 B | -1870 |
| Winding & Preloads | -29193 | 16477 | 23661 | 33071 | 37620 | --- | --- | -91800 | -77020 | -40000 | -40000 |
| All Loads | 16558 | 32421 | 12922 | 31270 | 35927 | --- | --- | 8220 | -9170 | -54280 | -42050 |
| All Loads Except Winding | --- | --- | --- | --- | --- | 11483 | -831 | --- | --- | --- | --- |

Using the stress areas of the screws,

$$\sigma_{\max}(\text{inner}) = \frac{-91800 \times 2\pi/60}{.226} = -42,500 \text{ psi at } 300 \text{ K}$$

$$\sigma_{\max}(\text{outer}) = \frac{-54280 \times 2\pi/60}{.334} = -17,020 \text{ psi at } 4.2 \text{ K}$$

Push Bars:

$$\sigma_r(\text{true}) = \sigma_r(\text{ANSYS}) \times \frac{\text{Total Area}}{\text{Area of Bars}} = \sigma_r(\text{ANSYS}) \frac{2 \pi r}{60 \times 1.25}$$

The worse case is again after winding and preloading at room temperatures for the inner push bar at $r = 25.225''$.

For these inner push bars,

$$\sigma_r(\text{true}) = \sigma_r(\text{ANSYS}) \times 2.11$$

$$\sigma_r(\text{true max}) = 23,980 \text{ at } 300 \text{ K}$$

True bending stresses are more complicated due to the G-10 bonded to the stainless steel push bars which is a parallel component as opposed to a series component in the radial case. The correct axial or bending modulus of 7.95×10^6 psi modulus was selected to get the correct bending deflections.

This modulus was calculated by considering both the discontinuities of the bars and their fictitious extra thickness. The ANSYS output gives correct deflections, but these deformations are in an imaging material. Since $\sigma = \epsilon E$ we must multiply axial bending stresses in ANSYS by $30/7.95 = 3.77$. Now we have correct stresses in a .455 thick solid stainless steel bar that has the correctly deformed shape. This means that we also have the correct bending moments in these bars if the assembly of STIF 42 elements are thought of as a simple beam. However, the actual beam or push bar is only .375" thick. Since $\sigma_{\text{bend}} \sim M/t^2$ we must multiply these axial bending stresses by an additional factor of $(.455/.375)^2$. Thus for the inner push bar,

$$\begin{aligned} \sigma_y(\text{true bending}) &= \sigma_y(\text{ANSYS}) \times \frac{30 \times 10^7}{7.95 \times 10^7} \times (.455/.375)^2 \\ &= \sigma_y(\text{ANSYS}) \times 5.56 \end{aligned}$$

$$\sigma_y(\text{true peak bending}) = -12,020 \times 5.56 = -67,000 \text{ psi at } 300 \text{ K}$$

Likewise for the outer push bar,

$$\begin{aligned}\sigma_y(\text{true bending}) &= \sigma_y(\text{ANSYS}) \times \frac{30 \times 10^7}{6.09 \times 10^6} \times (.755/.625)^2 \\ &= \sigma_y(\text{ANSYS}) \times 7.19\end{aligned}$$

$$\sigma_y(\text{true peak bending}) = -3754 \times 7.19 = -27,000 \text{ psi at } 4.2 \text{ K}$$

which occurs when all load cases are combined. Peak bending stresses in the inner bar are not nearly as high as they seem. The inner screws have a flat end of 7/16" diameter which not only distributes the load but also reduces the span between loads.

Outer Axial Support Bracket:

The outer axial support bracket is again another discontinuous structure which is modeled as being axisymmetric. Plots are shown only for the combined load case, but the axial loading causes virtually all the stress in this member. As before, stress results from ANSYS should be multiplied by the ratio True Area/Total Area = E(stainless steel)/E(ANSYS) = 14.3. However, the top two element rows are in reality made of eight separate very thick pieces of stainless. Thus the peak stresses found at the point loading are much less than $14.3 \times \sigma(\text{ANSYS})$. The true peak bearing stress at the point loading is given by $62,500 \text{ lbs}/(\pi/4 \times 3^2) = 8800 \text{ psi}$. The peak stress in the gussets which make up the bracket are found at the bottom connection to the outer cryostat wall.

$$\sigma(\text{True Von Mises}) = 1661 \times 14.3 = 23,750 \text{ psi}$$

$$\sigma(\text{True Stress Intensity}) = 1712 \times 14.3 = 24,500 \text{ psi}$$

$$\sigma(\text{True Radial}) = 1376 \times 14.3 = 19,700 \text{ psi}$$

These stresses only appear at 4.2 K.

3D FINITE ELEMENT ANALYSIS BY COMPUTERIZED ENGINEERING

As the cryostat was being machined Fermilab let out a contract to Computerized Engineering for a 1/4 3D model of the cryostat shell. The following load cases were run.

1. 900 psi radially outward on the outer cylinder.
2. 900 psi radially outward on the inner cylinder.
3. 500,000 lbs (TRIM #37) distributed on the bottom and top annular cryostat plates.
4. 150,000 lb load distributed sinusoidally ($P_r = 300 \sin \theta$ psi) on the outer wall which simulates the radially downward decentering forces.
5. Load cases 1, 2, and 3 combined.
6. Load cases 1, 2, 3 and 4 combined.

Figure 59 is the 3D ANSYS model. See Appendix A for the C.E. report details.

The following table is based on modified 3D results which correspond to 740 psi inner preload, 400 psi outer preload, and 462,000 lbs of axial loading which are the input values to my axisymmetric ANSYS runs. The stress in the gusset for the 3D run is divided by two to correspond to the addition of two more (total of 4) 1/2" gussets which was the case analyzed in the axisymmetric run.

Comparison of Von Mises Stress
(psi)

| Load Case | 3D | Axisymmetric |
|------------------------------------|--------|--------------|
| Inner Wall Load 740 psi | 19300 | 20223 |
| Outer Wall Load 400 psi | 7420 | 6987 |
| Axial Load, Cryostat 462,000 lb | 21,700 | 28371 |
| Axial Load Support gusset | 12,950 | 23750 |

Close agreement exists between the two models except for axial loading in the gussets. Much higher stresses appear in the axisymmetric model because of peak stresses at the single point restraint. The combined load cases really do not have any importance now that a detailed axisymmetric analysis has been performed.

Load case #4 is very important, however, because this case was not analyzed in the axisymmetric model. The following peak Von Mises stresses are found

SIGE = 5746 psi in the cryostat body

SIGE = 7155 psi in an axial support gusset (plate element)

There are now 4 gussets per post so this stress is actually much lower. The stress of 5746 psi is located in element 57 which is on the O.D. of the cryostat right at the end of the radial arm gussets.

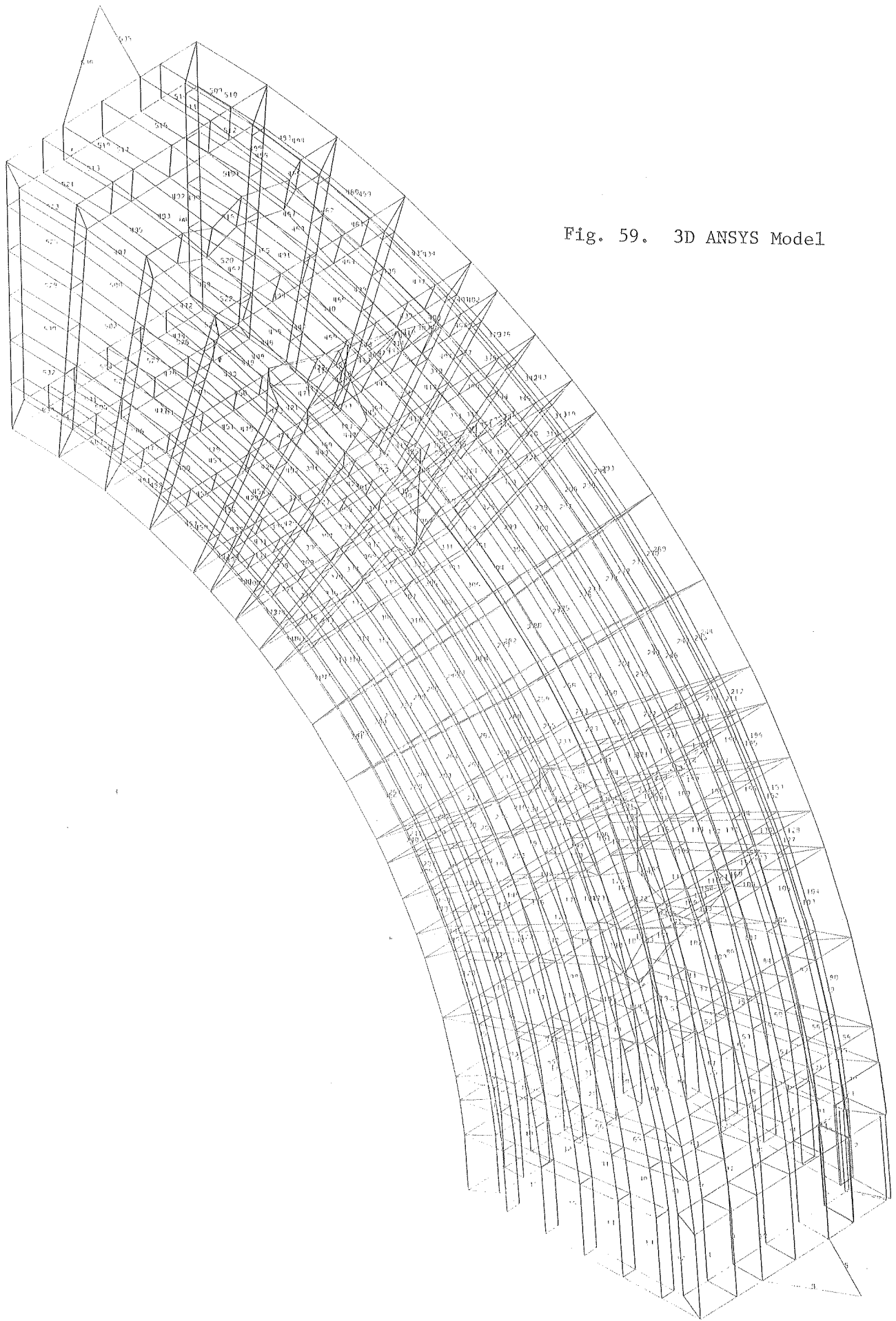


Fig. 59. 3D ANSYS Model

FINITE ELEMENT ANALYSIS OF RADIAL ARM BRACKET

In the previous section the 3D model gave us a maximum Von Mises stress of 5700 psi in the cryostat body for the 150,000 lb radially decentering load case. The welded brackets in which the radial arms are pinned were modeled as very simple pipe elements (STIF9). Bob Wands has performed an ANSYS analysis which looks in detail at these brackets and the cryostat around them. A point load force of 75,000 lbs is applied at the pin hole location of the bracket, and the 1/4 model with an additional plane of symmetry (actually 1/8 model) has the proper symmetry boundary conditions imposed on it. The following peak Von Mises stresses are found.

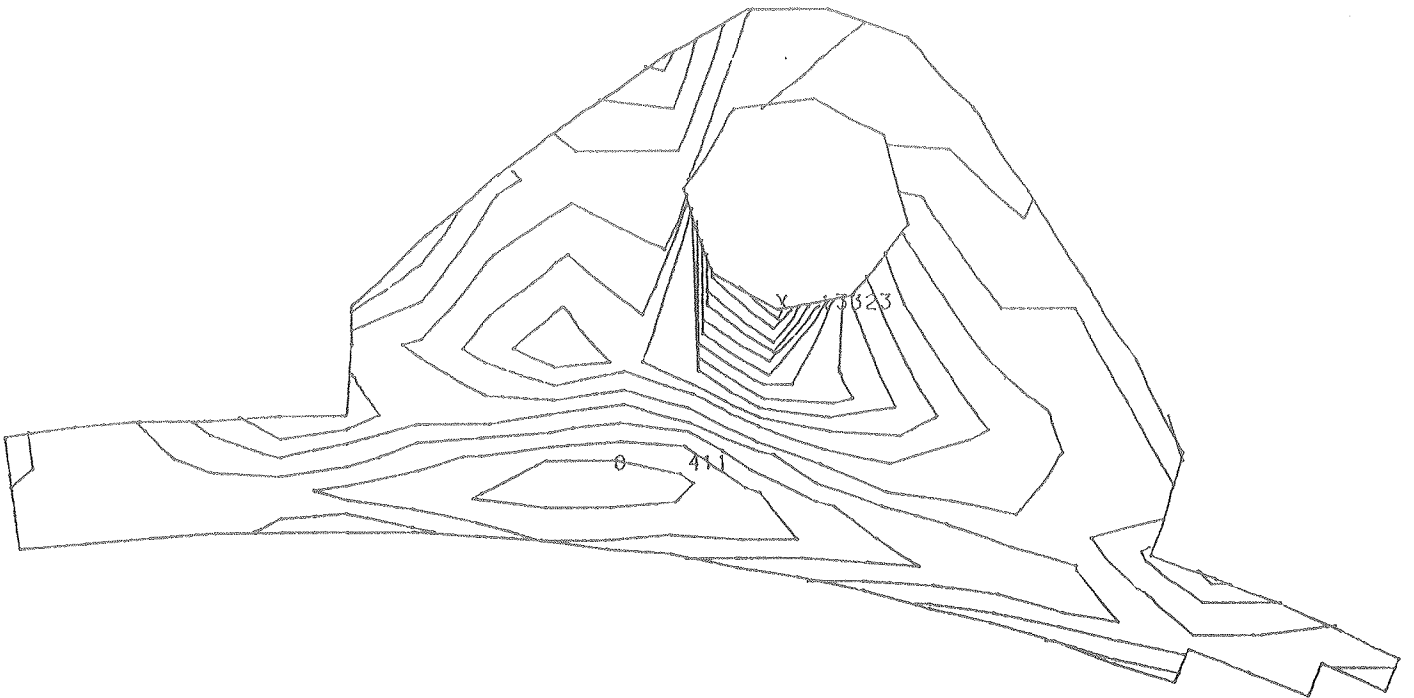
10,090 psi in the cryostat body

13,700 psi in the bracket

Figures 60 to 62 are cross sections through the bracket and outer wall. Note that the cross sections are not necessarily through the peak stress areas. Never the less, this gives a good indication of the stress pattern distribution.

STEP= 1 ITER= 1 TIME= 0

Fig. 60. Radial Arm Bracket



800.00

STEP= 1 ITER= 1 TIME= 0

X

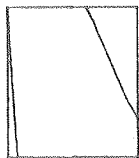
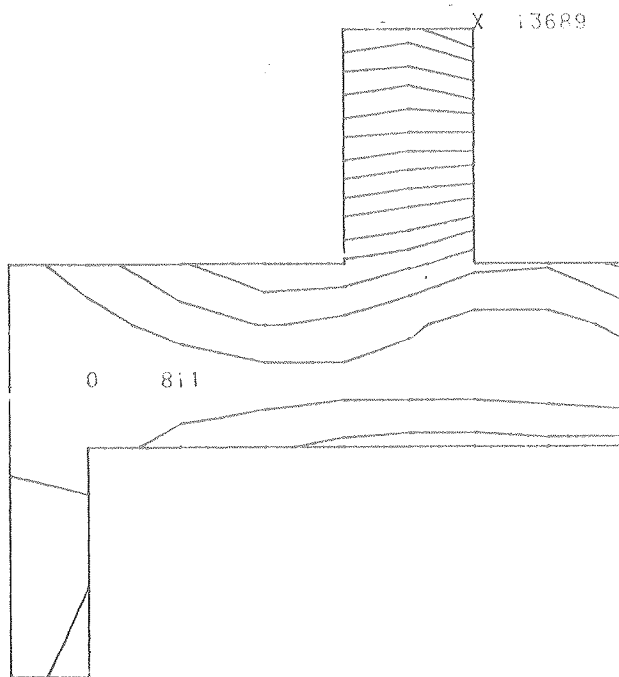
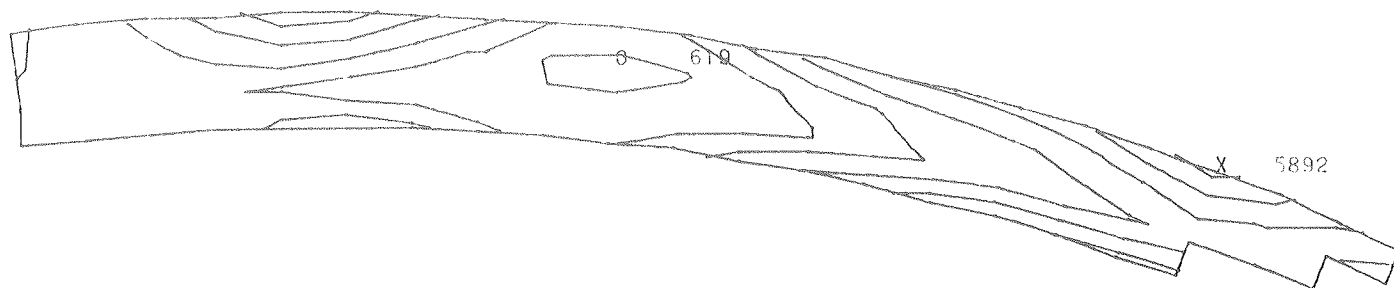


Fig. 61. Cross Section Through Radial Arm Bracket and Cryostat



STEP= 1 ITER= 1 TIME= 0

Fig. 62. Von Mises Stress
Distribution in Cryostat
Outer Wall Due to Radial
Arm Loading



Strength of Material Cryostat Analysis

Since the cryostat was designed with hand calculations it seems worthwhile to review some of these calculations. They serve as a check on the finite element work and provide insight to the stress distribution. The following loads are considered.

1. Uniform Pressures on the Cryostat Inner Surface
2. Axial Loads
3. Radial Decentering Loads

The cryostat was designed using a strength of materials approach and W. Young's solenoid stress program. The stress program provided radial pressure loads for the hand calculation, while the hand calculations provided the correct stiffnesses for the solenoid program. Axial and radial decentering loads were considered as independent problems.

Uniform Pressure Distributions:

The cryostat is modeled with a plane of symmetry through the midplane. Figure 63 shows the dimensions and definitions of pressure, moments, elongation angular deflection and internal forces. The problem is tackled by breaking the cryostat into discrete components and then equating all elongations and angular deflections at both corners to solve the resulting six simultaneous equations for internal forces and moments. I have written a HP41-C program called TOROID which solves for internal corner forces and moments which then can be used to calculate stresses. All of the following table numbers and case numbers refer to Roark and Young's Handbook of Stress and Strain.

Inner Cylinder:

Due to pressure P_i (Table 29, case 1b)

Let $q = -P_i$

$$1) \Delta R_b = -P_i R^2 / Et$$

$$2) \theta_b = 0$$

$$3) \Delta h_b = \frac{P_i R v \ell}{Et}$$

Due to H_b (Table 29, case 1a)

$$4) \Delta R_b = \frac{-H_b v R}{Et}$$

$$5) \theta_b = 0$$

$$6) \Delta h_b = \frac{H_b \lambda}{Et}$$

Due to V_b :

This case does not appear in Table 30 for thin walled cylinders. We need the case of a short thin walled cylinder with one end slope guided. Fortunately short beams on elastic foundations have exactly the same formulation as short thin cylinders, therefore Table 7, case 1 may be used. Replace EI and β in the beam formulation with D and λ in the cylinder case.

$$D = \frac{Et^3}{12(1-\nu^2)} \quad \lambda = [3(1-\nu^2)/R^2t^2]^{1/4}$$

Also replace load W on the beam with $-V_b$ at $x = 0$.

$$7) \theta_b = \frac{-V_b}{2D\lambda^2} \frac{C_2 Ca_3 - C_4 Ca_1}{C_{12}}$$

$$8) \Delta R_b = y_a = \frac{V_b}{2D\lambda^3} \frac{C_1 Ca_1 + C_3 Ca_3}{C_{12}}$$

where y_a is the deflection of the beam

Due to M_b (Table 7, case #4):

Replace M_o with $-M_b$ at $x = 0$

$$9) \theta_b = \frac{M_b}{2D\lambda} \frac{C_2 Ca_2 + C_4 Ca_4}{C_{12}}$$

$$10) \Delta R_b = y_a = \frac{-M_b}{2D\lambda^2} \frac{C_3 Ca_2 - C_1 Ca_4}{C_{12}}$$

Outer Cylinder:

Use the same procedure as for the inner cylinder but notice differences in sign convention.

Due to internal pressure (Table 29, case 1b):

$$11) \Delta R_a = P_o R^2 / Et$$

$$12) \theta_a = 0$$

$$13) \Delta h_a = \frac{-P_o R_a v l}{E t}$$

Due to H_a (Table 29, case 1a):

$$14) \Delta R_a = \frac{-H_a v R}{E t}$$

$$15) \theta_a = 0$$

$$16) \Delta h_a = \frac{H_a l}{E t}$$

Due to V_a (Table 7, case 1):

$$17) \theta_a = \frac{V_a}{2D\lambda^2} \frac{C_2 C_3 - C_4 C_1}{C_{12}}$$

$$18) \Delta R_a = y_a = \frac{-V_a}{2D\lambda^3} \frac{C_1 C_1 - C_3 C_3}{C_{12}}$$

Due to M_a (Table 7, case #4):

$$19) \theta_a = \frac{-M_a}{2D\lambda} \frac{C_2 C_2 + C_4 C_4}{C_{12}}$$

$$20) \Delta R_a = y_a = \frac{M_a}{2D\lambda^2} \frac{C_3 C_2 - C_1 C_4}{C_{12}}$$

Top Plate:

Treat this member as a thin annular plate except under loads V_a and V_b where it is considered to be a thick walled cylinder.

Due to V_b (Table 32, case 1a):

Replace q with $-V_b$ /thickness of plate

$$21) \Delta R_b = \frac{-V_b R_b}{E t} \left[\frac{(R_a^2 + R_b^2)}{(R_a^2 - R_b^2)} + \nu \right]$$

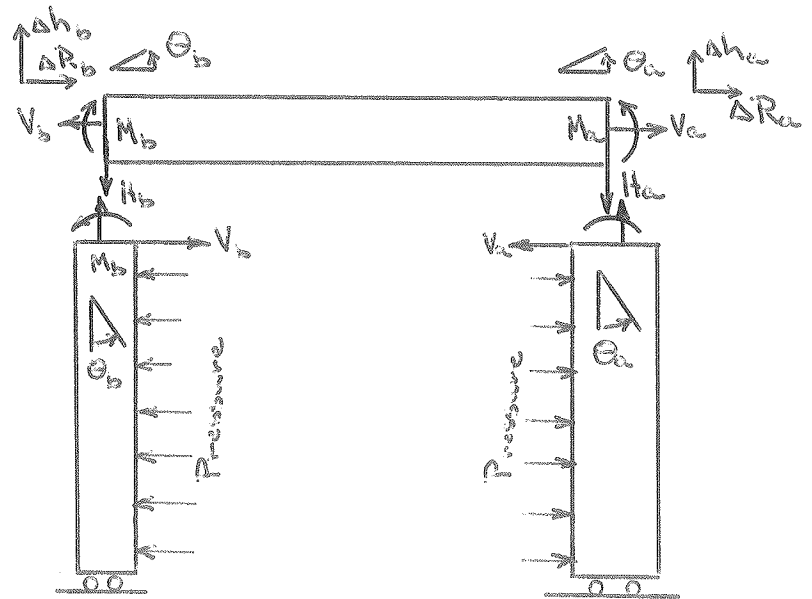


Figure 63

$$22) \Delta R_a = \frac{-V_b}{Et} \frac{2 R_a R_b^2}{R_a^2 - R_b^2}$$

Δl , the change in thickness of the plates, does not enter since the top edge is free. Very small differences in the final height of the cryostat would occur, however:

$$23) \theta_a = \theta_b = 0$$

$$\Delta h_a = \Delta h_b = 0$$

Due to V_a (Table 2, case 1c):

$$q = -V_a/t$$

$$24) \Delta R_a = \frac{V_a R_a}{Et} [(R_a^2 + R_b^2)/(R_a^2 - R_b^2) - \nu]$$

$$25) \Delta R_b = \frac{V_a}{Et} \frac{2 R_a^2 R_b}{R_a^2 - R_b^2}$$

$$26) \theta_a = \theta_b = \Delta h_a = \Delta h_b = 0$$

Due to M_b (Table 24 case 5a):

Treat as a thin annular plate simply supported at the O.D. Let $M_o = M_b$ and $r_o = R_b$. Note that pictures in Table 24 show some incorrect angles and deflections. The stated definitions and tabulations all have the correct sign convention, however.

$$27) \Delta h_b = y_b = \frac{M_b R_a^2}{D} \frac{C_1 L_8 - L_2}{C_7}$$

$$28) \theta_b = \frac{-M_b R_a L_8}{DC_7}$$

$$29) \theta_a = \frac{-M_b R_a}{D} \frac{C_4 L_8 - L_5}{C_7}$$

$$30) \Delta h_a = \Delta R_a = \Delta R_b = 0$$

Due to M_a (Table 24, case 5a):

Let $M_o = -M_a$ and $r_o = R_a$

C parameters are constant; L parameters are functions of the radius of

the applied load.

$$31) \Delta h_b = y_b = \frac{-M_a R_a^2}{D} \frac{C_1 L_8 - L_2}{C_7}$$

$$32) \theta_b = \frac{M_a R_a L_8}{DC_7}$$

$$33) \theta_a = \frac{M_a R_a}{D} \frac{C_4 L_8 - L_5}{C_7}$$

$$34) \Delta h_a = \Delta R_a = \Delta R_b = 0$$

Due to H_b (Table 24, case 1a):

Let $w = H_b$

$$35) \Delta h_b = y_b = \frac{-H_b R_a^3}{D} \frac{C_1 L_9 - L_3}{C_7}$$

$$36) \theta_b = \frac{H_b R_a^2 L_9}{DC_7}$$

$$37) \theta_a = \frac{H_b R_a^2}{D} \frac{C_4 L_9 - L_6}{C_7}$$

$$38) \Delta h_a = \Delta R_a = \Delta R_b = 0$$

Due to internal pressure P_T (Table 24, case 2a)

Let $q = -P_T$

$$39) y_b = \frac{P_T R_a^4}{D} \frac{C_1 L_{17} - L_{11}}{C_7}$$

$$40) \theta_b = \frac{-P_T R_a^3 L_{17}}{DC_7}$$

$$41) \theta_a = \frac{-P_T R_a^3}{D} \frac{C_4 L_{17} - L_{14}}{C_7}$$

$$42) y_a = \Delta R_a = \Delta R_b = 0$$

An extra force balance equation between H_a , H_b , and pressure P_T on the annular plate is required since this plate was considered to be simply supported on the O.D.

$$2\pi R_a H_a + 2\pi R_b H_b = \pi(R_a^2 - R_b^2)P_T$$

$$43) H_a = \frac{(R_a^2 - R_b^2)P_T}{2R_a} - \frac{R_b H_b}{R_a}$$

Now equate deflections and angular rotations at corners A and B. Neglect equations with zero deformations.

Radial change at B,

$$44) \text{eq's (1 + 4 + 8 + 10) = eq's (21+ 25)}$$

Radial change at A,

$$45) \text{eq's (11 + 14 + 18 + 20) = eq's (22 + 24)}$$

Angular change at B,

$$46) \text{eq's (7 + 9) = eq's (28 + 32 + 36 + 40)}$$

Angular change at A,

$$47) \text{eq's (17 + 19) = eq's (29 + 33+ 37 + 41)}$$

Axial extension at B,

$$48) \Delta h(\text{inner cylinder}) = \Delta h(\text{plate deformation}) + \text{change in length of outer cylinder}$$

$$\text{eq's (3 + 6) = eq's (13 + 16) + eq's (27 + 31 + 35+ 39)}$$

Force balance equation,

eq 43 in the form

$$49) OV_a + OV_b + H_a + \frac{R_b H_b}{R_a} + OM_a + OM_b = \frac{(R_a^2 - R_b^3)}{2R_a} P_T$$

This force balance equation takes the place of the axial extensions at corner A where the results would be meaningless because the annular plate was simply supported at this location.

Equation 44-49 are solved for the unknowns M_a , M_b , V_a , V_b , H_a , H_b with my program TOROID. The radial electromagnetic load case will be compared with the axisymmetric ANSYS run. A pressure of 400 psi is applied on the outer wall and -1090 psi (tensile) is applied to the inner wall.

Solving the equations yields,

$$V_a = 459 \text{ lbs/in}$$

$$V_b = -1795 \text{ lbs/in}$$

$$H_a = 83 \text{ lbs/in}$$

$$H_b = -121 \text{ lbs/in}$$

$$M_a = 335 \text{ in-lbs/in}$$

$$M_b = -826 \text{ in-lbs/in}$$

These loads plus the pressure loadings are imposed on the two cylinders and top annular plate. Stresses are then calculated using Table 7, 24, 29, and 32 in Roark and Young. Figure 6⁴ along with Table 3 compares the "hand" calculations with the 1/2 axisymmetric ANSYS model. Comparison is reasonably good especially at the midplane. Remember that the radial pressures we distributed uniformly in the hand calculations but were applied as line loads in ANSYS. This will result in somewhat different moments being generated. All stresses agree within 5000 psi even at the corners where large discrepancies are expected.

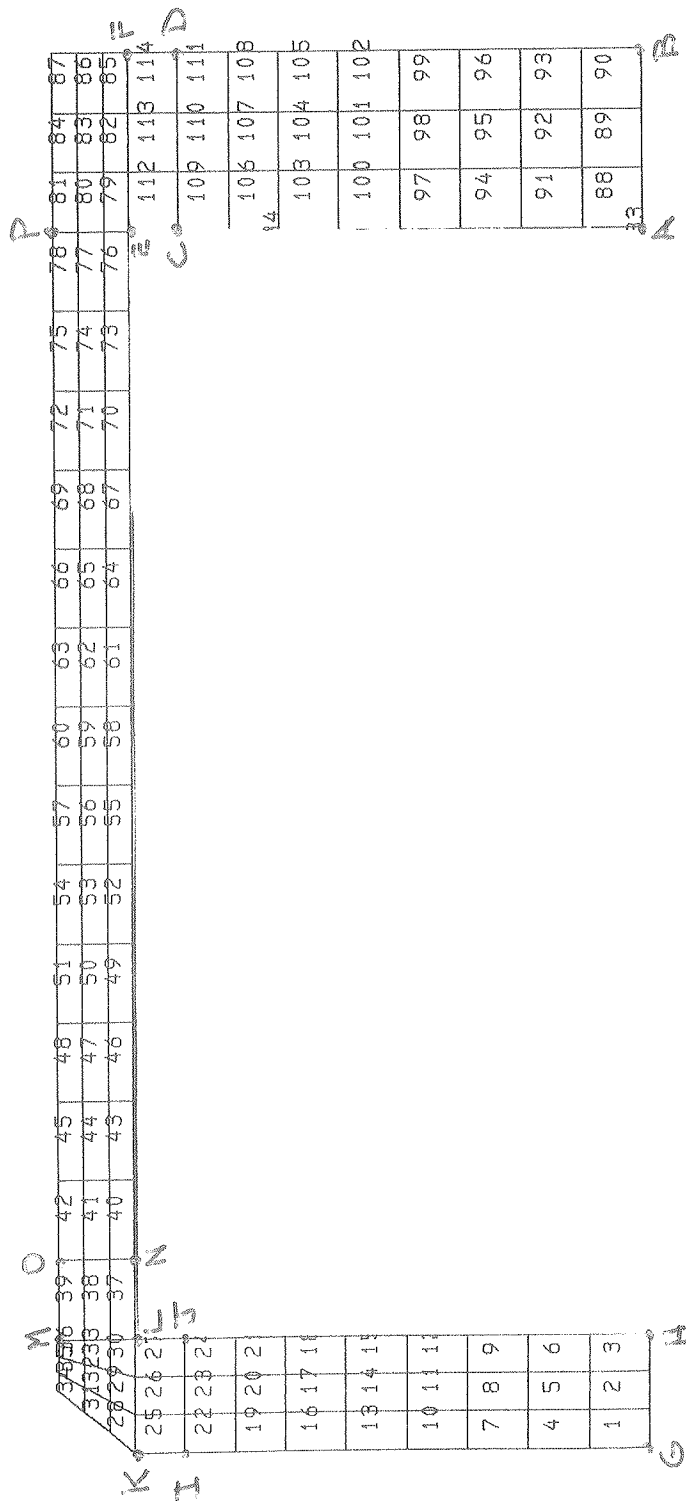


Fig. 64. Locations Used in Table 3

Stress Comparison*
 Table 3
 Inner & Outer Cylinders

| | σ_z | σ_z (ANSYS) | σ_{axial} | σ_{axial} (ANSYS) |
|---|------------|--------------------|------------------|--------------------------|
| A | 6370 | 5006 | -1650 | -1805 |
| B | 7370 | 6266 | 1650 | 1451 |
| C | --- | 6163 | --- | 996 |
| D | --- | 5646 | --- | 22.7 |
| E | 6675 | 7047 | 815 | 1073 |
| F | 6185 | 5574 | -815 | -64 |
| G | 15890 | 16290 | -15280 | -14550 |
| H | 25050 | 25852 | 15280 | 14937 |
| I | --- | 11400 | --- | -3501 |
| J | --- | 12640 | --- | 1222 |
| K | 12250 | 10750 | 4956 | -259 |
| L | 9270 | 7149 | -4956 | -1843 |

Annular Plate

| | σ_z | σ_z (ANSYS) | σ_r | σ_r (ANSYS) |
|---|------------|--------------------|------------|--------------------|
| L | 7820 | 7149 | -13530 | -8756 |
| M | 12170 | 10420 | 8214 | 7488 |
| N | 7425 | 5821 | -10720 | -13230 |
| O | 11400 | 10760 | 6560 | 8426 |
| E | 6600 | 7047 | 5090 | 2890 |
| P | 6710 | 4920 | -3730 | -3430 |

*Loads

-1150 psi outer wall and +420 psi inner wall for ANSYS
 -1090 psi outer wall and +400 psi inner wall for TOROID

The pressures are based on the average pressure found for the radial load case in ANSYS using the forces found on the preload screws.

Axial Loads:

Axial loads cause stresses in at least three different ways, each of which can be roughly estimated. They are: electromagnetic loads and axial restraints (Randolite posts) do not pass through the centroid of the cryostat. Thus a twisting moment appears which tends to roll the cryostat and create bending stresses in the hoop direction; axial loading from the conductor bends the bottom plate creating bending stresses in the radial direction; axial restraint from the Randolite posts is transferred through the gussets to the outer wall. These gussets may be treated as a simple beam.

Axial loads are assumed to be uniformly distributed in the θ direction. Neglecting the outer brackets and the coil inside, the cryostat has a centroid located at $r = 30.54$ and a moment of inertia about the centroid = 571 in^4 . This value is based on the nominal minimum thickness. Three different twisting moments act on the cryostat. For comparison with previous ANSYS calculations assume a total axial force of $4.62 \times 10^5 \text{ lbs}$. Thus the following three twisting moments act on the cryostat.

From axial support posts,

$$M_T = 4.62 \times 10^5 (38.5 - 30.54) = 3.68 \times 10^6 \text{ in lbs}$$

$$= 19160 \text{ in lbs/in at the centroid}$$

From axial electromagnetic forces,

The centroid of the axial force is given by $r = \frac{\sum(Fz_i r_i)}{\sum Fz_i} = 31.7''$ where the values from my TRIM run #47 were used. The i^{th} component refers to a specific column from FORGY.

$$M_T = -4.62 \times 10^5 (31.7 - 30.54) / (2\pi \times 30.54) = -2790 \text{ in lbs/in}$$

at the centroid

From the radial electromagnetic forces,

The centroid of the radial force is given by

$$z = \frac{\sum T_i z_i}{\sum T_i} = .11'' \text{ above the cryostat midplane}$$

Again FORGY results from TRIM 47 were used, and T_i refers to total tension on a given row. The total radial force is given by $2\pi \sum T_i = 4.08 \times 10^6 \text{ lbs}$.

$$M_T = \frac{-4.08 \times 10^6}{2\pi \times 30.54} \times .11 = -2340 \text{ in-lbs/in}$$

Total twisting moment = $14,030 \text{ in-lbs/in}$ at the centroid. But we will neglect

the radial component for comparison with the previous ANSYS run with only axial loading. Then,

$$M_T = 16,370 \text{ in-lbs/in}$$

Timoshenko³ gives an expression for the stress in a solid thick ring subjected to a uniform twisting moment. Modifying his formula to consider our cryostat as the difference of two solid rings yields,

$$\sigma = \frac{12 M_T a y}{r(h_o^3 \ln d_o/C_o - h_i^3 \ln d_i/C_i)}$$

where

- o = refers to outer solid
- i = refers to inner solid
- d = outer radius
- c = inner radius
- h = height
- y = distance from neutral axis
- a = radius of centroid = 30.54

$$\sigma = \frac{26160 y}{r}$$

The peak hoop stress is found at the top and bottom edge of the inner radius. Stresses are compressive in the top half and tensile in the bottom half and run in the hoop direction.

$$\sigma_{\max} = 5780 \text{ psi}$$

The more simple expression for a compact ring gives, $\sigma_{\max} = 4600$ psi ANSYS yields a max stress value of -6506 psi near the top inside corner. Stresses on the bottom edge are greater as bending of the bottom plate in the next section must also be considered. The case of a compact ring subject to eight concentrated moments⁴ (eight support posts) was also analyzed. An 8% variation with angle was found with the average peak stress differing from the uniformly distributed moment compact ring case by only 2%. The assumption of distributing the axial retaining loads in the axisymmetric ANSYS model is, therefore, valid.

The bottom plate was analyzed as an annular plate fixed at both the O.D. and I.D. under a line load of 5.08×10^5 lbs = 2600 lbs/in located at 31.15. These two values correspond to the centroid of only the axial forces which push against the bottom plate. In the following table, tangential bending stress are combined with the bending stresses from the cryostat roll.

Stresses in Bottom Annular Plate
Subjected to Axial Electromagnetic Loading

| radius | σ_r | $\sigma_r(\text{ANSYS})$ | $\sigma_\theta(\text{TOTAL})$ | $\sigma_\theta(\text{ANSYS})$ |
|-----------|------------|--------------------------|-------------------------------|-------------------------------|
| 24.75 Top | 29050 | 11630 | 13560 | 9804 |
| Bottom | -29050 | -13500 | -320 | -457 |
| 31.15 Top | -33330 | -17940 | -6970 | -3916 |
| Bottom | 33330 | 21240 | 15220 | 10570 |
| 34.5 Top | 47000 | 22620 | 17560 | 12300 |
| Bottom | -47000 | -27,530 | -10,110 | -4140 |

Substantial discrepancies exist between the two calculations, but considering the vast simplification of the annular plate model the differences are not unexpected. A more accurate treatment.

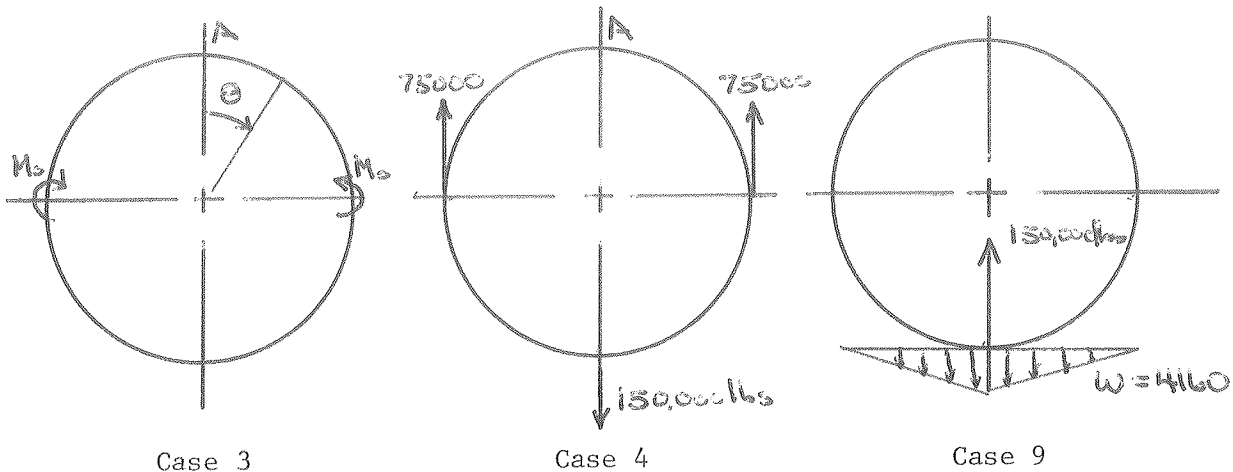
Simple estimates can be made for the stress in the gussets which comprise the axial support brackets. The original design was based on two 1/2" wide x 7" long gussets. The stress level was considered rather high and two additional 1/2" x 8" long gussets were added. As in the ANSYS model four 1/2" x 7" gussets are assumed for these calculations. Linear elastic theory for a cantilever beam predicts peak bending stresses of + 8600 psi at the top and bottom of the gusset and a peak shear stress of 6200 psi. But these gussets have extremely short span/depth ratios, and the assumption of a linear stress distribution is no longer valid. ANSYS gives radial bending stress values at the top and bottom of the cylinder - gusset junction of -13400 and 10970 psi.

Radial Decentering Loads:

Look only at radial vertical forces. The forces and moments for the horizontal radial forces are only 1/2 as large. 75,000 lbs of decentering loading is restrained by each arm.

Gussets welded to cryostat and connected to support arms are:

2 x 1-1/8" thick
12" span or arc length
3-3/8" eccentricity from outer wall



Use Roark & Young Table 17, Cases 3, 4 and 9 combined as shown above. Vertical downward forces are assumed to be distributed as in case 9. Load restraints are assumed to be at exactly $\theta = 90^\circ$. In case 3, $M_0 = 75,000 \times 3\text{-}3/8 = 2.53 \times 10^5$ in lbs.

The maximum moment is at point A

| | MA |
|--------|----------------------------|
| Case 3 | -34580 |
| 4 | -3.69×10^5 |
| 9 | 68740 |
| Total | -3.35×10^5 in lbs |

Assume the load is carried only by the outer wall.

$$I_{\text{wall}} = 1/12 \times 10.5 \times 1.57^3 = 3.87 \text{ in}^4$$

$$\text{max bending stress} = \frac{3.35 \times 10^5 \times 1.57/2}{3.87} = 68,000 \text{ psi}$$

Obviously the distribution of loads between the outer wall, annular plates, and inner wall is complex. Now assume that only the annular plates carry these bending moments. Use Table 16 for correction factors for thick curved beams. The moment of inertia, I , of the plates together = 104 in^4 and the correction factor for the inner radius is found to be 1.124. Then for the plates at point A

$$\sigma_{\text{bending}}(\text{max}) = 15,700 \text{ psi}$$

Peak Von Mises stresses in the cryostat body found in the 3D ANSYS analysis are only 5750 psi. Peak Von Mises stresses found with B. Wands analysis of this area is 10,090 psi.

Local stresses at the gussets can also be estimated as was done for the axial brackets. The span to depth ratio here is even much smaller. But assuming a linear distribution the maximum radial or bending stress = + 4700 psi.

COIL STRESS ANALYSIS WITH W. YOUNG'S PROGRAM

The radial and circumferential stresses in the Tohoku Bubble Chamber Magnet superconducting windings were analyzed with a computer program written by Warren Young at the University of Wisconsin [5]. Minor changes were made in the program to include radial preload and a step change in winding tension. The program is based on the following three concepts:

1. Equilibrium of radial forces
2. Compatability between radial displacement and circumferential strain
3. Compatability between radial displacements and changes in thickness between two adjacent layers

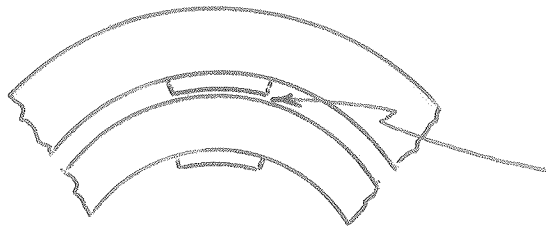
The coil was modeled as consisting of an inner ring, repetitive layers of coil, and an outer ring. This program can include cooling channels as an integral part of any layer. Using this feature is an easy way to model the push bars and set screws of the support rings and the G-10 spacers in the coil. Some further explanation of the parameters beyond that in Reference 5 is required, however. Examine the coil: The G-10 spacers cannot carry any hoop loads since they are discontinuous.

STA = avg. hoop load

STA/ECAR = stress in the narrow portion of the conductor.

Since one component of $\epsilon_{\theta} = \frac{STA}{ECAR} \frac{1}{E_T}$ from W. Young's program,

E_T = hoop modulus of the wire itself.



$$\sigma_r = \frac{S_r(I+1)}{CARI(I+1)}$$

SR(I+1) = average radial stress between layers I and I+1

$\frac{SR(I+1)}{CARI(I+1)}$ = radial stress at G-10 spacers between layers I and I+1

One component of the radial strain of layer I+1 $= \frac{SR(I+1)}{CARI(I+1)} \frac{1}{ER(I+1)}$

Thus,

ER = radial modulus of the composite, conductor and G-10 in series, based on a surface area equal to the area of contact between two components. This is different than E_r used in the finite element model.

Input Parameters for the Coil Stress Program:

The coil and reinforcement are divided into 3 components, the inner wall of cryostat, the coil, and the outer wall of the cryostat. The composite structure is difficult to analyze because the inner and outer reinforcement are connected through the top and bottom plates of the cryostat. Two cases are considered which bracket the possible values of stress in the coil. Case #2 is considered to be the most representative of the coil and will give the greatest hoop stresses in the coil.

1. Consider both inner and outer walls to be connected by the annular plates forming the top and bottom of the cryostat. The stiffest portion of the walls is at the junction of the rings and plates. Use an effective hoop modulus to represent an equivalent wall thickness at the corners of the cryostat. This case represents the maximum possible reinforcing as far the coil is considered.
2. Consider again both the inner and outer walls to be connected by the annular plates but use an effective hoops modulus to represent an equivalent wall thickness at the midplane of the coil.

Room temperature material properties are assumed for winding and preload. Liquid helium temperature properties are used for cooldown and energization. Various inner and outer cryostat wall thicknesses were used to simulate wire which is in the midplane and corners of the cryostat. Material properties for the conductor package are assumed to be linear. This is only true for the upper stress levels. For example, below 1300 psi average radial pressure the coil modulus, E_r , becomes highly nonlinear. Radial shear carried through G-10 spacers and radial friction at the cryostat interface is not considered. Finally, the radial components of field is assumed to have no effect on radial or hoop stresses due to Poisson's ratio. Hoop stresses for the cryostat/coil reinforcement are given as part of the program output. These values should not be used since they are based on fictitious wall thicknesses. Only the radial pressure on the cryostat walls should use as input in an analysis of cryostat stresses.

Inner Cryostat Wall Parameters:

Consider inner wall, push bars, insulators, and preload screws as a composite structure

Inner Radius: $R_{INS} = 23.75" = 60.325 \text{ cm}$

Inner Push Bars Thickness: $0.375"$

Push Bar G-10 Insulator = $0.03"$

Width: $W = 0.184" = 0.4674 \text{ cm}$

Thickness $T = 1" + 0.375 + 0.030 = 1.405" = 3.569 \text{ cm}$

$T_{CR} = \frac{0.375 + 0.030}{1.405} = 0.2883$

Inner Contact Area Ratio $CARI = 1$ (This could be any number, however)

Outer Contact Area Ratio $CARO = \frac{60 \times 1.25}{2\pi \times 25.155} = 0.475$

$E_{CAR} = E_{MAR} = \frac{1"}{1.405"} = 0.712$

CARO is the constant area ratio at the outer radius of the composite inner layer. It is the ratio of pushbar area divided by conductor area.

The inner pushbars carry no hoop loads. When computing peak stresses and total deformation E_{CAR} and E_{MAR} are used. The effective radial modulus of the inner wall is computed using the formula for materials in series.

Area of inner pushbar touching the coil = 10.83 in^2

Effective area of three 5/8" set screws = $3 \times 0.226 = 0.678 \text{ in}^2$

Assume the set screws extend 0.030"

$$\frac{1}{ER} = \frac{1}{1.405} \left[\frac{0.03}{4 \times 10^6} + \frac{1.375}{3 \times 10^7} + \frac{0.030}{0.678} \right] \times 3 \times 10^7$$

10.83

$ER = 26.3 \times 10^6 \text{ psi} \quad (18.13 \times 10^6 \text{ N/cm}^2)$

$$PRT = PRT = 0.3$$

$$CTER = (0.0075 \times 0.03 + 1.375 \times 0.003)/1.405 = 0.0031$$

(radial thermal contraction)

$$CTET = 0.0030 \text{ (hoop thermal contraction)}$$

$$FPRE = 0 \text{ (winding tension)}$$

$$CU = 0 \text{ (current)}$$

For the case where the inner wall is not considered to be attached to the top and bottom annular plates

$$ET = 3 \times 10^7 \text{ psi } (20.69 \times 10^6 \text{ N/cm}^2)$$

For a cylinder with uniform internal pressure

$$\sigma_{\theta} = \frac{P_r}{t} \text{ and } \Delta r = \frac{Pr^2}{Et}$$

Both stress and deflection are linear in pressure and inversely proportional in thickness.

From previous results with my program TOROID, hoop stresses and deflections are given for a 900 psi radial pressure on the actual cryostat walls. For a 900 psi pressure only on the inner wall we get,

$$\text{At the midplane } \phi_{\theta} = 15,748 \text{ psi}$$

$$\text{At the corner of the cryostat } \sigma_{\theta} = 5630 \text{ psi}$$

If the inner wall were free floating with an internal pressure of 900 psi,

$$\sigma_{\theta} = \frac{900 \times 24.25''}{1} = 21,830 \text{ psi}$$

The effective wall thicknesses must then be

$$\text{At the midplane} \quad t_{\text{effective}} = 1 \times \frac{21,830}{15,748} = 1.39''$$

$$\text{At the corner of cryostat} \quad t_{\text{effective}} = 1 \times \frac{21,830}{5630} = 3.88''$$

Rather than change wall thickness, the hoop modulus is modified to reflect the increased stiffness. This approach was chosen to keep a constant value of magnetic field for all computer runs. HZIN and HZOT are defined at the inner radius of the inner wall and the outer radius of the outer wall, not at the coil boundaries.

Since,

$$\Delta r = \frac{Pr^2}{Et} \quad \text{and} \quad Pr = \frac{\Delta r Et}{r^2}$$

A change in either E or t by the same proportion will change radial deformation and radial pressure by an identical amount. Thus an effective hoop modulus for coil reinforcement can be used in place of an effective wall thickness as far as deformation and stress in the coil is concerned.

However, hoop stress ($\sigma_{\theta} = Pr/t$) is unaffected by an increase in hoop modulus. Thus the computer results give erroneously large values of hoop stress for the cryostat by the factor of $E_{\text{effective}}/E_{\text{material}}$. This is unimportant since only radial pressure on the coil reinforcement (the cryostat) is used as input to a detailed stress analysis of the cryostat.

For the inner coil reinforcement when the cryostat is considered to be a closed shell:

At the cryostat/coil midplane:

$$ET = 41.6 \times 10^6 \text{ psi} \quad (28.68 \times 10^6 \text{ N/cm}^2)$$

At the cryostat corner:

$$ET = 116 \times 10^6 \text{ psi} \quad (79.98 \times 10^6 \text{ N/cm}^2)$$

During coil winding the inner cryostat wall is less stiff since the outer wall is not attached. In a similar manner the following results are obtained.

At the cryostat/coil midplane:

$$t_{\text{effective}} = 1.238"; \quad ET = 37.1 \times 10^6 \text{ psi} \quad (25.61 \times 10^6 \text{ N/cm}^2)$$

At the cryostat corner:

$$t_{\text{effective}} = 3.05"; \quad ET = 91.5 \times 10^6 \text{ psi} \quad (63.08 \times 10^6 \text{ N/cm}^2)$$

Outer Cryostat Wall Parameters:

All parameters are calculated in the same manner as the inner wall parameters.

Outer wall nominal thickness 1.56"

Push bar thickness 0.5"
 Push bar insulation .13"
 Preload screw length .48"
 $T = 1.56 + 0.5 + 0.065 + 0.275 = 2.67" = 6.782 \text{ cm}$
 $T_{CR} = (0.48 + 0.5 + 0.13)/2.67 = .4157$
 $CARI = (60 \times 1.25)/2\pi \times 33.67 = 0.355$
 CARO = 1.0 (any value is acceptable, however)
 ECAR=EMAR: $1.56/2.67 = 0.5843$
 W= $.184" = .4674 \text{ cm}$

Again ET is modified to reflect the additional stiffness of the closed shell.

| Condition | $t_{\text{effective}}$ | $ET_{\text{effective}}$ psi (N/cm ²) |
|-------------------------|------------------------|--|
| Free floating wall | 1.56" | 30×10^6 (20.69×10^6) |
| Middle of cryostat wall | 3.2" | 61.5×10^6 (42.4×10^6) |
| Corner of cryostat wall | 5.0" | 96.2 (66.3×10^6) |

$$ER = \frac{1}{2.67} \left[\frac{0.13}{4 \times 10^6} + \frac{1.56 + 0.5}{3 \times 10^7} + \frac{0.48}{3 \times 0.334 \times 3 \times 10^7} \right] = 10.83$$

ER= $9.74 \times 10^6 \text{ psi} = 6.72 \times 10^6 \text{ N/cm}^2$
 CTET=CTER= 0.0030
 FPRE= 0
 CU= 0
 PRT=PTR= 0.3

Coil and Miscellaneous Parameters:

Inner radius of the first turn = $23.75'' + 1.405'' = 25.155''$

Assume the outer radius of the last turn = $33.39''$ and that there are 63 layers in this coil. This equals $0.13071''/\text{layer}$. With a conductor thickness of $0.089''$, then G-10 thickness = $0.0417''$

| | |
|-------------|--------------------------------|
| T= | $0.13071'' = 0.332 \text{ cm}$ |
| W= | $0.178'' = 0.4521 \text{ cm}$ |
| TCR= | $0.0147/.13071 = 0.3191$ |
| ECAR = EMAR | $0.089/0.13071 = .6809$ |
| PRT = PTR | 0.3 |
| CU= | 675 Amps |

From actual conductor stress tests:

ET= $12.5 \times 10^6 \text{ psi}$ ($8.62 \times 10^6 \text{ N/cm}^2$) at 4.2K
 $8.2 \times 10^6 \text{ psi}$ ($5.65 \times 10^6 \text{ N/cm}^2$) at room temperature

ER= $1.2 \times 10^6 \text{ psi}$ ($8.27 \times 10^5 \text{ N/cm}^2$)

CTET= 0.00332; pure copper = 0.0033

CTER= 0.0046

Each layer to layer G-10 insulator has a $3/4''$ arc length in contact with the conductor.

The contact area ratio is therefore given by

| | | |
|-----------------|---|--------------------|
| $60 \times 3/4$ | = | 0.285 inner layer |
| ----- | = | 0.249 middle layer |
| 2πr | | 0.213 outer layer |

The average value was chosen since the program does not offer any easy method of varying the contact area ratio. Thus,

$$\text{CARI} = \text{CARO} = 0.249$$

Winding Tension = FPRE = 110 lbs (489 N) layers 1 to 39
 140 lbs (622 N) layers 40 to 63

My TRIM run No. 37 magnetic field values were used in this program as opposed to TRIM No. 47 for all other analyses. Below is a comparison and input values used in this program.

| | Actual | Used in this Analysis | TRIM 37 | TRIM 47 |
|-------------------|--------|--------------------------|---------|---------|
| Coil Inner Radius | 25.14 | 25.155 | 25.125 | 25.14 |
| Coil Outer Radius | 33.27 | 33.39 | 33.625 | 33.27 |
| Bzi (midplane) | - | - | 53.4 | 54.0 |
| Bzo (midplane) | - | - | -11.1 | -12.6 |
| HZIN | - | 64.06 | - | - |
| HZOT | - | -29.43 | - | - |
| Iron Bore Radius | 22.616 | - | 21.625 | 22.616 |

The current of 675 amps is approximately 4% less than that actually used, and the magnetic fields are slightly different than those which are anticipated by the more recent TRIM No. 47 run. These do not have a significant effect on the calculations due to other larger uncertainties. The next section summarizes the coil stresses and compares them to ANSYS results.

DISCUSSION AND SUMMARY OF COIL STRESSES

Table 4 compares the coil stress results from W. Young's program with ANSYS. This table and the output from the solenoid code is given in terms of average radial stress and true conductor hoop stress based on an area of .0167 sq inches. Output from ANSYS is average radial stress and average hoop stress, but the hoop stresses have been converted to true conductor stress for the following table and figures. Maximum, minimum, and average values are given for the ANSYS results. The two programs are in fairly good agreement with one another but some discrepancies between them do exist. Figures 65 to 76 are the axisymmetric ANSYS stress contour plots. Figures 77 to 80 are results only from W. Young's program. If one examines Figures 81 and 82, it becomes apparent that the stress solenoid program results are roughly equal to the average ANSYS results. The relatively small stresses from axial electromagnetic loads are added into the combined ANSYS stress values and not into the combined solenoid stress values. The biggest difference appear at the I.D. and O.D. where the bending of the push bars has a significant effect. See the previous Table 2 for peak ANSYS coil stresses.

The largest uncertainties in the coil stress calculations come from changes in the stress distribution in the winding process. During the winding process each coil was baked four different times under pressure. Baking embeds the conductor into the B-staged epoxy coated G-10 layer to layer spacers. This procedure increases the conductor/G-10 composite modulus from 3.7×10^5 psi to 1.2×10^6 psi. This in turn reduces conductor hoop stresses and coil motion when charging. An approximate .050" decrease in radius was measured each time the coil was baked. It is assumed that the layer next to the previously baked layer does not change radius during baking and that all layers in between change by a proportional amount.

The curve labeled theoretical winding stress in Figures 77 and 78 are the values predicted by the solenoid computer program. Radial stress in the coil after winding can be estimated very precisely since the radial stress must be zero at the outside and the torque on the inner screws is a good measure of the radial pressure at the inside of the coil. The curve labeled actual winding stress is drawn between these two points which has the same shape as the theoretical winding stress. Baking the coil has reduced this inner radial pressure from -860 psi to -230 psi. It is apparent that embedding the cable into the spacers must reduce the contact pressure between the two.

Baking has an even greater effect on the hoop stress distribution in the coil, and it is more difficult to estimate correctly. Conductor hoop stress is determined from the following three considerations.

1. Initial winding tension.
2. Change in radius of the cable due to the radial deformation of the cryostat and coil underneath the layer in question.
3. Change in radius of the cable from baking.

TABLE 4
Coil Stresses From W. Young's
Program and ANSYS
Average Radial and True Conductor Stresses
(psi)

| Load Cases | Layer 1 σ_r | Layer 32 σ_r | Layer 63 σ_r | Layer 1 σ_θ | Layer 32 σ_θ | Layer 63 σ_θ |
|---|-------------------------------|--------------------------------|--------------------------------|---------------------------------|--------------------------------|--------------------------------|
| Field Run #20 E = 1.2×10^6 E $^r_\theta$ = 12.5×10^6 | 1047 (1944/275) (954) | - 518 (-563/-518) (-538) | - 560 (-542/-262) (-408) | 10,840 (8810/6570) (7680) | 5,347 (6970/6880) (6920) | 954 (3250/2970) (3100) |
| Field Run #21 Same as run #20, except location is at cryostat corner | 1437 | - 360 | - 508 | 8,200 | 4,046 | 68 |
| Winding Run #22 E = 1.2×10^6 E $^r_\theta$ = 8.2×10^6 | - 860 | - 588 | - 23 | 699 | 2,757 | 8,832 |
| Cooldown Run #23 Same values as #20 | 61 (373/48) (183) | 281 (407/289) (345) | 397 (546/258) (407) | 3,070 (3170/1820) (2651) | 1,964 (1517/1499) (1507) | 1,785 (1688/810) (1143) |
| 100 psi preload from Inner Ring Run #24 Same values as run #22 | - 100 (-173/-42) (-100) | - 36 (-34/-31) (-33) | - 1 0 | 664 (798/697) (751) | 412 (12/409) (411) | 363 (311/310) (310) |
| 100 psi preload from Outer Ring Run #25 | - 34 (-133/-19) (-61) | - 59 (-77/-68) (-73) | - 98 (-140/-70) (-105) | - 232 (-185/-48) (-116) | - 428 (-353/-350) (-352) | - 718 (-625/-574) (-601) |

Note: All stresses from W. Young's program are through the coil midplane except where noted. Parenthesis denote the following values from the full model axisymmetric ANSYS analysis. Average ANSYS stresses are obtained by averaging all nodel stresses on a particular column. (Max/Min)
(Average)

ANSYS
84/ 4/ 5
15.9378
PLOT NO. 10
POST1
STEP=2
ITER=1
STRESS PLOT
SZ

ORIG SCALING
ZV=1
DIST=4.78
XF=29.3
EDGE
DMAX=.0183
MX=3961
MN=1540
INC=200

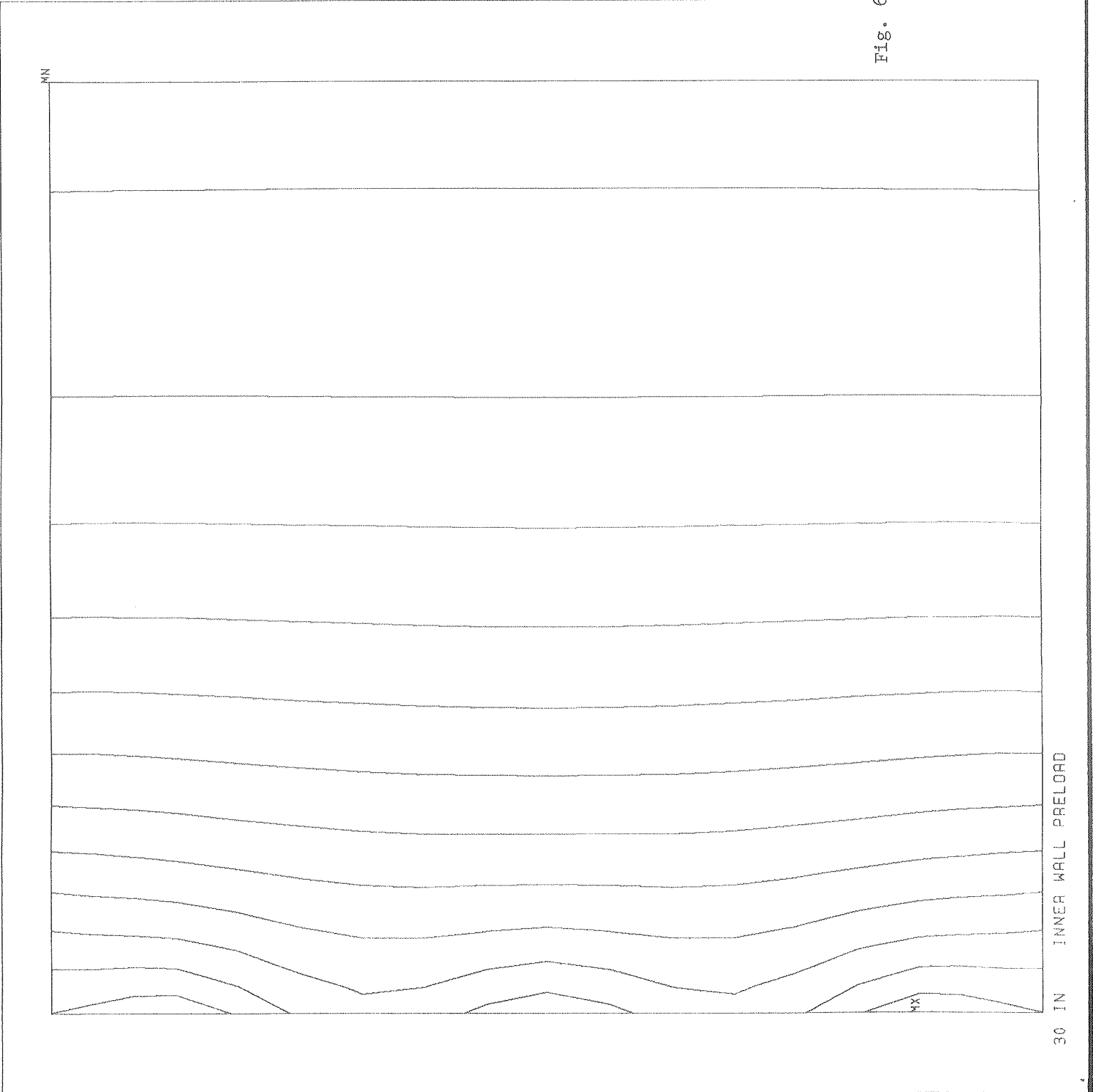


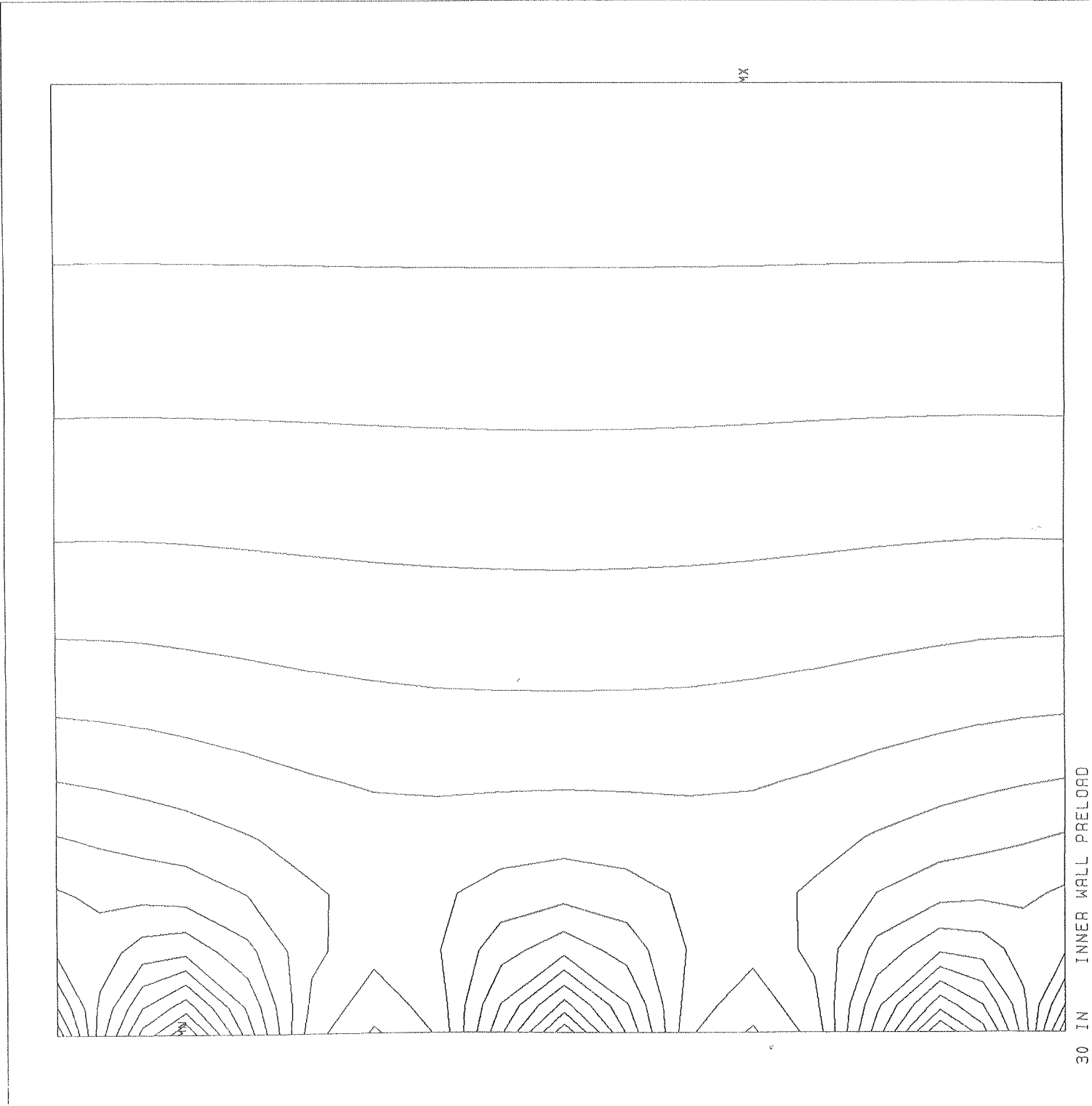
Fig. 65. Coil Stress

ANSYS
84/ 4/ 5
15.9386
PLOT NO. 11
POST1
STEP=2
ITER=1
STRESS PLOT
SX

ORIG SCALING
ZV=1
DIST=4.78
XF=29.3
EDGE
DMAX=.0183
MX=-1.16
MN=-1279
INC=80

Fig 66

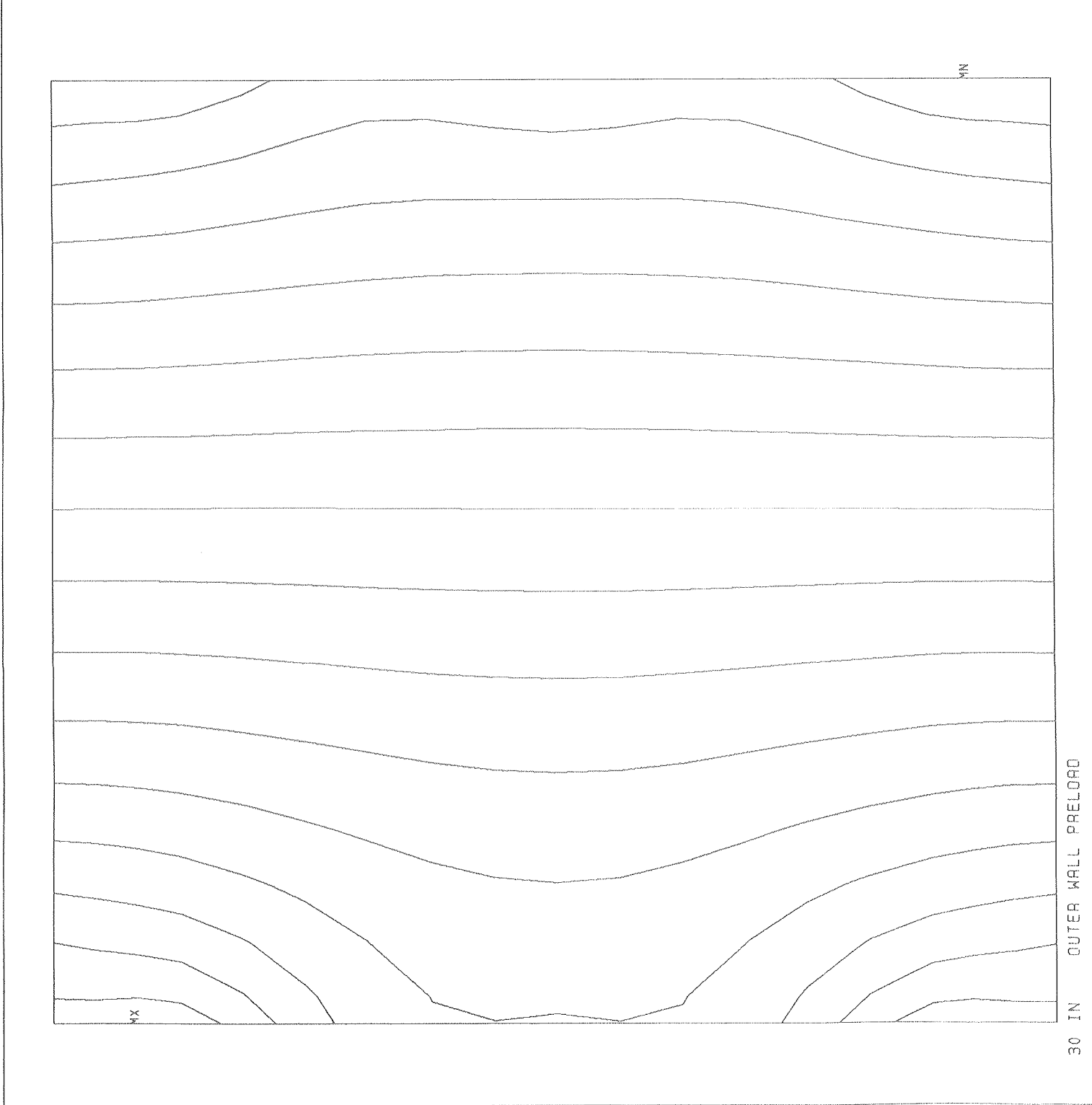
074



ANSYS
84/ 4/ 5
15.9614
PLOT NO. 16
POST1
STEP=3
ITER=1
STRESS PLOT
SZ

ORIG SCALING
ZV=1
DIST=4.78
XF=29.3
EDGE
DMAX=.0102
MX=-130
MN=-1682
INC=100

Fig 67

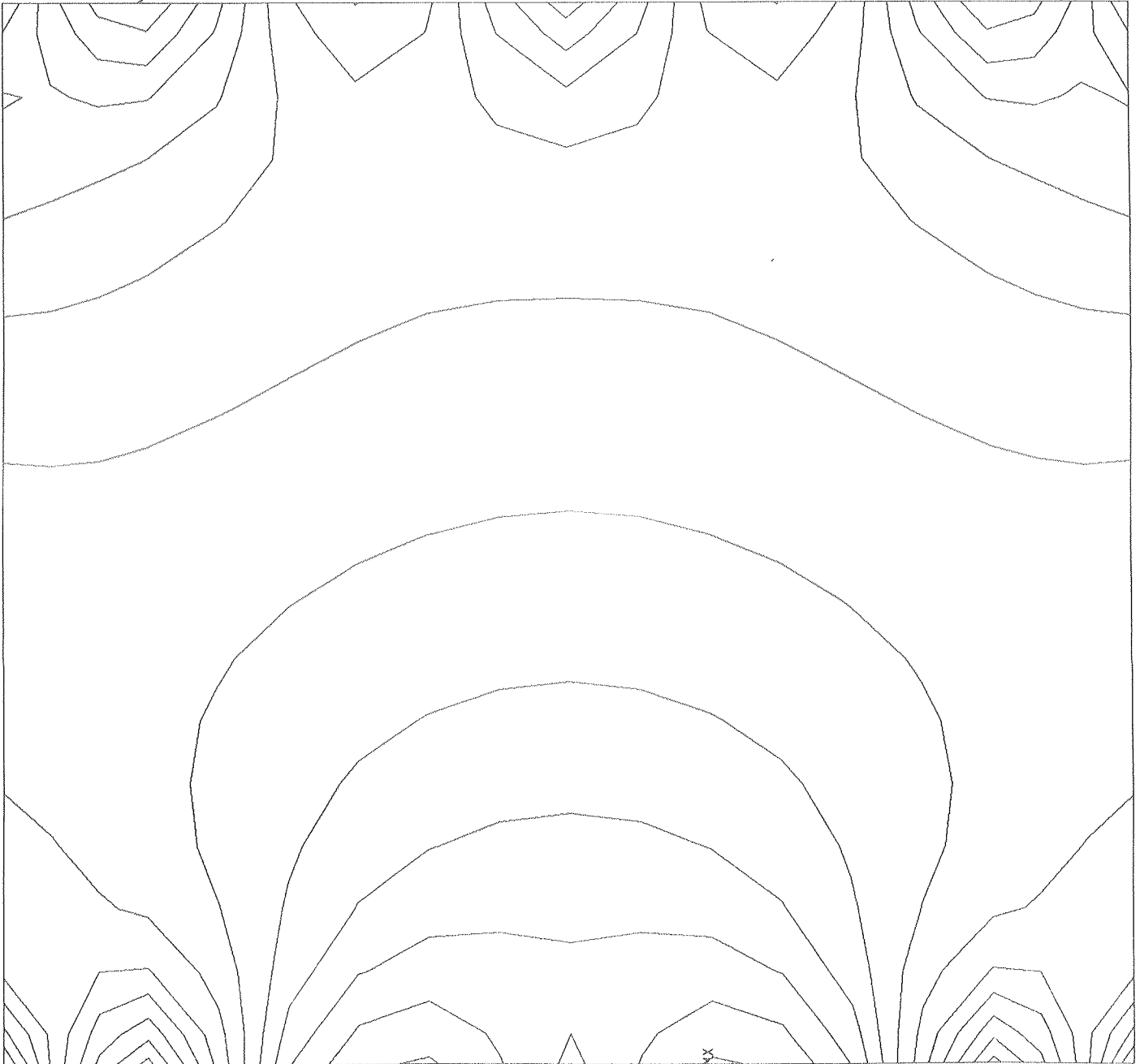


30 IN OUTER WALL PRELOAD

ANSYS
84/ 4/ 5
15.9625
PLOT NO. 17
POST1
STEP=3
ITER=1
STRESS PLOT
SX

ORIG SCALING
ZV=1
DIST=4.78
XF=29.3
EDGE
DMAX=.0102
MX=-74.6
MN=-560
INC=40

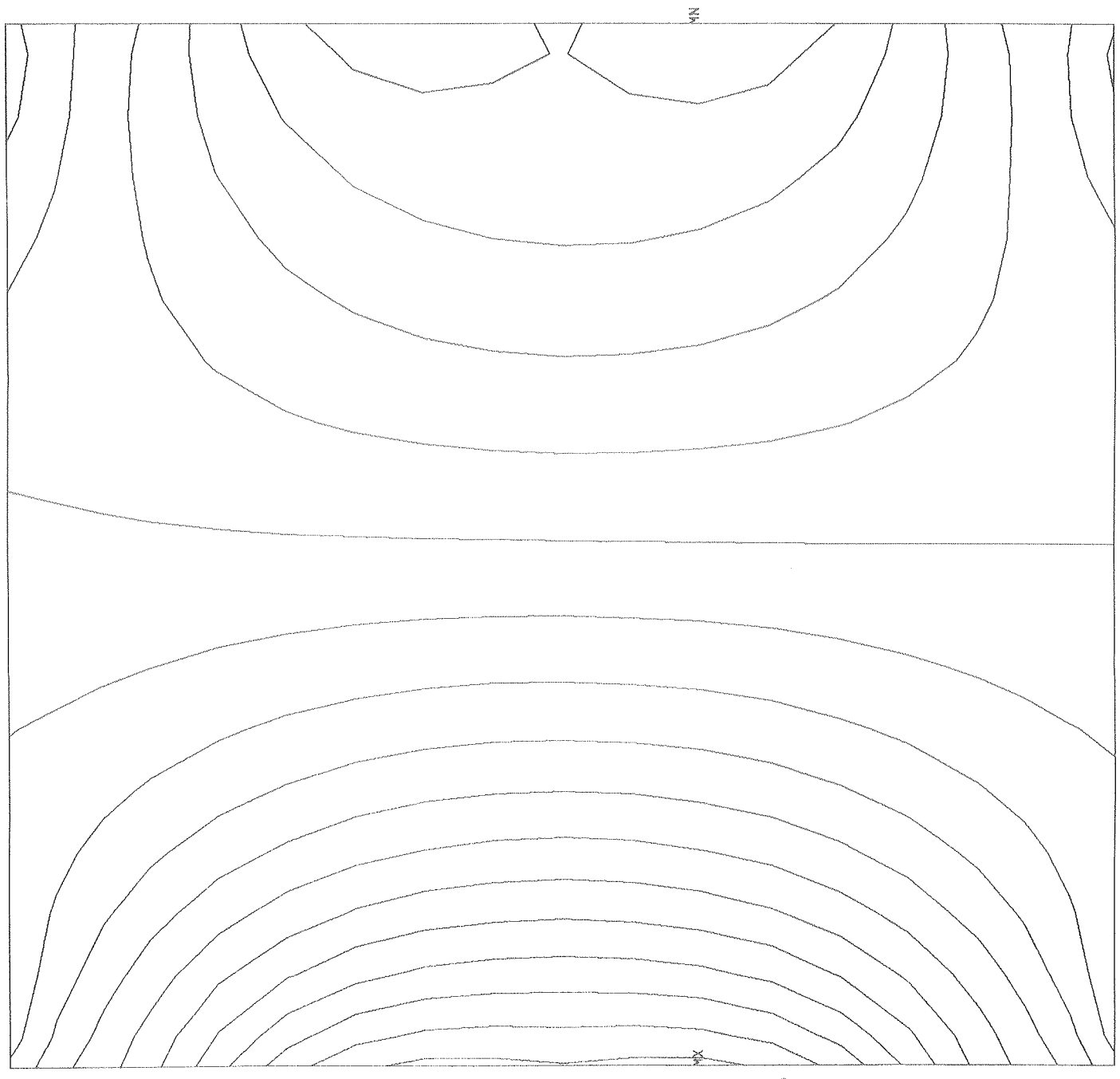
Fig 68



30 IN OUTER WALL PRELOAD

ANSYS
84/ 4/ 5
15.9842
PLOT NO. 22
POST1
STEP=4
ITER=1
STRESS PLOT
SZ
ORIG SCALING
ZV=1
DIST=4.78
XF=29.3
EDGE
DMAX=.108
MX=2130
MN=535
INC=100

Fig 69



30 IN. COOL DOWN TO 4.2K

ANSYS
84/ 4/ 5
15.9853
PLOT NO. 23
POST1
STEP=4
ITER=1
STRESS PLOT
SX
ORIG SCALING
ZV=1
DIST=4.78
XF=29.3
EDGE
DMAX=.108
MX=588
MN=47.3
INC=40

Fig 70

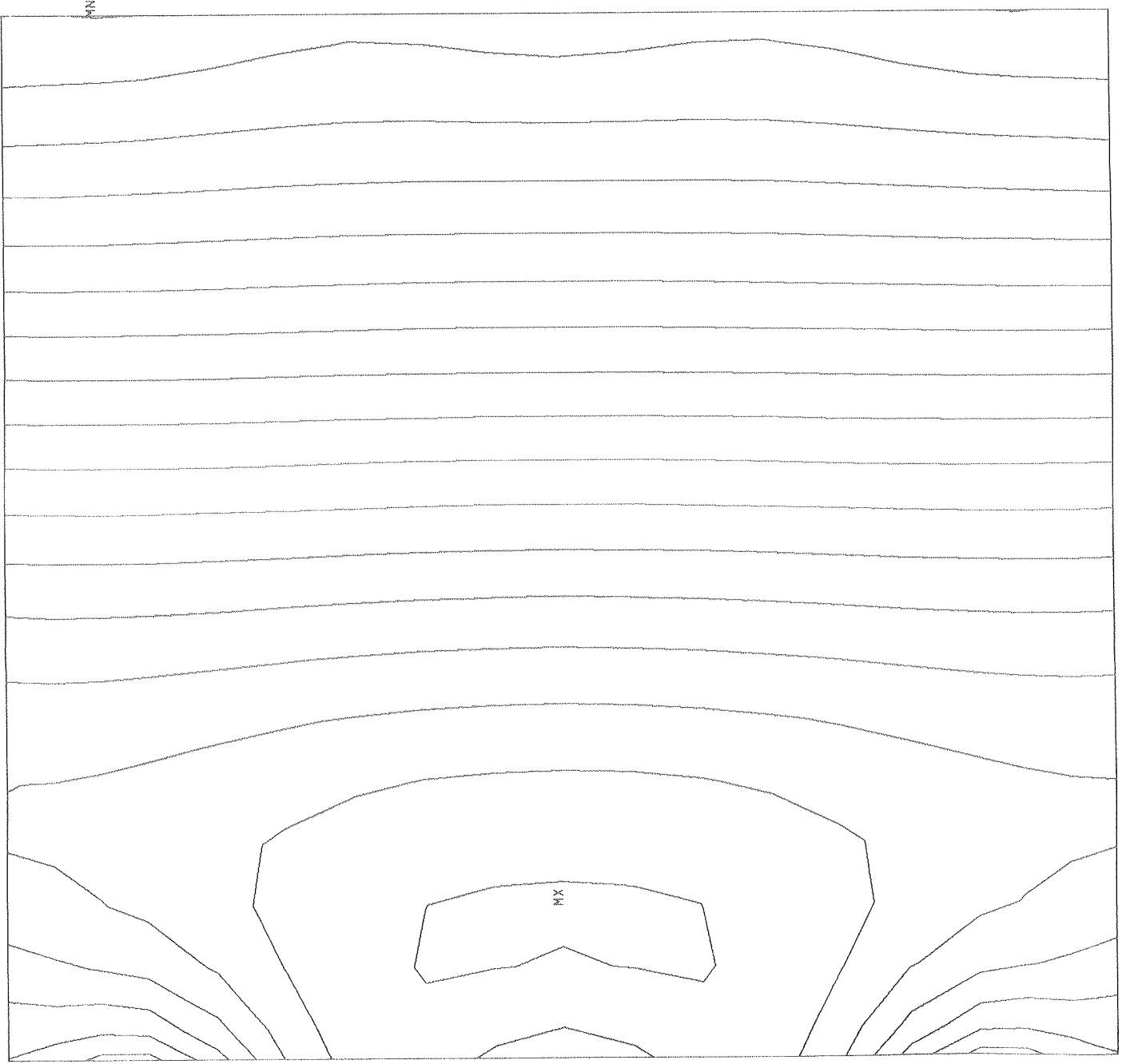


MY

MN

ANSYS
84/ 4/ 5
16.0144
PLOT NO. 28
POST1
STEP=5
ITER=1
STRESS PLOT
SZ
ORIG SCALING
ZV=1
DIST=4.78
XF=29.3
EDGE
DMAX=.0191
MX=6029
MN=1992
INC=250

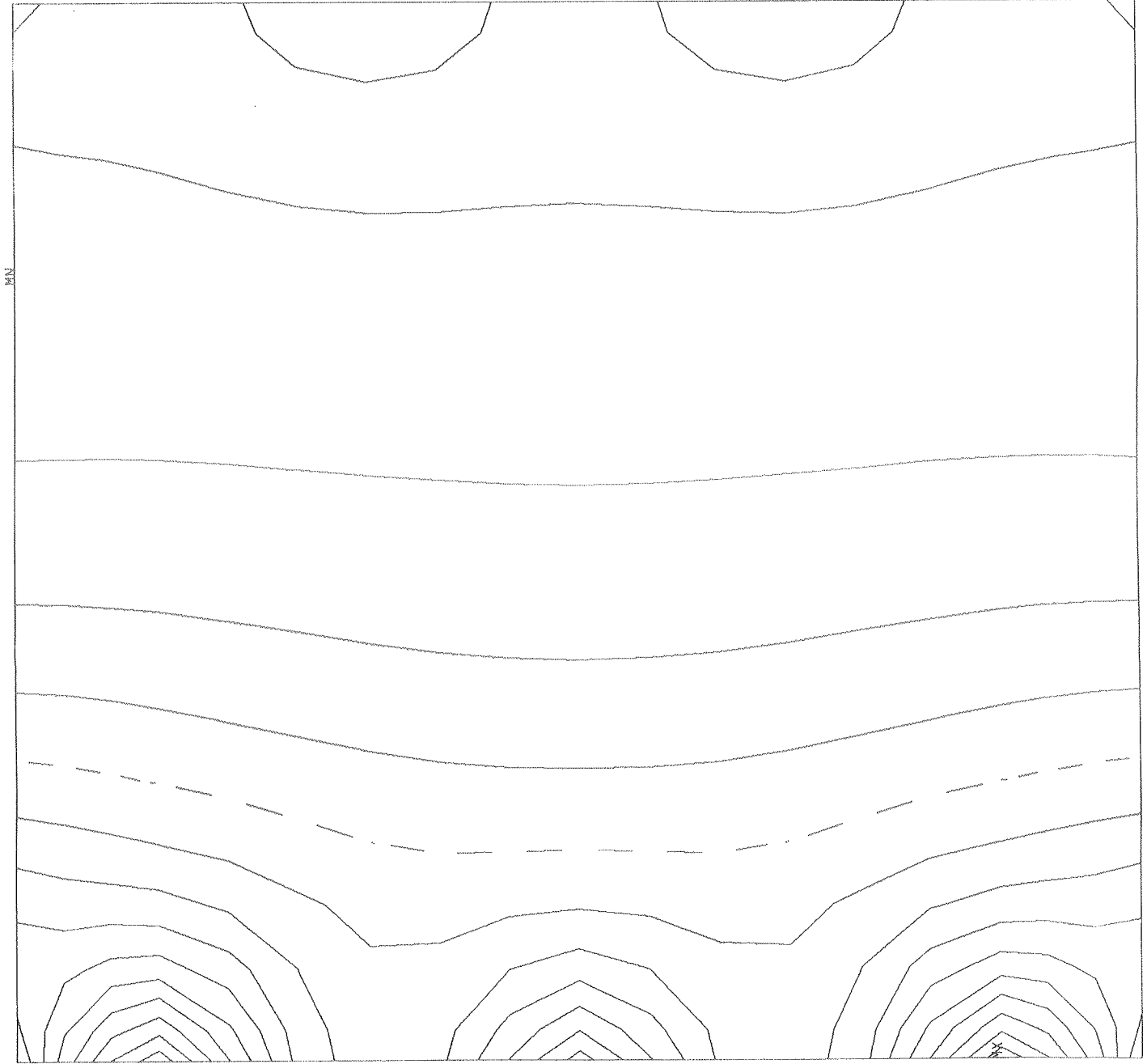
Fig 71



RADIAL E.M. LOADS

ANSYS
84/ 4/ 5
16.0158
PLOT NO. 29
POST1
STEP=5
ITER=1
STRESS PLOT
SX
ORIG SCALING
ZV=1
DIST=4.78
XF=29.3
EDGE
DMAX=.0191
MX=1944
MN=-677
INC=200

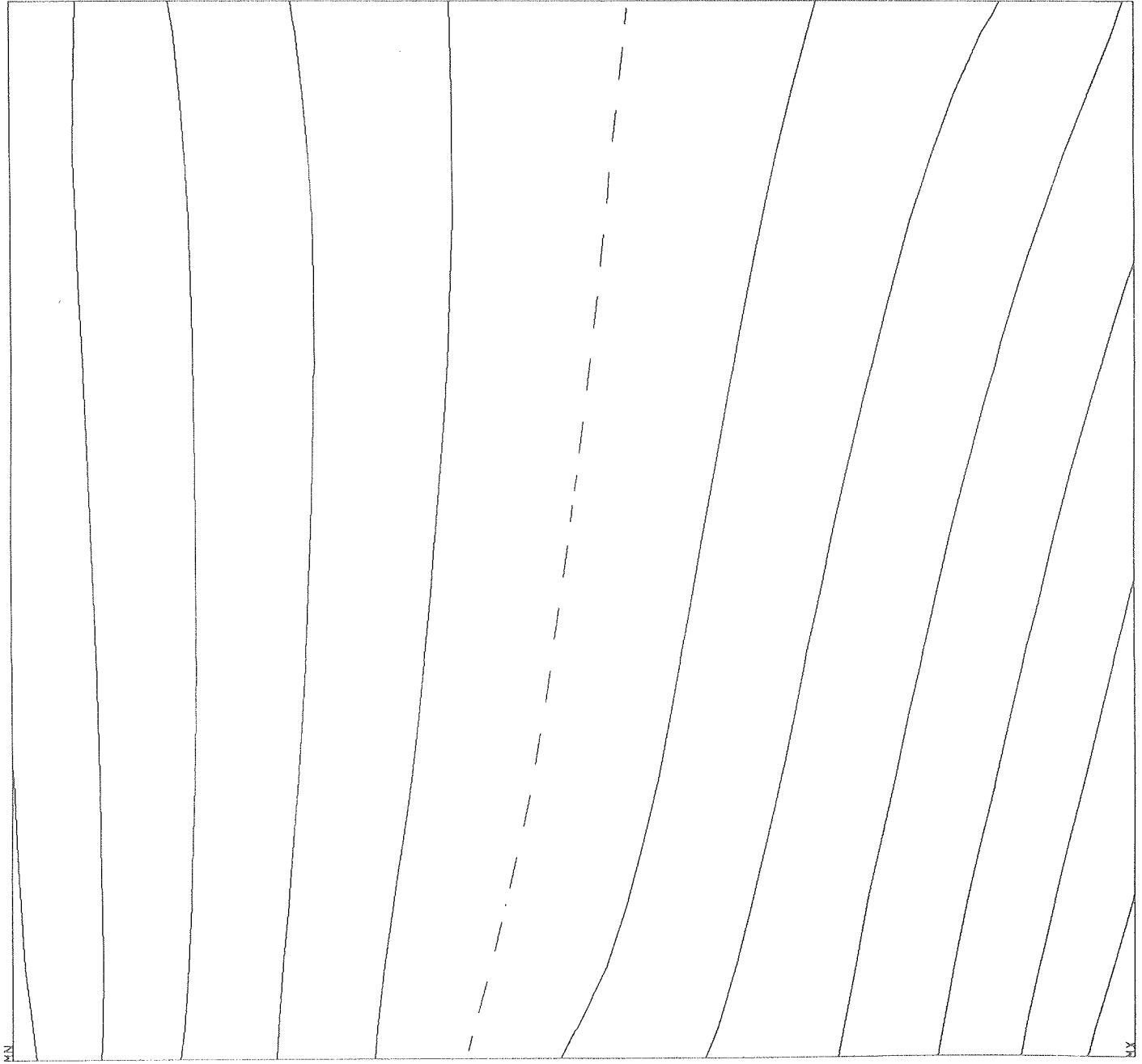
Fig 72



RADIAL E.M. LOADS

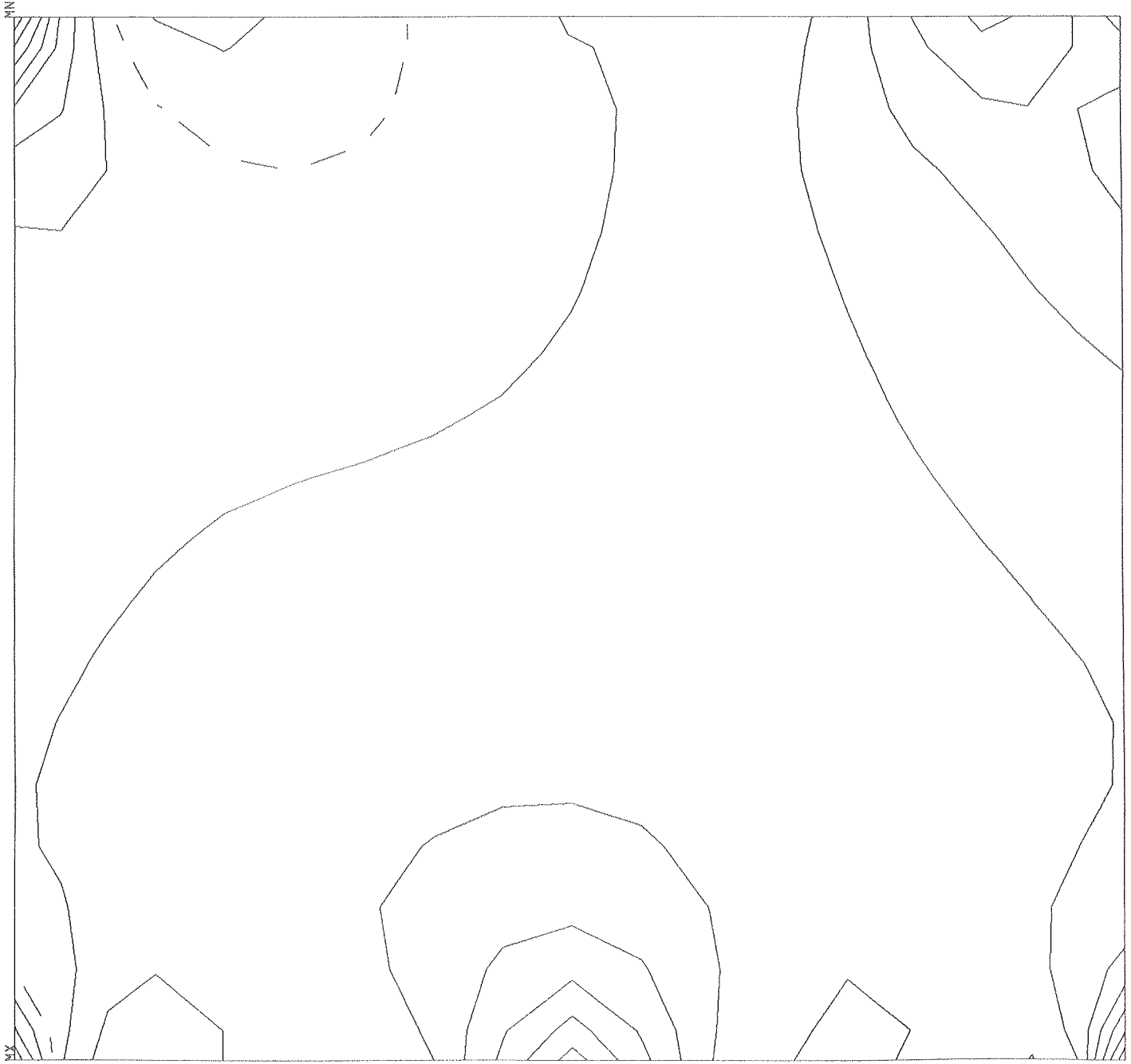
RNSYS
84/ 4/ 5
16.0386
PLOT NO. 34
POST1
STEP=6
ITER=1
STRESS PLOT
SZ
ORIG SCALING
ZV=1
DIST=4.78
XF=29.3
EDGE
DMAX=.0197
MX=1365
MN=-1077
INC=200

Fig 73



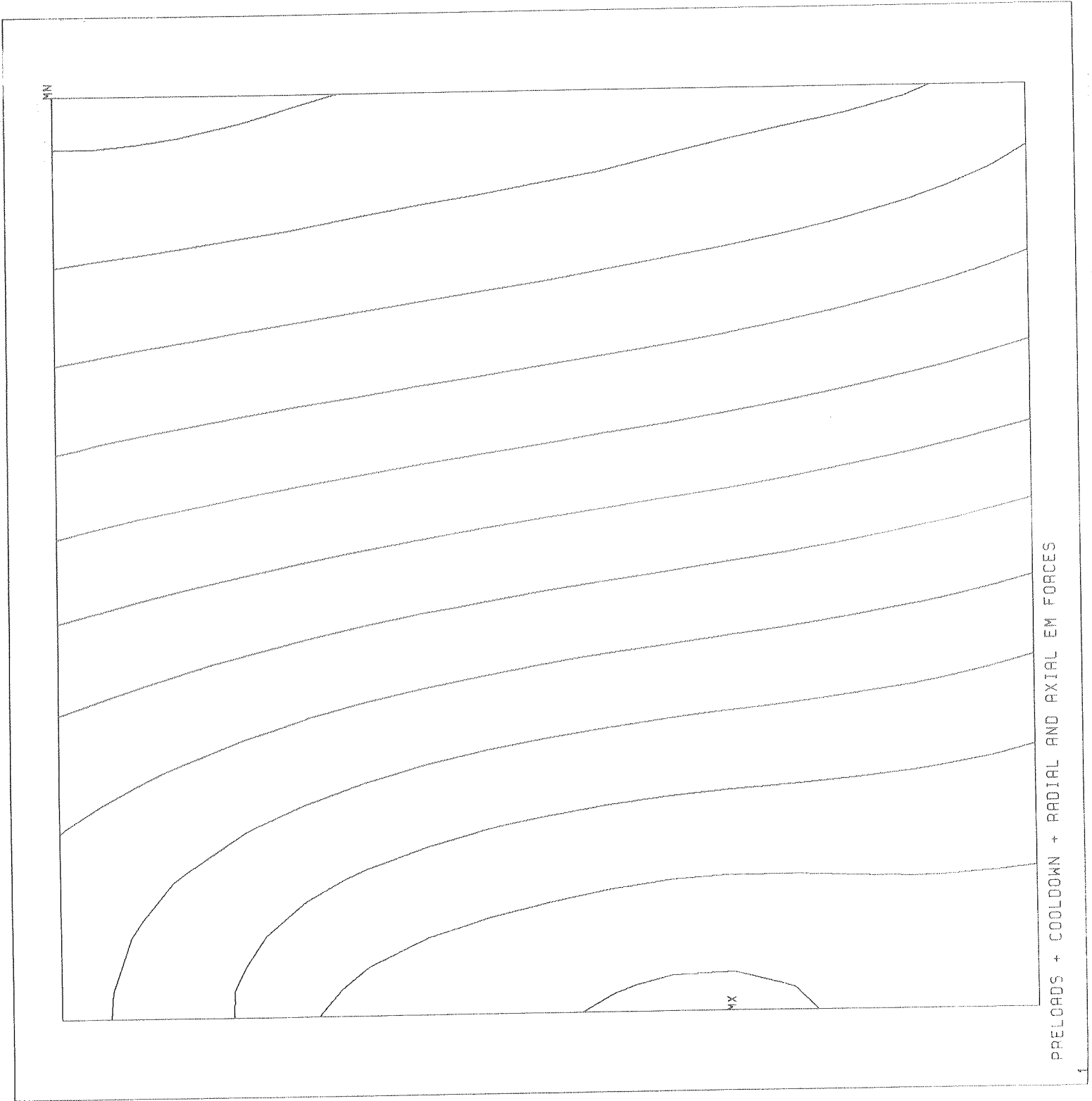
ANSYS
84/ 4/ 5
16.0397
PLOT NO. 35
POST1
STEP=6
ITER=1
STRESS PLOT
SX
ORIG SCALING
ZV=1
DIST=4.78
XF=29.3
EDGE
DMAX=.0197
MX=74.8
MN=-158
INC=20

Fig 74



ANSYS
84/ 5/30
9.8428
PLOT NO. 1
POST1
STEP=9999
ITER=1
STRESS PLOT
SZ
ORIG SCALING
ZV=1
DIST=4.78
XF=29.3
EDGE
DMAX=.0992
MX=11483
MN=2058
INC=800

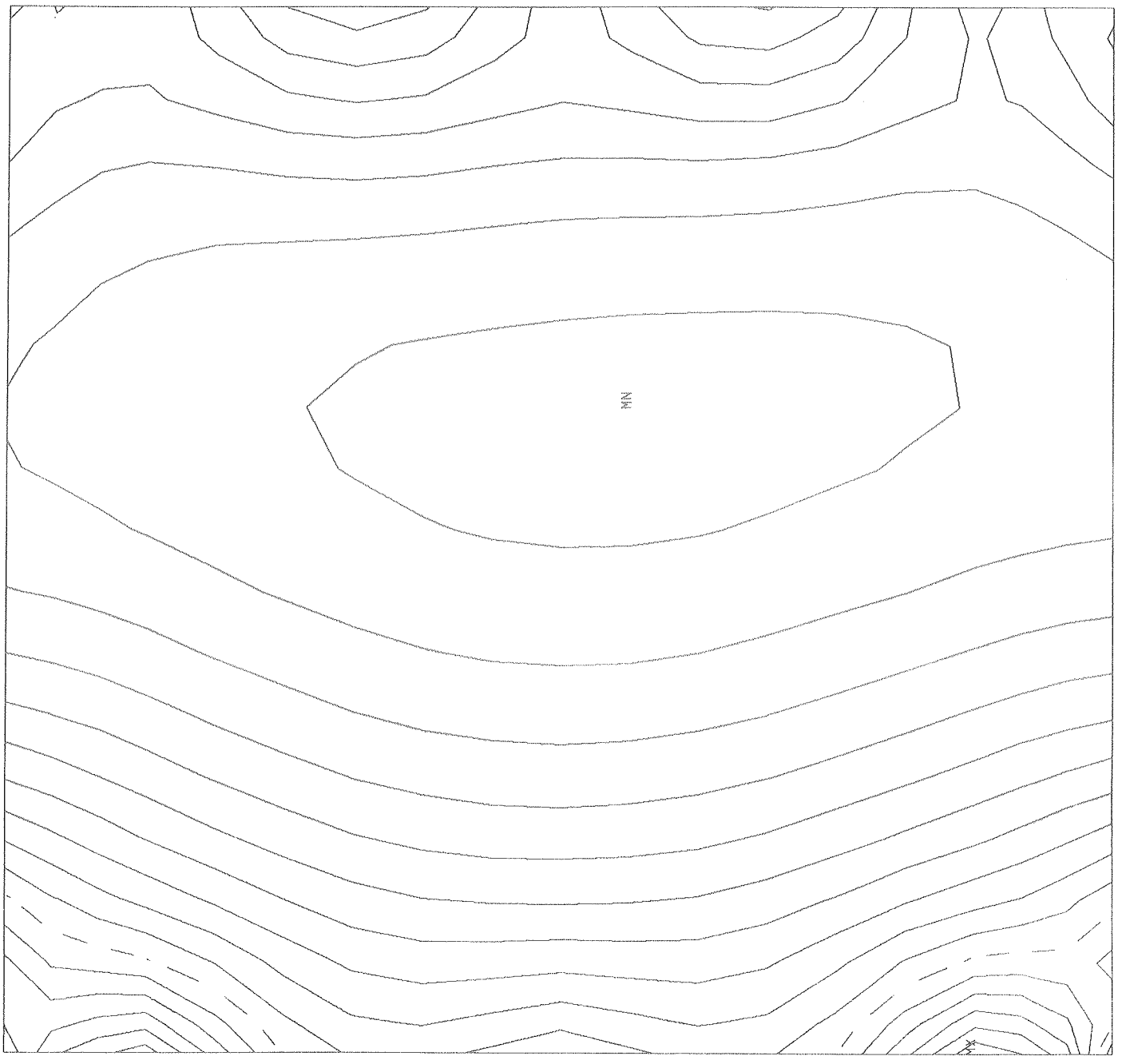
Fig 75



PRELOADS + COOLDOWN + RADIAL AND AXIAL EM FORCES

ANSYS
84/ 5/30
9.8436
PLOT NO. 2
POST1
STEP=9999
ITER=1
STRESS PLOT
SX
ORIG SCALING
ZV=1
DIST=4.78
XF=29.3
EDGE
DMAX=.0992
MX=467
MN=-831
INC=80

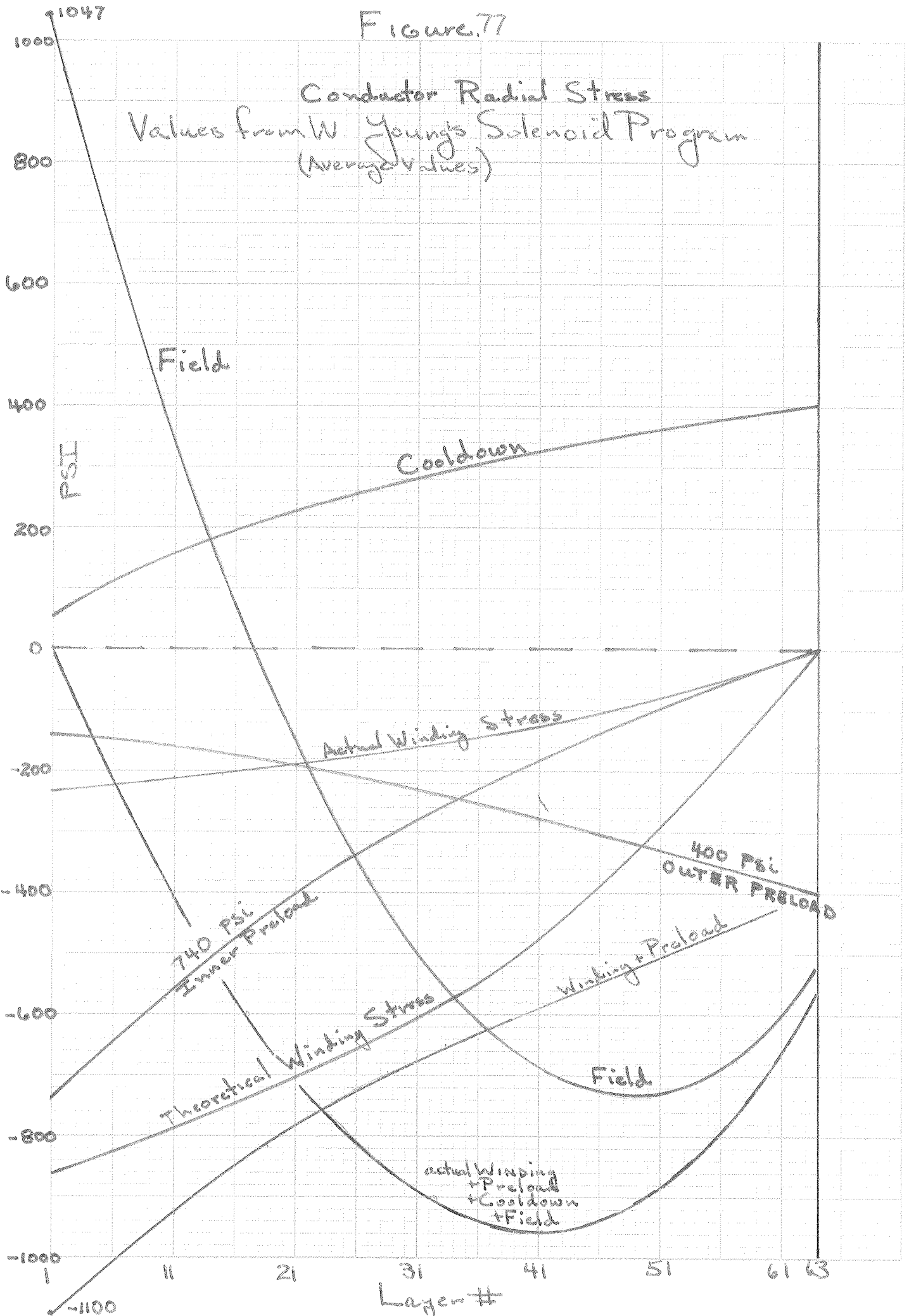
Fig. 76



PRELOADS + COOLDOWN + RADIAL AND AXIAL EM FORCES

Figure 77

Conductor Radial Stress
Values from W. Young's Solenoid Program
(Average Values)



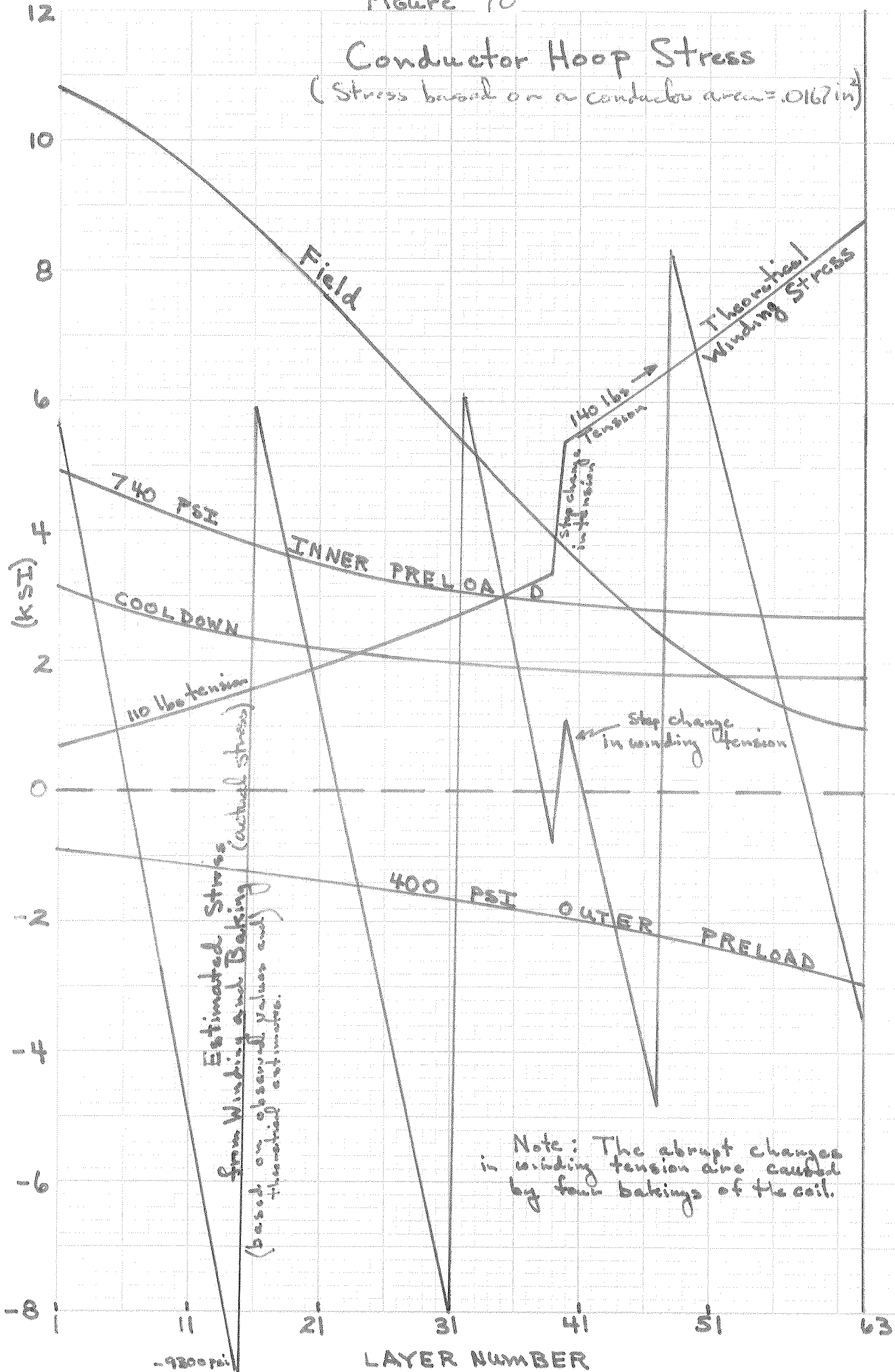
46 0782

NOE PASSED TO THE FACTS

Figure 78

Conductor Hoop Stress

(Stress based on a conductor area = .0167 in²)



46 0782

NSA Memorandum

-9300 psi

Figure 79
 Radial Displacement
 Values from W. Young's Selenoid Program

46 0782

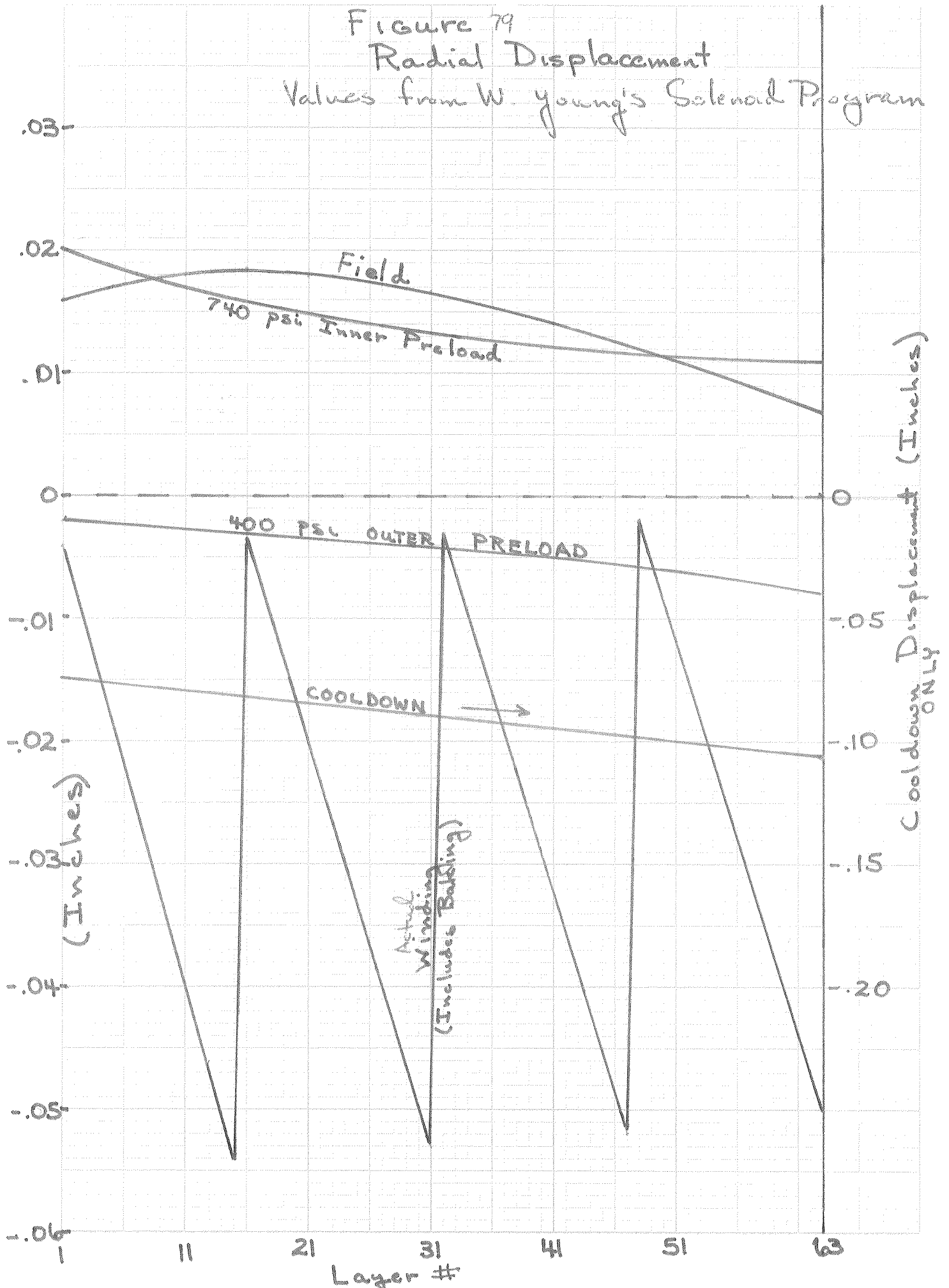
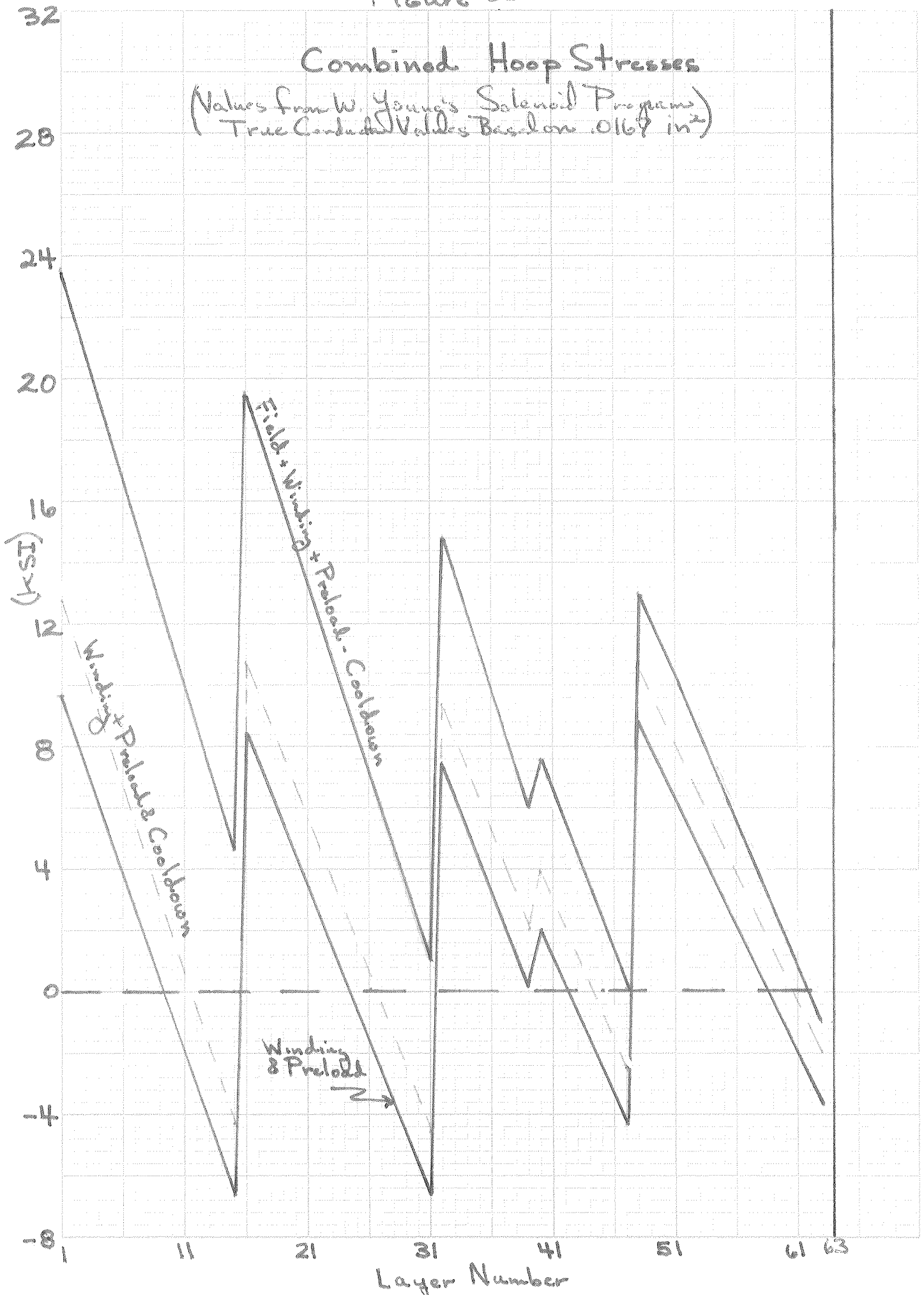


Figure 80

Combined Hoop Stresses

(Values from W. Young's Solenoid Program)
True Conductive Values Based on .0167 in²



45 0782

W. Young's Solenoid Program

Figure 81

Combined Radial Stress (average coil pressure)

Includes Preloading, cooldown, and electromagnetic loads except where noted.

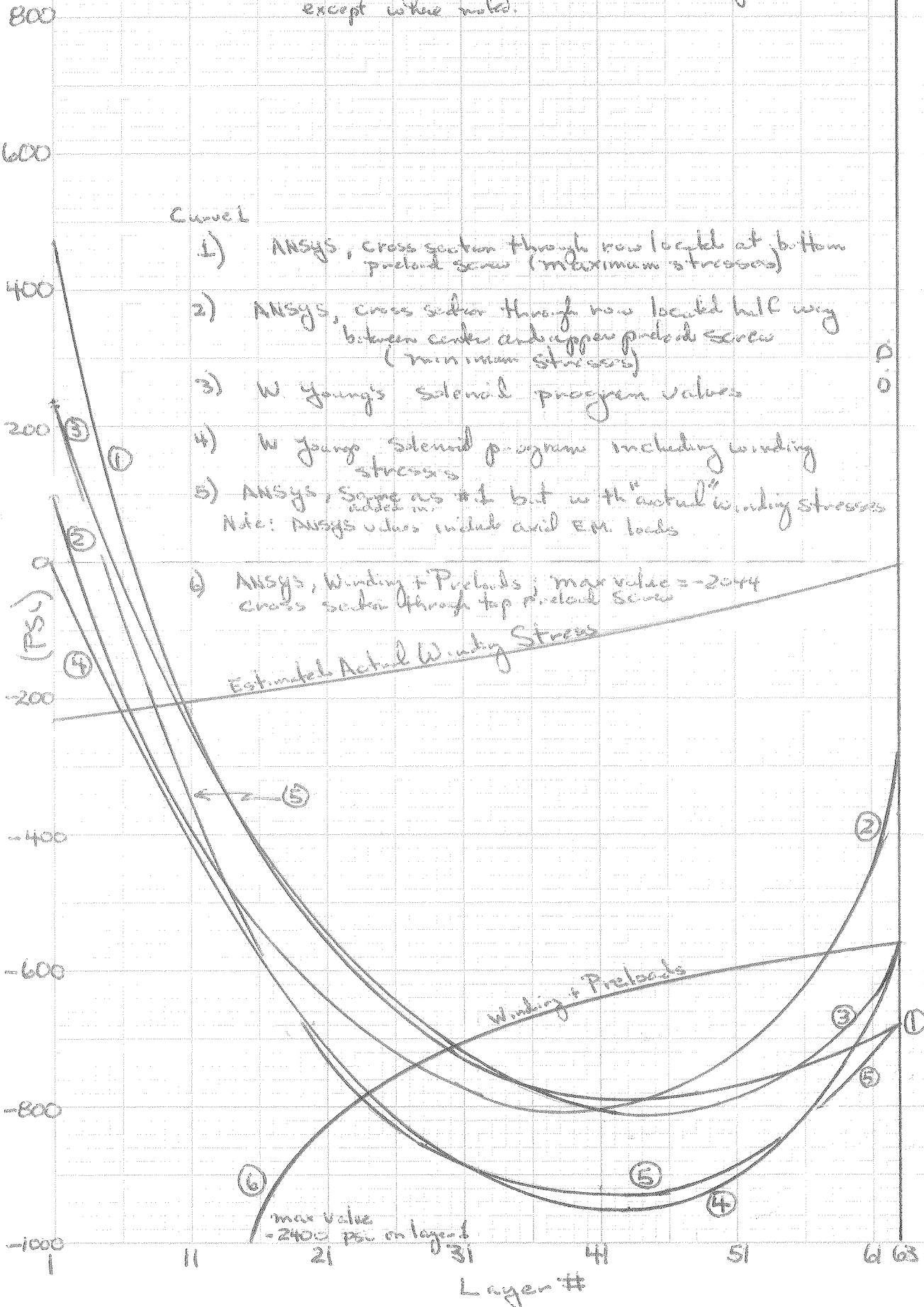
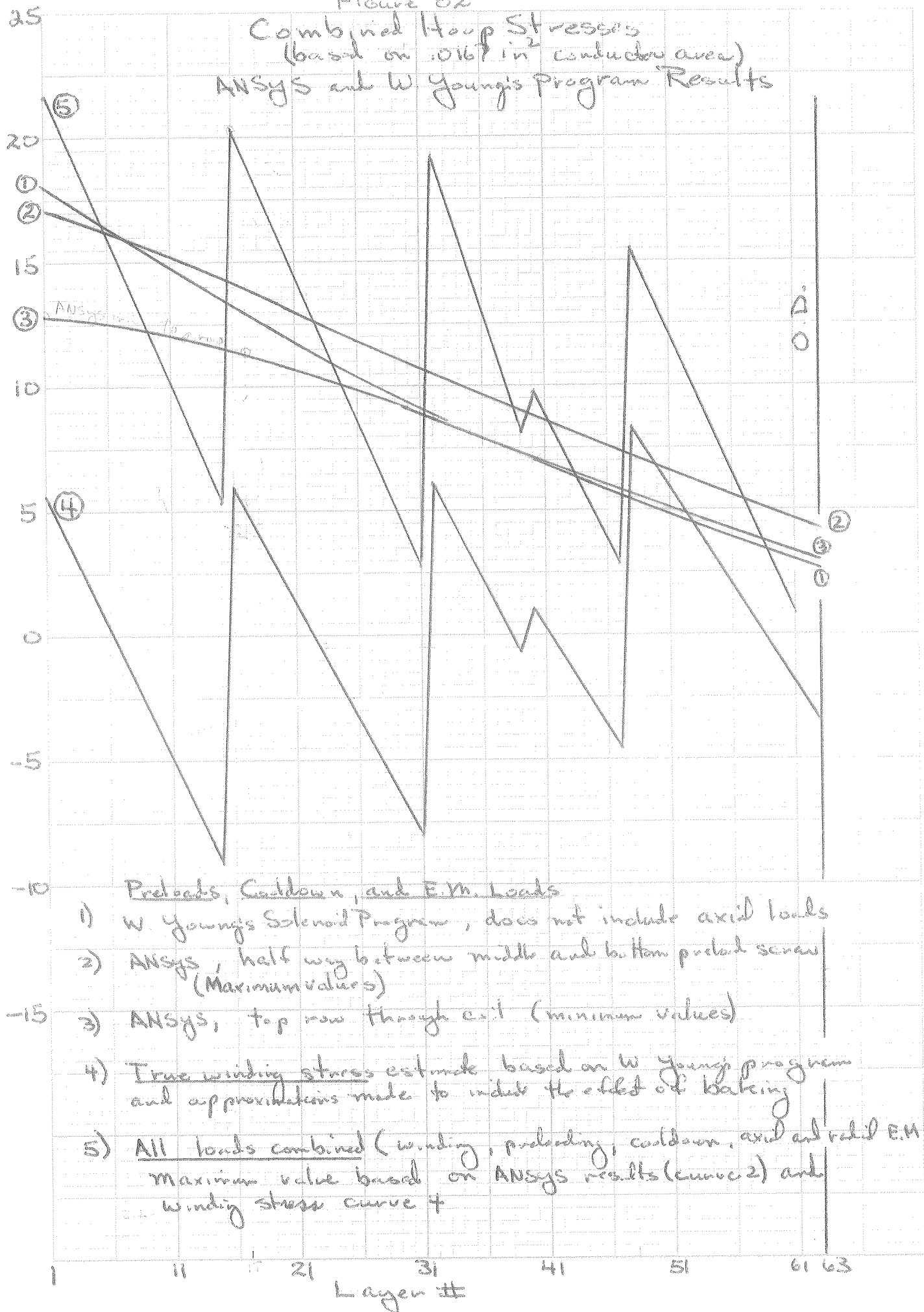


Figure 82

Combined Hoop Stresses
(based on .0167 in² conductor area)
ANSYS and W Young's Program Results



Predicts, Cutdown, and E.M. Loads

- 1) W. Young's Solenoid Program, does not include axial loads
- 2) ANSYS, half way between middle and bottom prelead screw (Maximum values)
- 3) ANSYS, top row through coil (minimum values)

4) True winding stress estimate based on W Young's program and approximations made to include the effect of baking

5) All loads combined (winding, preleading, cutdown, axial and radial E.M. loads) maximum value based on ANSYS results (curve 2) and winding stress curve 4

Winding tension was measured continuously and is known with $\pm 10\%$. Radial deformations are part of the output of Warren Young's program. This enables us to calculate the reduction in hoop tension from the overall change in radius of the coil using the relationship $\sigma_{\theta} = \Delta R/R E_{\theta}$. These stresses arise from the radial motion of the inner wall and the radial compression of the coil as a whole. ΔR for each layer is calculated by multiplying the ΔR 's from the program by the factor

$$\frac{230}{860} \frac{\text{actual pressure on inner wall}}{\text{theoretical pressure on inner wall}}$$

These values are, therefore, hoop stress values if we had wound the coil without baking and had ended up with a radial pressure of 230 psi on the inner layer.

The localized effects of baking are calculated using the same formula for σ_{θ} . These results are added in the previous hoop stress terms creating the sawtoothed curve called actual winding stress in Figure 78. Baking clearly has a dramatic effect upon hoop stress distribution when compared to the results from the theoretical winding stress curve. This sawtoothed pattern is still very pronounced when all hoop stresses are added together.

Summary of Coil Stresses:

The selection of proper radial preloads from the inner and outer ring is a compromise of the following conflicting requirements.

1. Compressive radial stress at every location in the coil is highly desirable. This will minimize conductor motion.
2. Hoop stress in the coil should be minimized. Tests at 4.2 K demonstrated that the cable can withstand cyclic loading in excess of 35,000 psi with no apparent damage. Critical current and RRR values were effected very little.
3. Compressive hoop stress in the conductor should be small enough to eliminate any possibility of buckling.
4. Preload values cannot exceed those physically possible with the 5/8" screws on the inside of the 3/4" screws on the outside. The limiting case is the preload on the coil I.D. A maximum of 7,400 lbs (970 psi average coil pressure) can be applied with each screw.

It is assumed that the ANSYS results are more accurate than those obtained from W. Young's program. However we must rely on this program for winding stresses. The following results are found from examining the Figures 81 and 81 for combined stresses.

$$+\sigma_{\theta}(\max) = 21,500 \text{ psi (under all loads combined; Fig. 82, Curve 5)}$$

$$-\sigma_{\theta}(\max) = -9300 \text{ psi (after winding and baking; Fig. 82, Curve 4)}$$

$$-\sigma_r(\max) = -2040 \text{ psi (avg coil)} = -7200 \text{ psi (Fig. 81, Curve 6)} \\ \text{(G-10/conductor interface after winding and preloading)}$$

$$+\sigma_r(\max) = 230 \text{ psi (under all loads combined; Fig. 81, Curve 5)}$$

Upon initial consideration, the peak hoop stress in the conductor appears quite high. However, the cable was cycled repeatedly to 35 ksi and once up to 45 ksi (.94% strain) without any apparent significant degradation in short sample or RRR. Furthermore, the peak stress occurs on the inner layer where 7 Energy Doubler strands were used to make up the cable as opposed to the usual 6 which was also the number used in the tested cable. Maximum compressive stress is no problem. The room temperature strength of the G-10 CR is 60,000 psi. For OFHC copper $\sigma_y \sim 7000$ psi and $\sigma_u = 30,000$ psi. A peak tensile radial load of 230 psi is found at a few spots on the inner layers. It is highly desirable that the coil always remain in radial compression. Because the modulus of the coil/G-10 package becomes nonlinear at a compressive pressures less than -1500 psi, it can be easily assumed that the coil is in fact always in radial compression. In a similar manner the peak hoop stress in the conductor is certainly limited to 21,500 psi due to the nonlinearity of yielding above 20,000 psi. In short, the predicted values represent upper bounds because the coil is highly nonlinear, and peak stresses will be redistributed throughout the coil.

Since the outer wall radial pressure is only -680 psi, one might suggest an increase in outer preload to increase radial pressures and decrease hoop loading. An increase in this preload, however, increases the compressive hoop stress. Local buckling of the conductor also needs to be considered. The concern here is potential layer to layer shorts. Maximum compressive stress is -9300 after winding and -4200 psi after cooldown. Both of these cases occur in layer #15 and #31.

Assume the conductor to be straight between the G-10 spacers. The conductor tends to make a sharp bend at each spacer rather than form a smooth circle. The expressions for buckling are given below

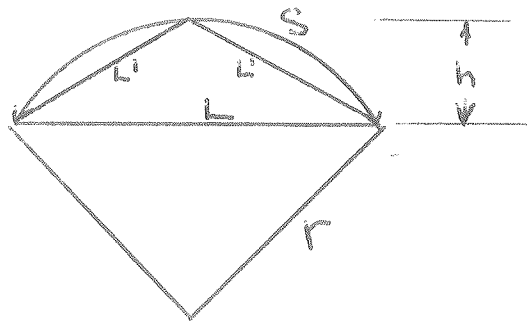
$$F_{cr} = \frac{\pi^2 E I}{l^2} \text{ for hinged ends}$$

$$F_{cr} = \frac{4\pi^2 E I}{l^2} \text{ for fixed ends}$$

where l is the span between the G-10 spacers. After cooldown layer #31 is most susceptible to buckling. The moment of inertia, I , must be known. This number cannot be calculated based on cross section since the conductor is a cable, not a monolith. Tests were made on the Instron to extract this number from simple bending tests treating the cable as a beam fixed between two supports. The cable

was found to have a moment of inertia, $I_z = 1.0 \times 10^{-5} \text{ in}^4$, which surprisingly is almost identical to the estimated value. The 4.2 K buckling stress ($E = 12.5 \times 10^6 \text{ psi}$) for layer #31 is 24,000 psi. The room temperature buckling stress ($E = 8.2 \times 10^6 \text{ psi}$) for layer #15 is 20,500 psi. Both of these values are based on the assumption of hinged ends. Any amount of additional constraint from radial pressure will increase these values. Buckling should not be a problem.

Local deformation is next calculated in the unlikely event of buckling. The worst case is after winding at layer #15 where $\epsilon_0 = -9300/8.2 \times 10^6 = .0011$. Assume a straight conductor which buckles locally such that the arc length of the curved path equals the length of the conductor in the relaxed condition. At this point further deformation would be impossible.



$$L_0 = 1.58'' = S$$

$$\Delta L = 1.58 \times .0011 = .0017''$$

$$L = L_0 - \Delta L = 1.5783$$

$$\text{Using Huyghen's approximate formula } L' = \frac{3S+L}{8} = .78979$$

$$\text{Then } h = .032''$$

$$\text{and } r = \frac{L^2}{8h} = 9.7'' = \text{local radius of curvature}$$

After winding, preload, and cooldown local deformation could at most be .017'' which is about one half the thinnest layer to layer spacer. Perforated mylar in layers 1 to 26 and solid dimpled mylar for the rest of the coil has been inserted between the spacers to prevent any possibility of layer to layer shorts. The first 26 layers of both coils had new very high quality cable which should be additionally resistant to buckling.

PEPRELOAD SCREW TORQUE VALUES

The inner layer is preloaded by sixty 1-1/4" wide bars using the 5/8-11 UNC socket set screws on each bar. The outer layer is similarly loaded except these preload screws are 3/4-10 UNC.

$$\text{Load on an inner screw} = \frac{P_i \times \pi \times 50.45 \times 8.69}{3 \times 60} = 7.65 P_i \text{ lb}_f$$

$$\text{Load on an outer screw} = 10.12 P_o \text{ lb}_f$$

Figure 83 is a torque vs. load curve for a 5/8" set screw with antisieze lubricant. Annealed screws do not have the preloading capacity of the as-fabricated screws. Annealing the screws was initially considered to reduce their residual magnetism created by cold working during their manufacture. No preload set screws used in the cryostat are annealed. The absolute maximum load which is possible is 7500 lbs. Failure is through excessive deformation of the broached socket. Unbrako gives a minimum tensile strength of 18,000 lbs for stainless socket head cap screws. The stress area of a 5/8 UNC screw = 0.226 sq in.

Thus,

$$18,000 \text{ lbs} = 80,000 \text{ psi}$$

$$7,500 \text{ lbs} = 33,000 \text{ psi}$$

Clearly the inner screws can withstand more force than that which is possible to achieve with a torque wrench. Winding and an additional 740 psi inner preload create an average pressure of 970 psi on the inner layer of conductor. This is equivalent to 7400 lbs on each 5/8" screw.

No torque vs. load measurement were made with the 3/4" screws. An approximation to this curve is given by

$$T(\text{in-lbs}) = K F d$$

where d is the nominal diameter. The inner screws have a $K = 0.166$ up to 6000 lbs. For an average bolt and nut, $K = 0.199$ for 5/8" UNC and $K = 0.194$ for 3/4" UNC [3]. Assume the same ratio for our well lubricated screws.

For the 3/4-10 UNC screws

$$T(\text{in-lbs}) = 0.162 F \times 0.75 = 0.121 F \text{ (lbs)}$$

Coil preloading consists of the following two step process:

1. Preload with inner screws by an additional 740 psi average coil pressure (970 psi total). The outer screws should not be in contact at this time. From Fig. 6.

$$T = 70 \text{ ft-lbs}$$

2. Preload with outer screws for an average outer layer pressure of 400 psi = 4040 lbs per screws. Using the formula for torque of a 3/4" screw.

$$T = 489 \text{ in-lbs} = 41 \text{ ft-lbs}$$

Inner screws for cryostat # one were made from 303 SS, and the inner screws for cryostat # two were made from 304 SS. The 303 SS was found to be much more brittle than the 304. Torque was limited to 70 ft-lbs. in the 304 screws rounding out the broached sockets. Torque was limited to the same value in the 303 screw by a cracking of the socket. A 303 SS screw was machined down to the bottom of the drill point of the socket. The screw was placed in a stainless nut extending .070" past the nut to represent its maximum extension into the cryostat. This set up represents the absolute minimum amount of non-cracked thread engagement. Failure occurred at 28,600 lbs. A 304 stainless screw tested in an identical manner failed at 25,000 lbs. Cracked screws have a minimum safety factor of 3.8.

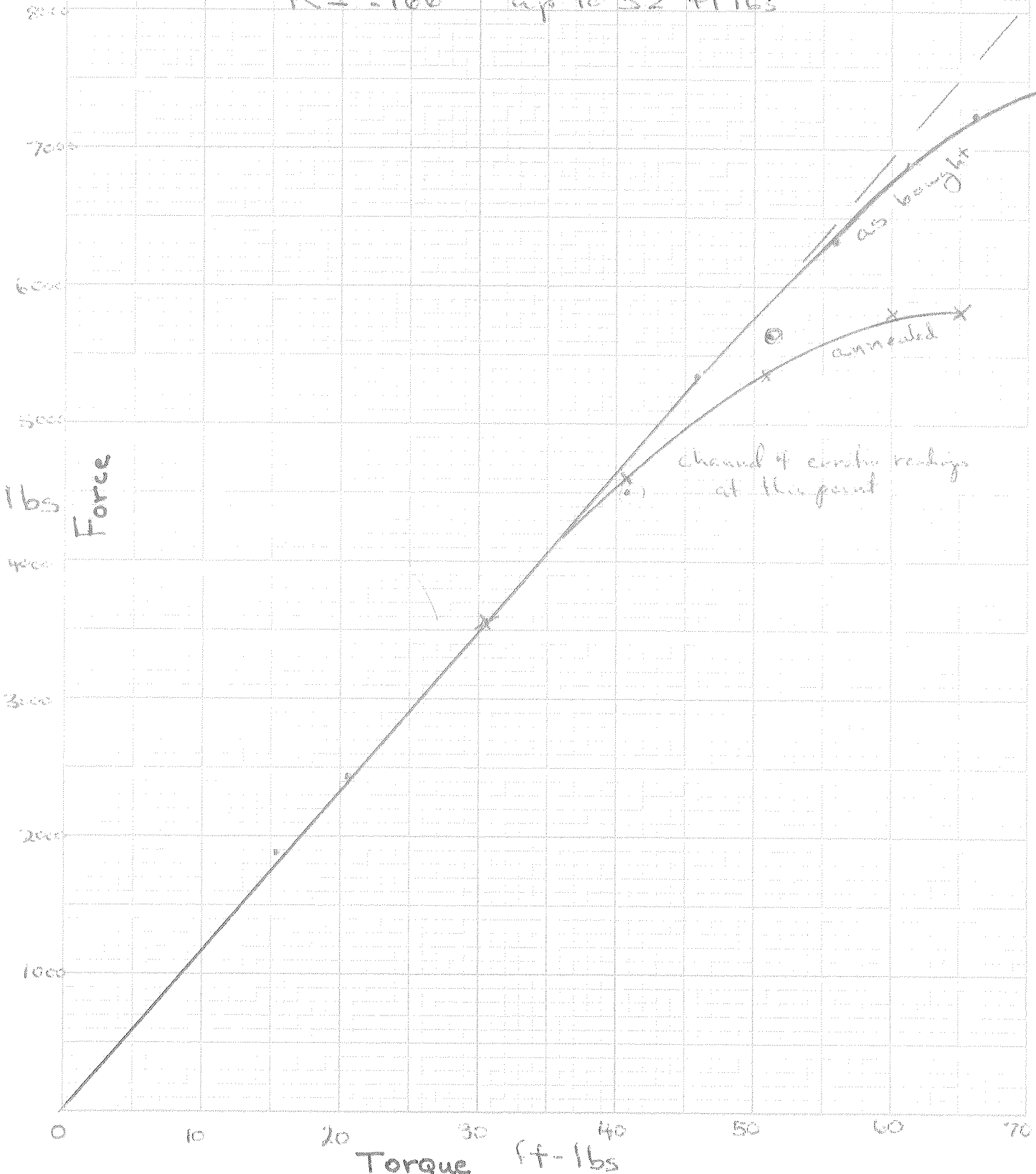
Figure 83

5/8-11 UNC stainless on stainless
with anti-siege

$$\text{Torque (in lbs)} = K F_c d \quad d = \frac{9}{8}$$

$$K = .166 \quad \text{up to } 52 \text{ ft-lbs}$$

46 0782



46 0782

SPECIAL AREA STRESS ANALYSISPressure Rating of Preload Screw Covers:

Preload screws on both the O.D. and I.D. are covered by a welded stainless steel cover. Each screw has a drill hole through it so that trapped helium volumes can be easily vented to the interior of the cryostat.

Effective diameter at outside of weld = 1.0"

Nominal thickness = .125"

Minimum machined thickness = .083"

Assume the edges are fixed. Use Roark and Young, Table 24, Case 10b.

$$M_{\max} = M_{ra} = -.125 wa = -.0625 w$$

$$\sigma_{\max} = \frac{6 M}{t^2} = 54.4 w$$

$$\text{Burst pressure} \sim \frac{250,000}{54.4} = 4600 \text{ psi}$$

Stress Concentrations Due to Preload Screw Holes:

The stress concentrations caused by the preload screws are difficult to analyze. Nevertheless, close approximation can be made by considering multiple holes in plates as opposed to cylinder.⁶ Only the inner cylinder will be analyzed since the highest stresses occur here, and the screws are closer together than on the outer cylinder. The holes are 5/8" diameter, separated by 3.25" axially and 2.5" circumferentially. Stress is increased by reduction of area and by genuine stress concentration. Overall stress distribution patterns are complex, but in general the principal stresses are hoop compression and axial bending. Axial bending is actually considered to be cylindrical bending where $M_{\text{hoop}} = \nu M_{\text{axial}}$.

In the hoop direction,

$$\sigma_{\text{nominal}} = \sigma_{\text{gross}} \times 3.25 / (3.25 - .625) = 1.24 \sigma_{\text{gross}}$$

In the axial direction,

$$\sigma_{\text{nominal}} = \sigma_{\text{gross}} \times 2.5 / (2.5 - .625) = 1.33 \sigma_{\text{gross}}$$

Identical cases cannot be found in the literature. Peterson has examples closest to our situation. The results are summarized below. See Figures 84 and 85.

Rectangular pattern of holes subject to uniaxial tension (hoop):

$$K_{TN} = 2.47$$

$$\sigma_{\max} = 2.47 \sigma_{\text{gross}}$$

Single row of holes subject to cylindrical bending (axial):

$$K_T = 1.81 \text{ holes aligned in axial direction}$$

$$K_T = 1.47 \text{ holes aligned in hoop direction}$$

$$\sigma_{\max} = 1.81 \times 1.24 \sigma_{\text{gross}} = 2.24 \sigma_{\text{gross}}$$

For comparison,

Single hole in infinite plate subject to uniaxial stress:

$$\sigma_{\max} = 3.0 \sigma$$

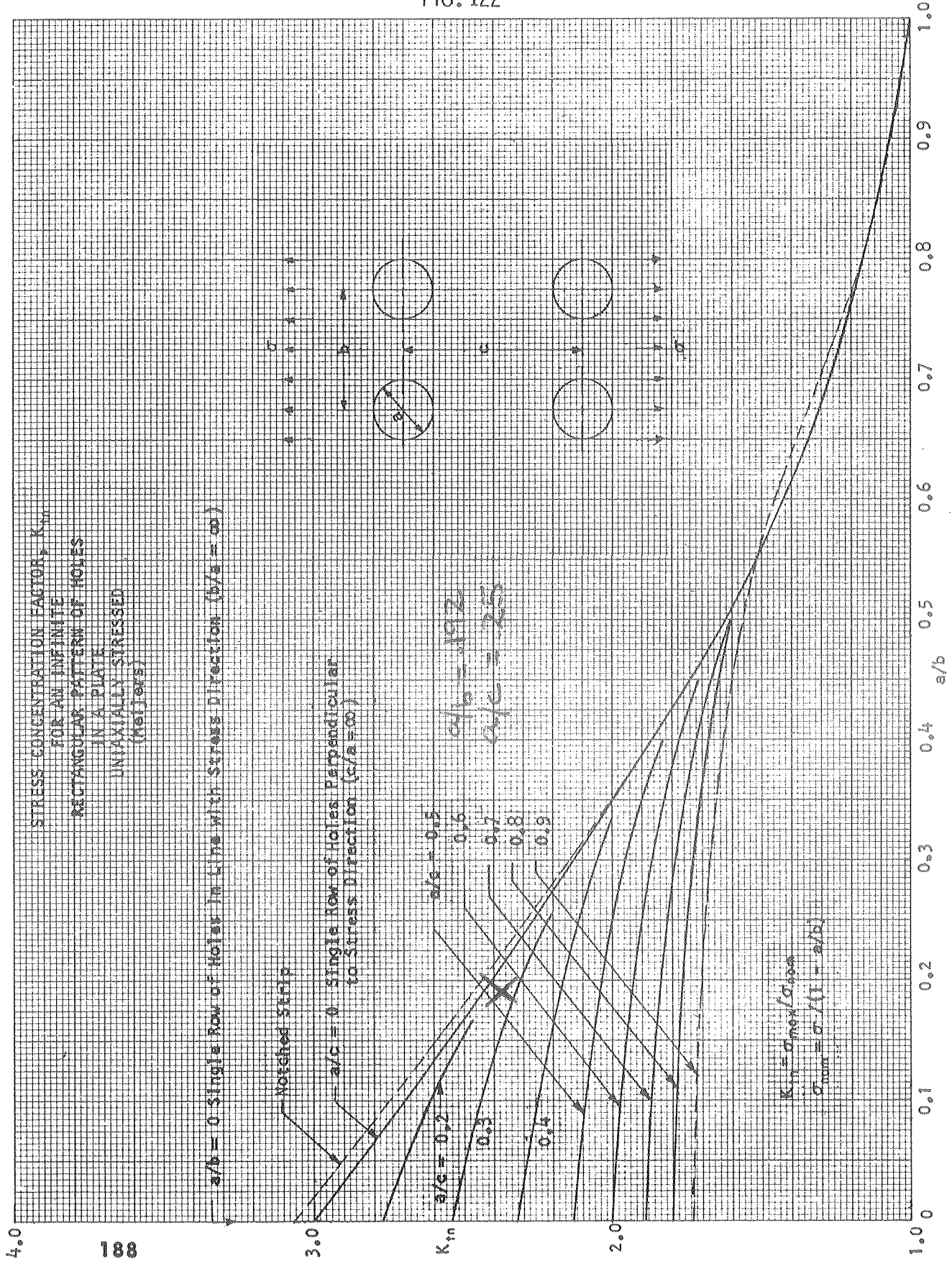
Single hole in infinite plate subject to cylindrical bending:

$$\begin{aligned} \sigma_{\max} &= 1.9 \sigma \quad \text{infinitely thin} \\ &= 2.34 \sigma \quad \text{dia/thickness} = .624/1.0 \end{aligned}$$

Conclusion:

A reasonable stress concentration for all cases would be 2.5 based on the gross stress values. The pressure of the screw hole covers should reduce the stress further but is not considered.

FIG. 122



4.0

188

3.0

K_{tn}

2.0

1.0

a/b

1.0

0.9

0.8

0.7

0.6

0.5

0.4

0.3

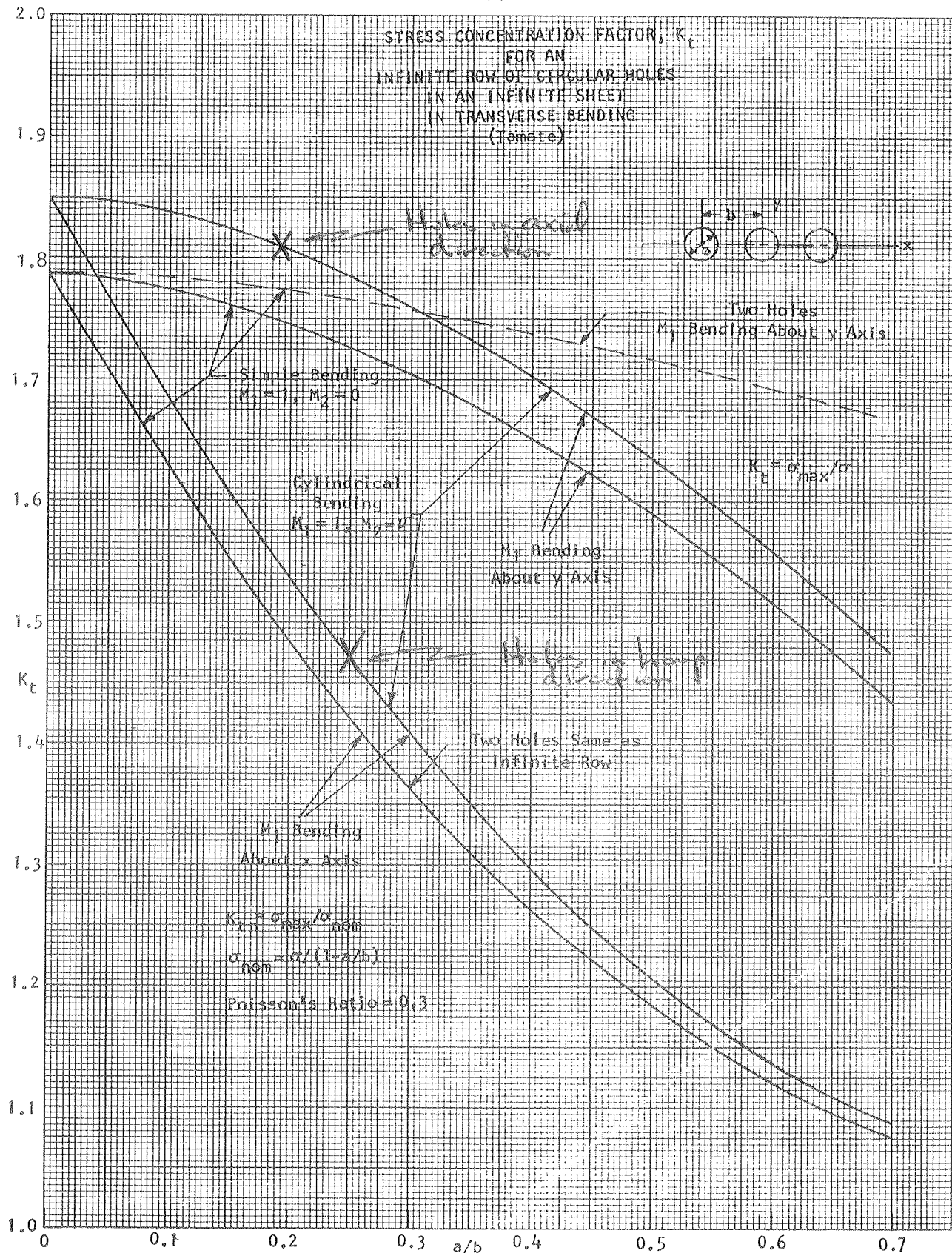
0.2

0.1

0.0

Fig 85
- Peterson -

FIG. 161



SUMMARY OF CRYOSTAT STRESS CALCULATIONS AND COMPARISON TO ASME
PRESSURE VESSEL CODE

Coil stresses are summarized in a prior section and are not discussed here. The cryostat body is made entirely of 304 SS with all major welds made with KRYOKAY 316L-15 SMA. The following material properties are assumed.^{7,8,9,10}

| Material | Temperature | σ_y (ksi) | σ_w (ksi) | S_m^* (ksi) |
|--------------|-------------|------------------|------------------|---------------|
| 304 | 293 K | 35 | 85 | 23 |
| 304 | 4 K | 60 | 250 | 40 |
| 316L-15(SMA) | 293 K | 57 | 78 | 26 |
| 316L-15(SMA) | 4 K | 95 | 175 | 58 |

Although this is not a code vessel, the design will be compared to the ASME code.

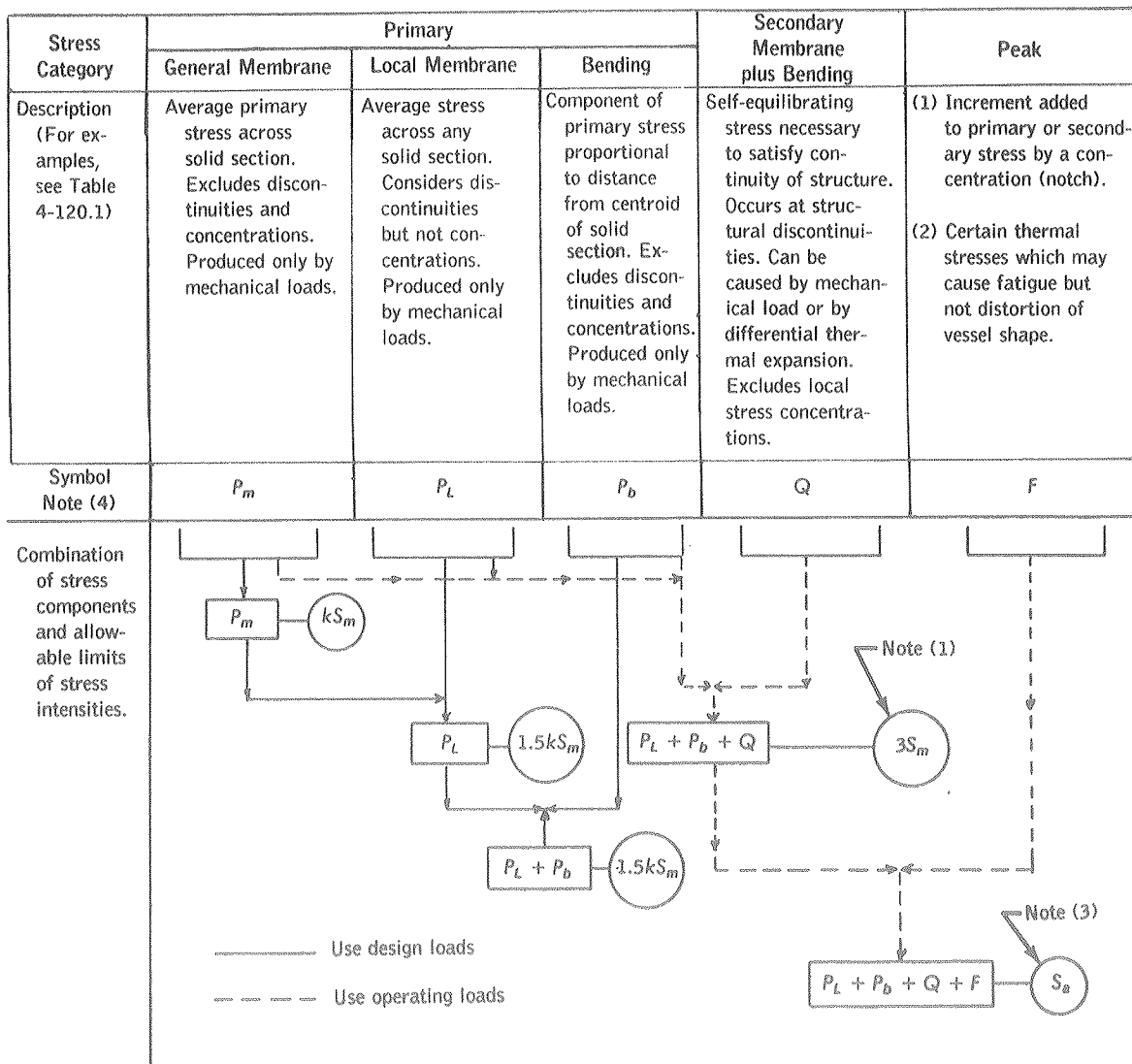
Section VIII, Division 2 will be the basis for comparison. This division places limits on various combinations of stress intensities. See Article AD-140, Appendix 1 and Appendix 4. The stress intensity value for room temperature 304 stainless plate is $S_m = 20$ ksi. See Table AHA-1. This value assumes yield strength of 30 ksi. Stress intensity values, S_m , are the smaller of $2/3 \sigma_y$ or $1/3 \sigma_u$. If we extend this philosophy to our materials, the values found in the table above are computed*. Only troublesome areas are examined.

Cross Section Through the Inner Wall Midplane:

After winding and preloading the peak cryostat stress is found at this location. Obviously this stress occurs at room temperature. Figure 86 is a copy of the procedural outline used in Division 2. From the ANSYS run the following stress values are obtained.

| | Inner Radius | Outer Radius |
|-------|---------------------------------|---------------------------------|
| S_z | = $-13930 \times 1.24 = -17270$ | = $-29190 \times 1.24 = -36200$ |
| S_x | = -783 | = -7174 |
| S_y | = $23661 \times 1.33 = 31460$ | = $-24060 \times 1.33 = -32000$ |
| S.I. | = 37620 | = 22290 |

The factors 1.24 and 1.33 appear because of the reduction in areas due to the screw holes. Primary membrane stress values are averaged through the thickness. The r, θ , and z or (x, z, y i ANSYS) are essentially the principal directions. Small values of shear stress in the xy ANSYS plane are neglected. The primary membrane values are given below.



NOTES:

- (1) This limitation applies to the range of stress intensity. The quantity $3S_m$ is defined as three times the average of the tabulated S_m values for the highest and lowest temperatures during the operation cycle. In the determination of the maximum primary-plus-secondary stress intensity range, it may be necessary to consider the superposition of cycles of various origins that produce a total range greater than the range of any of the individual cycles. The value of $3S_m$ may vary with the specific cycle, or combination of cycles, being considered since the temperature extremes may be different in each case. Therefore, care must be exercised to assure that the applicable value of $3S_m$ for each cycle, and combination of cycles, is not exceeded except as permitted by 4-136.4.
- (2) The stresses in Category Q are those parts of the total stress which are produced by thermal gradients, structural discontinuities, etc., and do not include primary stresses which may also exist at the same point. It should be noted, however, that a detailed stress analysis frequently gives the combination of primary and secondary stresses directly and, when appropriate, this calculated value represents the total of P_m (or P_L) + P_b + Q and not Q alone. Similarly, if the stress in Category F is produced by a stress concentration, the quantity F is the additional stress produced by the notch, over and above the nominal stress. For example, if a plate has a nominal stress intensity, S, and has a notch with a stress concentration factor, K, then $P_m = S$, $P_b = 0$, $Q = 0$, $F = P_m (K - 1)$ and the peak stress intensity equals $P_m + P_m (K - 1) = KP_m$.
- (3) S_a is obtained from the fatigue curves, Figs. 5-110.1, 5-110.2 and 5-110.3. The allowable stress intensity for the full range of fluctuation is $2 S_a$.
- (4) The symbols P_m , P_L , P_b , Q, and F do not represent single quantities, but rather sets of six quantities representing the six stress components σ_t , σ_l , σ_r , τ_{tb} , τ_{lr} , and τ_{rl} .
- (5) The k factors are given in Table AD-150.1.

FIG. 4-130.1 STRESS CATEGORIES AND LIMITS OF STRESS INTENSITY

$$P_m = -26735 \text{ for } S_z$$

$$-270 \text{ for } S_y$$

$$-3979 \text{ for } S_x$$

$$P_m(SI) = 26735 - 270 = 27000 \text{ psi} > S_m$$

This is an apparent code violation. According to Table 4-120:1 it may be possible to consider this inner wall as being subjected to only local membrane stresses P_L and secondary stresses Q . If this interpretation is correct, then

$$P_L(SI) = 27000 < 1.5 S_m = 30,000 \text{ and the code is satisfied.}$$

Next check $P_L + P_b$ at the inner radius

$$P_L = -26735 \text{ for } S_z$$

$$P_b = 9465 \text{ for } S_z$$

$$31460 \text{ for } S_y$$

$$P_L + P_b(SI) = 17270 + 31460 = 48730 > 1.5 S_m$$

Another apparent code violation. The bending stresses are treated as primary rather than secondary because they originate from the basic constraint of the inner wall by the top and bottom annular plates. The origin of the stresses are mechanical preload, however. As the inner wall deflects, the preload through the bolts from pushing against the coil relaxes. Any permanent deformation creates a permanent relaxation in stresses. Thus on subsequent cooldown/charging cycles we can never experience a ratcheting of increasing strain. In this sense all our stresses can be interpreted by the Code to be secondary. The basic characteristic of secondary stresses is that they are self limiting. These stresses can be thought of as secondary by the peculiar nature of their origin. Considered in this manner,

$$P_L + P_b + Q = Q = 37620 \times 1.3 = 49000 < 3 S_m = 60,000$$

and the code is satisfied. $3 S_m = 2 \sigma_y$ is the maximum value that secondary stresses will "shake down to elastic action".¹¹ The longitudinal seam weld is made between the bolt holes, and therefore, has the benefit of the full cross section. At this point $P_L + P_b + Q = 37620$ psi. This weld was radiographed and found to have no visible flaws. At 4.2 K under full radial and axial electromagnetic loads, the combined stress intensity through this section is $\sim 4500 \times 1.3 = 5850$ psi, and the code is clearly satisfied.

Cross Section Through the Inner Wall/Annular Plate Weld:

The worse case is again after preloading at room temperature.

| | Root of Weld | Top of Weld | Average |
|-------|--------------|-------------|---------|
| S_z | -1282 | 503 | -389 |
| S_y | 1121 | -17 | 552 |
| S_x | 10460 | 11220 | 10840 |
| SI | 12230 | 11240 | |

$$P_m = 10840 + 389 = 11230 < S_m = 20000$$

$$P_L + P_b = 10460 + 1282 = 11742 < 1.5 S_m = 30000$$

$$P_L + P_b + Q = 12230 < 3 S_m = 60000$$

$$P_L + P_b + Q = 2025 \text{ at the root of the weld under full load at } 4.2 \text{ K}$$

This weld presents no problem. Division 1 requires spot radiography for this weld which was not performed. If we use, however, the joint efficiency of .60 for single-welded butt joints for non-radiographed welds, we would still have an adequate safety margin. As in the cross section through the midplane, these stresses could be considered as entirely secondary due to the peculiar nature of the mechanical loading.

Cross Section Through Outer Wall Midplane:

The maximum stress occurs at 4.2 K under combined electromagnetic loads. For the combination of all loads except radially decentering loads, the following stresses are found.

| | Inner Radius | Outer Radius |
|-------|-----------------------------|---------------------------|
| S_z | $2670 \times 1.24 = 3311$ | $3186 \times 1.24 = 3951$ |
| S_x | -2505 | 84 |
| S_y | $-5205 \times 1.25 = -6506$ | $3009 \times 1.25 = 3761$ |
| SI | 8050 | 3654 |

Using the same method as for the inner wall;

$$P_m \text{ (SI)} = 5000 < S_m = 40000$$

$$P_L + P_b \text{ (SI)} = 9820 < 1.5 S_m = 60000$$

$$P_L + P_b + Q \text{ (SI)} = 8050 \times 1.24 = 9980 < 3 S_m = 120,000$$

The code is satisfied by a wide margin, but the local effects of the radial arm gussets, axial support bracket, and helium vent hole must also be considered. The longitudinal seam weld was fully radiographed and found to have no flaws.

B. Wands' analysis showed that the maximum Von Mises stress in the cryostat wall due to the 75,000 radial arm loading was 10,090 psi. The 3D ANSYS analysis gave a Von Mises stress of 5750. Maximum tensile membrane load in the outer wall at the bracket location should be $75,000 / (10.5 \times 1.56) = 4600$ psi. For the axial brackets, hand calculations gave an 8% variation in peak stress between uniformly distributed moments and 8 discrete concentrated moments. Assume the bottom of the axial support gussets are at the midplane. Peak stress and radial arm bracket stress occur here so that combining these stresses is a worse case. Using the true area of the gussets, we find from the axisymmetric calculations $S_x = 19700$, $S_y = 6360$, and $SI = 24480$. The combination of axial support bracket stresses is a worse case analysis since they don't occur at the same location. These axial support bracket stresses are actually the summation of local and secondary stresses. Consider the 10,090 psi Von Mises stress to exist from 4600 psi and 5400 psi of hoop bending. Then

$$P_m (SI) \sim 3631 + 4600 + 1211 = 9400 < S_m 40,000$$

$$P_L + P_D (SI) \sim 3951 + 10090 - 84 = 14000 < 1.5 S_m = 60,000$$

$$P_L + P_D + Q (SI, \max) \sim 24480 + 10,090 = 35000 < 3 S_{mm} = 120,000$$

The method of addition of $P_L + P_D + Q$ is incorrect because the stress intensities were added together rather than being computed from the addition of the individual stress components. Nevertheless, this represents an upper bound and is still far less than the code allowable value of $3 S_m$.

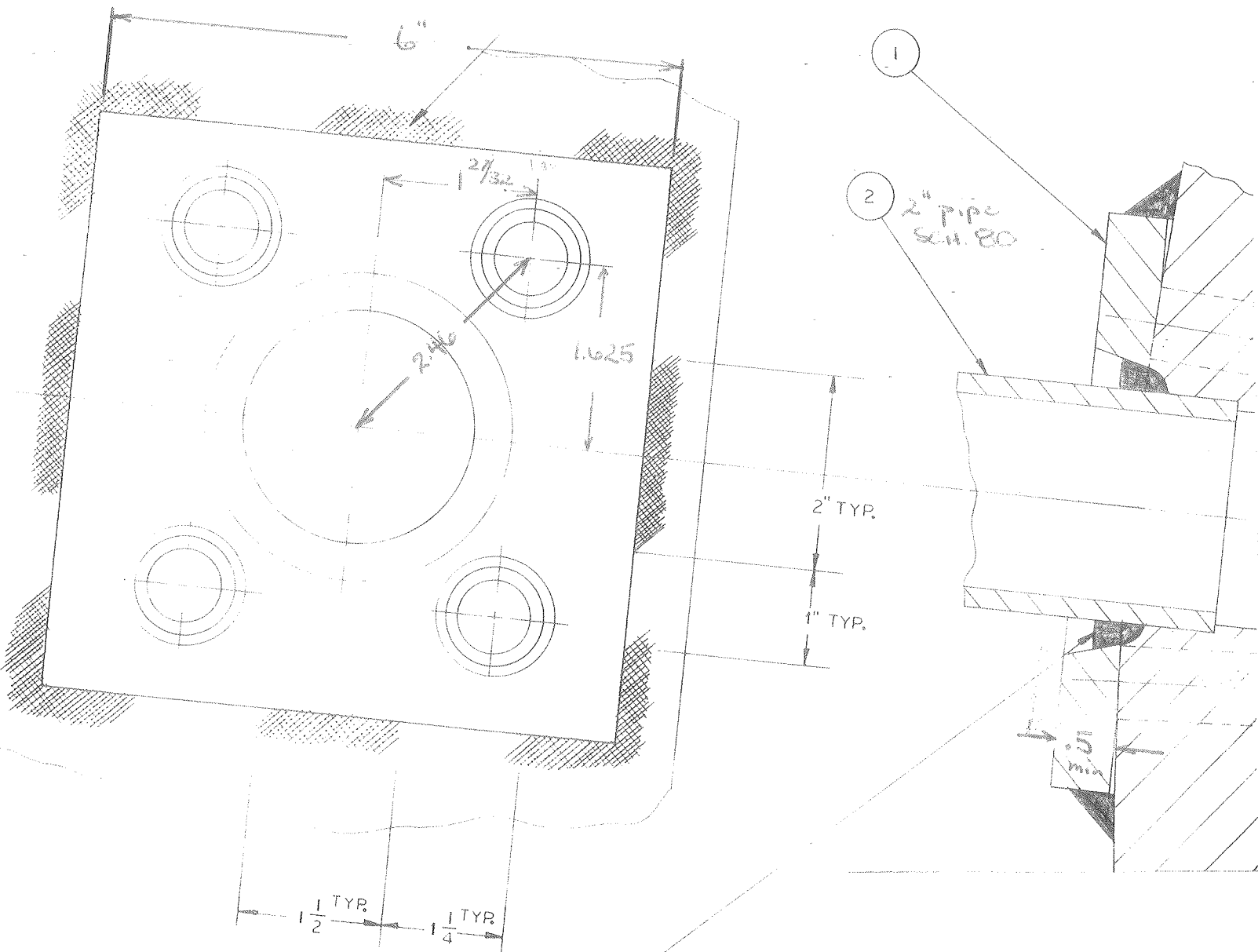
Finally the helium vent hole must be considered. The area required is given by $A = dt_r F$ where d is the diameter of the opening, t_r is the minimum wall thickness, and $F=1$ for the longitudinal plane. Based on the worse case analysis above we have approximately 4 times the required outer wall thickness or $t_r \sim 1.56/4 = .39$ ". The preload bolt holes complicate the picture. Assume that the vent hole and bolt hole combination is equal to one large hole with diameter 5.67". Then $A = 5.67 \times .39 = 2.2 \text{ in}^2$. Limits of reinforcing are greater than the axial height of the cylinder. Thus the area available for reinforcing the vent/bolt hole is $(1.56 - .39) \times (10.5 - 5.67) = 5.65 \text{ in}^2$ or 2-1/2 times the required amount. The code is difficult to interpret for this case and a reinforcing pad was added for extra safety. Figure 87 shows this reinforcing. In the longitudinal plane this reinforcing pad + nozzle combination adds about 2-1/2 in^2 of reinforcing or the entire amount required. Note also that in Division 1 2" pipe single openings in vessels greater than 3/8" thick do not require reinforcing. In conclusion the vent hole has roughly 3-1/2 times the required reinforcing.

Cross Section Through High Stress Point of Bottom Annular Plate

The highest stress point in the bottom annular plate occurs at the outer push bar where a spar element was used in ANSYS to simulate a partial transfer of

Figure 87

FINAL Drawing # 2771-MC-156003



TYPICAL FOR ALL WELDING

TIG WELD ROOT PASS. USE 316L FILLER ROD,
USE 316 L KRYO-KAY TO COMPLETE WELD.
WELD TO BE VACUUM TIGHT

axial load in shear to this member. From Fig. 52 the stress intensity ($P_L + P_b + Q$) is found to be 35900 psi which is less than $1 S_m$. Obviously P_m and $P_L + P_b$ satisfy the code also. Furthermore, this stress intensity value is due in part to a stress concentration component from the point loading approximation.

Cross Section Through the Bottom Outer Ring Closure Weld:

Again peak stresses occur under full field conditions at 4.2 K.

| | Root of Weld | Face of Weld | Average |
|-------|--------------|--------------|---------|
| S_x | 24740 | -28070 | -1665 |
| S_y | 11630 | 2380 | 7005 |
| S_z | 16560 | -963 | 7799 |
| SI | 17900 | 30880 | -- |

$$P_m \text{ (SI)} = 7799 + 1665 = 9464 < S_m = 58000$$

$$P_L + P_b \text{ (SI)} = 28070 + 2380 = 30450 < 1.5 S_m = 87000$$

$$24740 - 11630 = 13110 \text{ at the root of the weld}$$

$$P_L + P_b + Q \text{ (SI)} = 30880 < 3 S_m = 174000$$

$$17900 \text{ at the root of the weld}$$

Division II normally requires fully radiography for this weld except that ultrasonic testing may be used when radiography is impossible as in our case. In addition this joint should be a Type 1 double welded butt joint. This is a single welded butt joint without a backing strip.

This weld was made using a qualified weld procedure and a certified welder. The two closure welds were the only welds made using a certified welder. The welding test reports are given in Appendix B along with the ultrasonic test results. A crack was found along the root of the weld. This is interpreted as incomplete filling in the landing of the weld during the first TIG pass due to concern of overheating the conductor and insulators. No other weld defects were found. Division I uses a joint efficiency of .6 for single welded butt joints without a backing strip. Using this value we still have a minimum factor of 3.7 above code requirement at the root of the weld.

Inner Push Bar:

The maximum stress occurs at room temperature after winding and preloading at the upper preload screw location. The maximum bending stress in this bar is 67,000 psi at the junction with the top inner screw. If the code were applied, the following results are obtained.

$$P_m \text{ (SI)} = 39800 > S_m$$

$$P_L + P_b \text{ (SI)} = 42900 > 1.5 S_m$$

$$P_L + P_b + Q \text{ (SI)} = 42900 < 3 S_m$$

The code is violated unless all stresses are considered secondary due to the nature of the mechanical load. No significant differences in coil diameter were found. Machined inner bar stock probably has a significantly higher yield stress than the assumed 30,000 psi. Furthermore, the preload screws distribute the load and reduce the span which should appreciably lower the peak stresses. Finally, it is impossible for the inner bar to fail. The bar would yield slightly and the preload on the coil would relax.

Inner Preload Screws:

The maximum load is again after winding and preloading. Preloading and winding place 7400 lbs on each 5/8" UNC inner preload screw. These screws were tested and have an absolute minimum load capacity of 25,000 lbs. The safety factor is 3.38. Again this exceeds the code allowable values of 1/4 on the ultimate and 2/3 on the yield. As with the inner push bar, excessive loadings cause yielding and load relaxation.

Summary

In conclusion this vessel was not originally designed with the ASME pressure vessel code in mind since Fermilab policy did not require Code use (explicitly or implicitly) at that time. The magnet does, however, obey the majority of the Code requirements when the rules are modified or interpreted according to the intent of its basic design philosophy. In any event all components have an appropriate safety factor.

REFERENCES

1. W. Craddock, R. Kephart, M. Kobayashi, and M. Mruzek, "Coil Conversion of the Fermilab 30-Inch Bubble Chamber Magnet", *Advances in Cryogenic Engineering*, Vol. 27, p. 119.
2. Westendorp and Kilb, "Stresses in Magnetic Field Coils" *Proceedings of the 1968 Summer Study on Superconducting Devices and Accelerators, Part III*, p. 714-726, BNL 50155.
3. Timoshenko, *Strength of Materials, Part II*, p. 138.
4. Tabakman and Valentign, "Machine Design", October 22, 1964.
5. Boom, Peterson, Young, et. al., *Wisconsin Superconductive Energy Storage Project, Vol. 1, Appendix VI A*, July 1974.
6. Peterson, *Stress Concentration Factors*.
7. NBS, *LNG Users Handbook (1979)*.
8. D.T. Read, H.I. McHenry, P.A. Steinmeyer, and R.D. Thomas, "Metallurgical Factor Affecting the Toughness of 316L SMA Weldments at Cryogenic Temperatures", *Materials Studies for Fusion Energy, Vol. II*, p. 315, NBSIR 79-1609, June 1979.
9. Dalden, Seth, Whipple, *CEC, Vol. 28*, p. 839.
10. Teledyne Mckay, *Selector Chart*.
11. ASME, *Criteria of the ASME Boiler and Pressure Vessel Code for Design by Analysis in Sections III and VIII, Division 2*, 1969.